Available online at www.sciencedirect.com
ScienceDirect
Nuclear Data Sheets 107 (2006) 3061–3118
Nuclear Data Sheets
www.elsevier.com/locate/nds

Benchmarking ENDF/B-VII.0

Steven C. van der Marck*
Nuclear Research and Consultancy Group NRG,
P.O. Box, 1755 ZG Petten, the Netherlands

(Received September 26, 2006)

The new major release VII.0 of the ENDF/B nuclear data library has been tested extensively using benchmark calculations. These were based upon MCNP-4C3 continuous-energy Monte Carlo neutronics simulations, together with nuclear data processed using the code NJOY. Three types of benchmarks were used, *viz.*, criticality safety benchmarks, (fusion) shielding benchmarks, and reference systems for which the effective delayed neutron fraction is reported. For criticality safety, more than 700 benchmarks from the International Handbook of Criticality Safety Benchmark Experiments were used. Benchmarks from all categories were used, ranging from low-enriched uranium, compound fuel, thermal spectrum ones (LEU-COMP-THERM), to mixed uranium-plutonium, metallic fuel, fast spectrum ones (MIX-MET-FAST). For fusion shielding many benchmarks were based on IAEA specifications for the Oktavian experiments (for Al, Co, Cr, Cu, LiF, Mn, Mo, Si, Ti, W, Zr), Fusion Neutronics Source in Japan (for Be, C, N, O, Fe, Pb), and Pulsed Sphere experiments at Lawrence Livermore National Laboratory (for ^{6}Li, ^{7}Li, Be, C, N, O, Mg, Al, Ti, Fe, Pb, D_2O, H_2O, concrete, polyethylene and teflon). For testing delayed neutron data more than thirty measurements in widely varying systems were used. Among these were measurements in the Tank Critical Assembly (TCA in Japan) and IPEN/MB-01 (Brazil), both with a thermal spectrum, and two cores in Masurca (France) and three cores in the Fast Critical Assembly (FCA, Japan), all with fast spectra.

In criticality safety, many benchmarks were chosen from the category with a thermal spectrum, low-enriched uranium, compound fuel (LEU-COMP-THERM), because this is typical of most current-day reactors, and because these benchmarks were previously underpredicted by as much as 0.5% by most nuclear data libraries (such as ENDF/B-VI.8, JEFF-3.0). The calculated results presented here show that this underprediction is no longer there for ENDF/B-VII.0. The average over 257 benchmarks deviates only 0.017% from the measured benchmark value. Moreover, no clear trends (with *e.g.* enrichment, lattice pitch, or spectrum) have been observed. Also for fast spectrum benchmarks, both for intermediately or highly enriched uranium and for plutonium, clear improvements are apparent from the calculations. The results for bare assemblies have improved, as well as those with a depleted or natural uranium reflector. On the other hand, the results for plutonium solutions (PU-SOL-THERM) are still high, on average (over 120 benchmarks) roughly 0.6%. Furthermore there still is a bias for a range of benchmarks based on cores in the Zero Power Reactor (ANL) with sizable amounts of tungsten in them.

The results for the fusion shielding benchmarks have not changed significantly, compared to ENDF/B-VI.8, for most materials. The delayed neutron testing shows that the values for both thermal and fast spectrum cases are now well predicted, which is an improvement when compared with ENDF/B-VI.8.

*) Electronic address: vandermarck@nrg-nl.com

0090-3752/$ – see front matter
doi:10.1016/j.nds.2006.11.002

Contents

I. INTRODUCTION

In December 2006 a version of the ENDF/B-VII general purpose nuclear data library was released: ENDF/B-VII.0 [1]. Over the last several years there has been a concerted effort by many people to bring the quality of this nuclear data library to a new, higher level. Especially the underprediction of $k_{\rm eff}$ for many criticality safety benchmarks with a thermal spectrum has received much attention.

To get a first impression of the quality of the library, results are presented here for many benchmark calculations, involving criticality safety, (fusion) shielding, and the effective delayed neutron fraction. The benchmark definitions for the criticality safety cases are given by the International Criticality Safety Benchmark Evaluation Project (ICSBEP [2]), whereas for the shielding cases they are given by Refs. [3–6]. For the effective delayed neutron fraction, we refer to Refs. [7–9] for descriptions of the most important critical configurations for which calculational results are presented here.

The results of the criticality safety calculations show, among other things, that when using ENDF/B-VII.0 nuclear data, the prediction of $k_{\rm eff}$ for the thermal spectrum benchmarks is much closer to the benchmark value than for *e.g.* ENDF/B-VI.8. Also for fast spectrum benchmark cases the criticality safety benchmark results have improved considerably.

All results reported in this paper were obtained by use of the Monte Carlo neutronics code MCNP, version 4C3 [10]. The cross sections were processed using NJOY, version 99.125 for almost all isotopes. For ^{235}U and ^{239}Pu, NJOY version 99.161 was used, because in these cases a new section MT460 for photon production from fission product decay was introduced. All cross sections were processed at room temperature.

The values given in this paper are for the preliminary ENDF/B-VII (beta3) files. These files are equivalent to the final evaluated files released as ENDF/B-VII.0 so that conclusions and observations made here are applicable to the ENDF/B-VII.0 library.

II. BRIEF DESCRIPTION OF THE CRITICALITY BENCHMARKS

Almost all benchmarks were taken from the *International Handbook of Evaluated Criticality Safety Benchmark Experiments* (ICSBEP, [2]). In Ref. [2], these benchmarks are subdivided in main categories according to three criteria.

1. The main fissionable isotope. The systems containing uranium-235 are subdivided according to the enrichment in ^{235}U: there is low enriched uranium (LEU: wt% ^{235}U < 10), intermediate enriched (IEU: $10 <$ wt% ^{235}U < 60) and high enriched (HEU: wt% ^{235}U > 60). There are also plutonium systems (PU), mixed uranium/plutonium systems (MIX), and ^{233}U systems (U233).
2. The physical form of the fissile material: there are metal systems (MET), compound (COMP), solution (SOL) and miscellaneous systems.
3. The neutron spectrum: if more than half of the fissions occurs for neutrons with energy below 0.625 eV the spectrum is thermal (THERM), if more than half occurs between 0.625 eV and 100 keV it is intermediate (INTER), and if more than half occurs over 100 keV it is fast (FAST). If none of these applies, the spectrum is classified as MIXED.

The benchmark series identifier consists of the three components mentioned above, plus an additional sequence number.

For each of the benchmark series for which calculations have been performed, a brief description is given below.

A. High-enriched uranium (HEU) benchmarks

1. *Fast spectrum*

heu-met-fast-001 (1 case, 'Godiva') A bare sphere of highly enriched uranium (LANL, 1950s). The uranium enrichment was 94% ^{235}U.
The isotopes in this benchmark model are ^{234,235,238}U.

heu-met-fast-005 (6 cases) Cores of uranium metal alloy and reflectors of molybdenum and beryllium (Obninsk, 1987). The amount of reflector material (^{9}Be) and the amount of molybdenum between fuel and reflector was varied. The uranium enrichment was 90% ^{235}U.
The isotopes in these benchmark models are ^{nat}C, ^{27}Al, $^{28-30}$Si, $^{46-50}$Ti, $^{50,52-54}$Cr, ^{55}Mn, $^{54,56-58}$Fe, $^{58,60-62,64}$Ni, $^{92,94-98,100}$Mo, and ^{234,235,236,238}U.
In cases $2-6$ ^{9}Be is also present.

heu-met-fast-007 (43 cases) Uranium metal slabs moderated with polyethylene, plexiglas and teflon (ORNL, 1960s). Some of the polyethylene moderated experiments also had a polyethylene reflector. The H/^{235}U ratio was varied between 0 and 5. The uranium enrichment was 93% ^{235}U.
The isotopes in these benchmark models are ^{1}H, ^{nat}C, ^{234,235,236,238}U. In cases 27-31 ^{16}O is also used, and in cases 32-34 ^{19}F is also used.

heu-met-fast-022 (1 case) A sphere of highly enriched uranium with C, Fe and W impurities, reflected by duraluminum (VNIIEF, Russia, 1962). The uranium enrichment was 90% ^{235}U.
The isotopes in this benchmark model are ^{nat}C, ^{27}Al, $^{54,56-58}$Fe, ^{63,65}Cu, $^{182-184,186}$W, ^{234,235,238}U.

heu-met-fast-027 (1 case) A sphere of highly enriched uranium with C, Fe and W impurities, reflected by lead (VNIIEF, Russia, 1962). The uranium enrichment was 90% ^{235}U.
The isotopes in this benchmark model are ^{nat}C, $^{54,56-58}$Fe, $^{182-184,186}$W, $^{204,206-208}$Pb, ^{234,235,238}U.

heu-met-fast-028 (1 case, 'Topsy', 'Flattop-25') A sphere of highly enriched uranium reflected by normal uranium (LANL, 1960s). The uranium enrichment was 93% ^{235}U.
The isotopes in this benchmark model are ^{234,235,238}U.

heu-met-fast-057 (6 cases) Uranium metal spheres and cylinders, reflected by lead (LLNL, 1950s). The uranium enrichment was 93% ^{235}U.
The isotopes in these benchmark models are ^{9}Be, $^{40,42-44,46,48}$Ca, $^{54,56-58}$Fe, $^{58,60-62,64}$Ni, $^{204,206-208}$Pb, ^{234,235,238}U.

heu-met-fast-060 (1 case) A cylindrical assembly of uranium metal and tungsten, with aluminum reflectors (ZPR-9 assembly 4, ANL, 1960s). The uranium enrichment was 93% ^{235}U.
The isotopes in this benchmark model are ^{1}H, ^{nat}C, ^{19}F, $^{24-26}$Mg, ^{27}Al, $^{28-30}$Si, ^{35,37}Cl, $^{46-50}$Ti, $^{50,52-54}$Cr, ^{55}Mn, $^{54,56-58}$Fe, $^{58,60-62,64}$Ni, ^{63,65}Cu, $^{92,94-98,100}$Mo, $^{182-184,186}$W, ^{234,235,236,238}U.

heu-met-fast-064 (3 cases) Three cylinders of lead reflected highly enriched uranium (VNIITF, Russia, 1991). The uranium enrichment was 96% ^{235}U.
The isotopes in these benchmark models are ^{nat}C, $^{28-30}$Si, $^{50,52-54}$Cr, ^{55}Mn, $^{54,56-58}$Fe, $^{182-184,186}$W, $^{204,206-208}$Pb, ^{234,235,238}U.

heu-met-fast-067 (2 cases) Cylindrical assemblies of uranium metal with tungsten, graphite (assembly 5) and aluminum (assembly 6), reflected by dense aluminum. (ZPR-9 assemblies 5 and 6, ANL, 1960s). The uranium enrichment was 93% ^{235}U.
The isotopes in these benchmark models are ^{1}H, ^{nat}C, ^{19}F, $^{24-26}$Mg, ^{27}Al, $^{28-30}$Si, ^{35,37}Cl, $^{46-50}$Ti, $^{50,52-54}$Cr, ^{55}Mn, $^{54,56-58}$Fe, ^{63,65}Cu, $^{58,60-62,64}$Ni, $^{92,94-98,100}$Mo, $^{182-184,186}$W, ^{234,235,236,238}U.

heu-met-fast-072 (1 case, 'Zeus') An iron/HEU core surrounded by a copper reflector in the Los Alamos Critical Experiment Facility (LANL, 2002). In this report only configuration 1 (out of two) was computed. The uranium enrichment was 93% ^{235}U.
The isotopes in these benchmark models are ^{10,11}B, ^{nat}C, ^{14,15}N, $^{24-26}$Mg, ^{27}Al, $^{28-30}$Si, ^{31}P, $^{32-34,36}$S, $^{46-50}$Ti, ^{nat}V, $^{50,52-54}$Cr, ^{55}Mn, $^{54,56-58}$Fe, $^{58,60-62,64}$Ni, ^{63,65}Cu, ^{nat}Zn, ^{nat}Ga, $^{92,94-98,100}$Mo, $^{204,206-208}$Pb, ^{234,235,236,238}U.

2. *Intermediate spectrum*

heu-comp-inter-004 (1 case) A k_∞ experiment at the HECTOR reactor (Winfrith, UK, 1960s): a graphite moderated uranium oxide core. The benchmark model is an infinite medium with a material composition appropriate to the interpolated boron/^{235}U ratio. The uranium enrichment was 92% ^{235}U.
The isotopes in these benchmark models are ^{1}H, ^{10,11}B, ^{nat}C, ^{16}O, $^{40,42-44,46,48}$Ca, ^{234,235,236,238}U.

heu-comp-inter-005 (5 cases) Several k_∞ experiments at the COBRA facility (Obninsk, Russia, 1980s, 1990s), containing uranium and nickel (KBR-7 assembly), stainless steel (KBR-9), stainless steel and molybdenum (KBR-10), chromium (KBR-15), and zirconium (KBR-16). The uranium enrichment was 90% ^{235}U.
The isotopes in these benchmark models are ^{nat}C, ^{16}O, $^{28-30}$Si, $^{46-50}$Ti, $^{50,52-54}$Cr, ^{55}Mn, $^{54,56-58}$Fe, $^{58,60-62,64}$Ni, ^{235,238}U. Also used are ^{59}Co (case 1), $^{92,94-98,100}$Mo (case 3) and ^{1}H, $^{90-92,94,96}$Zr, $^{174,176-180}$Hf (case 5).

heu-met-inter-001 (1 case) A cylindrical assembly of uranium and iron, reflected by stainless steel (ZPR-9 assembly 34, ANL, 1979). The uranium enrichment was 93% ^{235}U.
The isotopes in this benchmark model are ^{1}H, ^{nat}C, ^{19}F, $^{24-26}$Mg, ^{27}Al, $^{28-30}$Si, ^{35,37}Cl, $^{50,52-54}$Cr, ^{55}Mn, $^{54,56-58}$Fe, $^{58,60-62,64}$Ni, ^{63,65}Cu, $^{92,94-98,100}$Mo, ^{234,235,236,238}U.

heu-met-inter-006 (4 cases, 'Zeus') The initial set of Zeus experiments at the Los Alamos Critical Experiments Facility (LANL, 1999-2001): uranium metal interspersed with graphite plates in a cylindrical stack, surrounded by copper reflector. The C/^{235}U ratio varied between 51.2 to 13.6. The uranium enrichment was 93% ^{235}U.
The isotopes in these benchmark models are ^{nat}C, $^{24-26}$Mg, ^{27}Al, $^{28-30}$Si, $^{46-50}$Ti, $^{50,52-54}$Cr, ^{55}Mn, $^{54,56-58}$Fe, ^{63,65}Cu, ^{234,235,236,238}U.

3. *Thermal spectrum*

heu-met-therm-001 (2 cases) A polyethylene moderated and reflected uranium system with silicon (LANL, 1999). The uranium enrichment was 93% ^{235}U.
The isotopes in these benchmark models are ^{1}H, ^{nat}C, ^{16}O, $^{28-30}$Si, ^{234,235,236,238}U.
Thermal scattering data for H in CH_2 are used.

heu-met-therm-003 (7 cases) Lattices of oralloy cubes in water (LANL, 1955). The number of cubes and their spacing were varied. The uranium enrichment was 94% ^{235}U.

The isotopes in these benchmark models are ^{1}H, ^{nat}C, ^{16}O, ^{234,235,238}U.
Thermal scattering data for H in H_2O are used.

heu-met-therm-006 (23 cases) Lattices of SPERT-D fuel elements, reported by ORNL, 1964-65. The fuel elements consisted of plates of a uranium-aluminium alloy. The experiments were water-moderated and water-reflected. In some of the cases uranyl nitrate solution (with and without boron) was substituted for the water. The lattice configuration was varied. The uranium enrichment was 93% ^{235}U.
The isotopes in these benchmark models are ^{1}H, ^{16}O, $^{24-26}$Mg, ^{27}Al, $^{28-30}$Si, $^{46-50}$Ti, $^{50,52-54}$Cr, ^{55}Mn, $^{54,56-58}$Fe, ^{63,65}Cu, and ^{234,235,238}U. Thermal scattering data for H in H_2O are used.
For cases 17 and 18 $^{106,108,110-114,116}$Cd is also present, while for cases 4 and $19-23$ ^{nat}C, ^{14}N, ^{31}P, $^{32-34,36}$S, and $^{58,60-62,64}$Ni are present too. Besides, cases $20-23$ have ^{10,11}B.

heu-met-therm-008 (2 cases) A polyethylene moderated and reflected uranium system with aluminium (LANL) The uranium enrichment was 93% ^{235}U.
The isotopes in these benchmark models are ^{1}H, ^{nat}C, $^{24-26}$Mg, ^{27}Al, $^{28-30}$Si, $^{46-50}$Ti, $^{50,52-54}$Cr, ^{55}Mn, $^{54,56-58}$Fe, ^{63,65}Cu, ^{234,235,236,238}U.
Thermal scattering data for H in CH_2 are used.

heu-met-therm-009 (1 case) A polyethylene moderated and reflected uranium system with magnesium oxide (LANL, 2001) The uranium enrichment was 93% ^{235}U.
The isotopes in these benchmark models are ^{1}H, ^{6,7}Li, ^{10}B, ^{nat}C, ^{16}O, $^{24-26}$Mg, ^{27}Al, ^{39,40,41}K, $^{40,42-44,46,48}$Ca, ^{55}Mn, $^{54,56-58}$Fe, $^{106,108,110-114,116}$Cd, ^{234,235,236,238}U.
Thermal scattering data for H in CH_2 are used.

heu-met-therm-010 (2 cases) A polyethylene moderated and reflected uranium system with gadolinium (LANL, 2001). Two thicknesses of Gd foil were used. The uranium enrichment was 93% ^{235}U.
The isotopes in these benchmark models are ^{1}H, ^{nat}C, $^{152,154-158,160}$Gd, ^{234,235,236,238}U.
Thermal scattering data for H in CH_2 are used.

heu-met-therm-013 (2 cases) A polyethylene moderated and reflected uranium system with iron (LANL, ~2002). Two thicknesses of iron plates were used. The uranium enrichment was 93% ^{235}U.
The isotopes in these benchmark models are ^{1}H, ^{nat}C, $^{54,56-58}$Fe, ^{234,235,236,238}U.
Thermal scattering data for H in CH_2 are used.

heu-met-therm-014 (1 case) $2 \times 2 \times 23$ array of uranium with silicon oxide, moderated and reflected by polyethylene (LANL, ~2002) The uranium enrichment was 93% ^{235}U.
The isotopes in these benchmark models are ^{1}H, ^{nat}C, ^{16}O, $^{28-30}$Si, ^{234,235,236,238}U.
Thermal scattering data for H in CH_2 are used.

heu-met-therm-016 (2 cases) $2 \times 2 \times 23$ array of uranium with Ni-Cr-Mo-Gd alloy, moderated and reflected by polyethylene (LANL) The uranium enrichment was 93% ^{235}U.
The isotopes in these benchmark models are ^{1}H, ^{10,11}B, ^{nat}C, ^{16}O, $^{24-26}$Mg, ^{27}Al, $^{28-30}$Si, ^{31}P, $^{40,42-44,46,48}$Ca, $^{46-50}$Ti, ^{nat}V, $^{50,52-54}$Cr, ^{55}Mn, $^{54,56-58}$Fe, ^{59}Co, $^{58,60-62,64}$Ni, ^{63,65}Cu, ^{79}Br, $^{90-92,94,96}$Zr, ^{93}Nb, $^{92,94-98,100}$Mo, ^{107,109}Ag, $^{106,108,110-114,116}$Cd, $^{152,154-158,160}$Gd, ^{174,176,177,178,179,180}Hf, ^{181}Ta, $^{182-184,186}$W, $^{204,206-208}$Pb, ^{234,235,236,238}U.
Thermal scattering data for H in CH_2 are used.

heu-met-therm-018 (2 cases) A polyethylene moderated and reflected uranium system with concrete (LANL, 2003). The uranium enrichment was 93% ^{235}U.
The isotopes in these benchmark models are ^{1}H, ^{6,7}Li, ^{10,11}B, ^{nat}C, ^{16}O, ^{23}Na, $^{24-26}$Mg, ^{27}Al, $^{28-30}$Si, ^{31}P, ^{32}S, ^{39,40,41}K, $^{40,42-44,46,48}$Ca, ^{45}Sc, $^{46-50}$Ti, $^{54,56-58}$Fe, ^{103}Rh, $^{106,108,110-114,116}$Cd, ^{113,115}In, ^{151,153}Eu, $^{152,154-158,160}$Gd, ^{234,235,236,238}U.
Thermal scattering data for H in CH_2 and for H in H_2O are used.

heu-met-therm-022 (1 case) A core in the Advanced Test Reactor of Idaho National Laboratory (1994). It consisted of a serpentine arrangement of highly enriched uranium-aluminide fuel plates, moderated by water and reflected by beryllium. The uranium enrichment was 93% ^{235}U.
The isotopes in this benchmark are , ^{10,11}B, ^{nat}C, ^{16}O, $^{24-26}$Mg, ^{27}Al, $^{28-30}$Si, $^{46-50}$Ti, $^{50,52-54}$Cr, $^{54,56-58}$Fe, ^{63,65}Cu, ^{55}Mn, ^{nat}Zn, $^{234-236,238}$U

heu-sol-therm-001 (10 cases) Cylindrical reflected tank with uranyl nitrate, minimally reflected. The uranium concentration was varied and the critical height was determined. The uranium enrichment was 93% ^{235}U.
The isotopes in these benchmark models are ^{1}H, ^{nat}C, ^{14}N, ^{16}O, ^{27}Al, $^{28-30}$Si, ^{31}P, $^{32-34,36}$S, $^{50,52-54}$Cr, ^{55}Mn, $^{54,56-58}$Fe, $^{58,60-62,64}$Ni, $^{92,94-98,100}$Mo, ^{234,235,236,238}U. Thermal scattering data for H in H_2O are used.

heu-sol-therm-002 (14 cases) Cylindrical reflected tank with uranyl nitrate, with a concrete reflector. The uranium concentration was varied and the critical height was determined. The uranium enrichment was 93% ^{235}U.
The isotopes in these benchmark models are ^{1}H, ^{nat}C, ^{14}N, ^{16}O, ^{23}Na, $^{24-26}$Mg, ^{27}Al, $^{28-30}$Si, $^{32-34,36}$S, $^{39-41}$K, $^{40,42-44,46,48}$Ca, $^{46-50}$Ti, $^{50,52-54}$Cr, ^{55}Mn, $^{54,56-58}$Fe, and ^{234,235,236,238}U.

Thermal scattering data for H in H_2O are used.
In cases $5-14$ there is also ^{63,65}Cu, in cases $1-4$ ^{31}P, $^{58,60-62,64}$Ni, and $^{92,94-98,100}$Mo.

heu-sol-therm-004 (6 cases) Reflected uranyl-fluoride solutions in heavy water (LANL, 1950s). The D/^{235}U ratio varied from 34 to 431. The uranium enrichment was 94% ^{235}U.
The isotopes in these benchmark models are ^{1,2}H, ^{16}O, ^{19}F, $^{28-30}$Si, $^{50,52-54}$Cr, ^{55}Mn, $^{54,56-58}$Fe, $^{58,60-62,64}$Ni, ^{234,235,238}U.
Thermal scattering data for D in D_2O and H in H_2O are used.

heu-sol-therm-009 (4 cases) Water reflected 6.4-liter spheres of highly enriched uranium oxyfluoride (UO_2F_2) solutions (ORNL, 1950s). The fuel concentration was varied. The uranium enrichment was 93% ^{235}U.
The isotopes in these benchmark models are ^{1}H, ^{16}O, ^{19}F, ^{27}Al, $^{28-30}$Si, ^{55}Mn, ^{63,65}Cu, ^{234,235,236,238}U. Thermal scattering data for H in H_2O are used.

heu-sol-therm-010 (4 cases) Water reflected 9.7-liter spheres of highly enriched uranium oxyfluoride (UO_2F_2) solutions (ORNL, 1950s). The fuel concentration and the temperature were varied. The uranium enrichment was 93% ^{235}U.
The isotopes in these benchmark models are ^{1}H, ^{16}O, ^{19}F, ^{27}Al, $^{28-30}$Si, ^{55}Mn, ^{63,65}Cu, ^{234,235,236,238}U. Thermal scattering data for H in H_2O are used.

heu-sol-therm-013 (4 cases, 'ORNL-1', ..., 'ORNL-4') Uranyl nitrate solutions poisoned with boric acid in an unreflected sphere (at ORNL, 1950s). The uranium enrichment was 93% ^{235}U.
The isotopes in these benchmark models are ^{1}H, ^{14}N, ^{16}O, ^{27}Al, $^{28-30}$Si, ^{55}Mn, ^{63,65}Cu, ^{nat}Zn, ^{234,235,236,238}U. Thermal scattering data for H in H_2O are used.
For cases $2-4$ ^{10,11}B are also present.

heu-sol-therm-032 (1 case) Unreflected 48-inch sphere of highly enriched uranyl nitrate solution (ORNL, 1950s). The uranium enrichment was 93% ^{235}U.
The isotopes in this benchmark model are ^{1}H, ^{14}N, ^{16}O, ^{27}Al, $^{28-30}$Si, ^{55}Mn, $^{54,56-58}$Fe, ^{63,65}Cu, ^{233,234,235,236,238}U. Thermal scattering data for H in H_2O are used.

heu-sol-therm-038 (30 cases) Two interacting slab tanks with highly enriched uranyl nitrate solution with various absorber-reflector plates (LANL, 1988). The absorber-reflector plates were made of poly-ethylene, borated poly-ethylene, boraflex, pyrex, stainless steel, hot rolled steel, lead, beryllium, depleted uranium, or cadmium. The uranium enrichment was 93% ^{235}U.
The isotopes in these benchmark models are ^{1}H, ^{9}Be, ^{10,11}B, ^{nat}C, ^{14}N, ^{16}O, ^{23}Na, $^{24-26}$Mg, ^{27}Al, $^{28-30}$Si, ^{31}P, $^{32-34,36}$S, $^{46-50}$Ti, $^{50,52-54}$Cr, ^{55}Mn, $^{54,56-58}$Fe, $^{58,60-62,64}$Ni, ^{63,65}Cu, $^{92,94-98,100}$Mo, $^{106,108,110-114,116}$Cd, $^{204,206-208}$Pb, ^{234,235,236,238}U.
Thermal scattering data for H in H_2O and for H in CH_2 are used.

heu-sol-therm-039 (6 cases) Mixture of highly enriched uranium hexafluoride (UF_6) and hydrofluoric acid (HF), low H/U ratio, in a hot-water reflected tank (Valduc, 1960s). The uranium concentration was varied. The uranium enrichment was 93% ^{235}U.
The isotopes in these benchmark models are ^{1}H, ^{nat}C, ^{16}O, ^{19}F, $^{28-30}$Si, ^{55}Mn, $^{54,56-58}$Fe, $^{58,60-62,64}$Ni, ^{63,65}Cu, ^{234,235,236,238}U. Thermal scattering data for H in H_2O are used.
The temperature for these benchmark cases does not match the temperature for which the cross sections were processed. In the results for ENDF/B-VII.0 presented in this paper, the only temperature correction applied was the one that is default in MCNP. This is not as it should be done, but is a result of the short time in which the present results needed to be finalized. For runs based on ENDF/B-VI.8 we have performed a check on the influence of this temperature discrepancy, based on the method in Ref. [15]. The result was a difference of, on average, 100 pcm between a good temperature treatment, and the default MCNP one, with the latter giving higher results. We included the ENDF/B-VII.0 results in this paper, because the discrepancy between calculation and benchmark value is roughly 2-3%, much larger than what can be explained by the temperature treatment.

heu-sol-therm-042 (8 cases) Unreflected cylinders (5 ft and 9 ft diameter) of highly enriched uranyl nitrate solution. The uranium concentration was varied. The uranium enrichment was 93% ^{235}U.
The isotopes in these benchmark models are ^{1}H, ^{nat}C, ^{14}N, ^{16}O, $^{50,52-54}$Cr, $^{54,56-58}$Fe, $^{58,60-62,64}$Ni, $^{92,94-98,100}$Mo, ^{234,235,236,238}U. Thermal scattering data for H in H_2O are used.

4. *Mixed spectrum*

heu-comp-mixed-003 (1 case) Heterogeneous assemblies of uranium dioxide fuel elements in a zirconium hydride moderator block, with beryllium reflector (RCC Kurchatov, 1992-1993). The uranium enrichment was 96% ^{235}U.
The isotopes in these benchmark models are ^{1}H, ^{9}Be, ^{10,11}B, ^{nat}C, ^{16}O, ^{27}Al, $^{28-30}$Si, $^{46-50}$Ti, $^{50,52-54}$Cr, ^{55}Mn, $^{54,56-58}$Fe, $^{58,60-62,64}$Ni, $^{90-92,94,96}$Zr, ^{93}Nb, $^{92,94-98,100}$Mo, ^{174,176,177,178,179,180}Hf,

$^{182-184,186}$W, ^{234,235,236,238}U.
Thermal scattering data for H in ZrH are used.

heu-met-mixed-005 (5 cases) Critical experiments with heterogeneous compositions of highly enriched uranium, silicon dioxide and polyethylene (Obninsk, 1999). The uranium enrichment was 90% ^{235}U.
The isotopes in these benchmark models are ^{1}H, ^{6,7}Li, ^{10,11}B, ^{nat}C, ^{14}N, ^{16}O, ^{23}Na, $^{24-26}$Mg, ^{27}Al, $^{28-30}$Si, ^{32}S, ^{39,40,41}K, $^{40,42-44,46,48}$Ca, $^{46-50}$Ti, ^{nat}V, $^{50,52-54}$Cr, ^{55}Mn, $^{54,56-58}$Fe, $^{58,60-62,64}$Ni, ^{63,65}Cu, $^{92,94-98,100}$Mo, $^{106,108,110-114,116}$Cd, $^{206-208}$Pb, ^{234,235,236,238}U.
Thermal scattering data for H in CH_2 and for H in H_2O are used.

B. Intermediate-enriched uranium (IEU) benchmarks

1. Fast spectrum

ieu-met-fast-001 (4 cases, 'Jemima') Bare cylindrical configurations of enriched and natural uranium (LANL, 1952-1954). The core average uranium enrichment was 36-55% ^{235}U.
The isotopes in these benchmark models are $^{24-26}$Mg, ^{27}Al, $^{50,52-54}$Cr, ^{55}Mn, $^{54,56-58}$Fe, $^{58,60-62,64}$Ni, ^{63,65}Cu, ^{234,235,238}U.

ieu-met-fast-002 (1 case) Cylindrical assembly with a core of alternating plates of enriched and natural uranium surrounded by a natural uranium reflector (LANL, 1956). The core average uranium enrichment was 16% ^{235}U.
The isotopes in this benchmark model are ^{234,235,238}U.

ieu-met-fast-007 (3 cases, 'Big Ten') Three models of a large mixed-uranium-metal cylindrical core with 10% average uranium enrichment, surrounded by a thick depleted uranium reflector (LANL, 1971). The total uranium mass was ten metric tons. This core is modeled in three different benchmark models: detailed, simple and two-zone. The core average uranium enrichment was 10% ^{235}U.
The isotopes in these benchmark models are $^{28-30}$Si, $^{50,52-54}$Cr, ^{55}Mn, $^{54,56-58}$Fe, $^{58,60-62,64}$Ni, ^{93}Nb, ^{234,235,236,238}U.

ieu-met-fast-010 (1 case) A cylindrical assembly of uranium metal, 9% average enrichment, with a thick depleted uranium reflector (ANL, ZPR-9, U9 benchmark assembly, 1980). The core average uranium enrichment was 9% ^{235}U.
The isotopes in these benchmark models are ^{1}H, ^{nat}C, ^{19}F, ^{27}Al, $^{28-30}$Si, ^{35,37}Cl, $^{50,52-54}$Cr, ^{55}Mn, $^{54,56-58}$Fe, $^{58,60-62,64}$Ni, ^{63,65}Cu, $^{92,94-98,100}$Mo, ^{234,235,236,238}U.

ieu-met-fast-012 (1 case) A critical assembly of uranium metal, aluminium and steel, reflected by depleted uranium (ZPR-3 assembly 41, 1962). The core average uranium enrichment was 16% ^{235}U.
The isotopes in this benchmark model are ^{nat}C, ^{27}Al, $^{28-30}$Si, $^{50,52-54}$Cr, ^{55}Mn, $^{54,56-58}$Fe, $^{58,60-62,64}$Ni, and ^{234,235,236,238}U.

ieu-met-fast-014 (2 cases) Cylindrical assemblies of uranium metal and tungsten with aluminum reflectors (ANL, ZPR-9 assemblies 2 and 3, 1964). Case 2 (assembly 3) had more tungsten than case 1 (assembly 1). The core average uranium enrichment was 16% ^{235}U (case 1) and 21% ^{235}U (case 2).
The isotopes in these benchmark models are ^{1}H, ^{nat}C, ^{19}F, $^{24-26}$Mg, ^{27}Al, $^{28-30}$Si, ^{35,37}Cl, $^{46-50}$Ti, $^{50,52-54}$Cr, ^{55}Mn, $^{54,56-58}$Fe, $^{58,60-62,64}$Ni, ^{63,65}Cu, $^{92,94-98,100}$Mo, $^{182-184,186}$W, ^{234,235,236,238}U.

2. Intermediate spectrum

ieu-comp-inter-001 (4 cases) For k_∞ experiments for combinations of uranium, thorium metal and varying amounts of polyethylene (IPPE, Obninsk, 1990-1994). The H/^{235}U ratio varied from 0 to 70. Various combinations of 36% ^{235}U and 90% ^{235}U were used.
The isotopes in these benchmark models are ^{1}H, ^{nat}C, ^{16}O, ^{27}Al, $^{28-30}$Si, $^{46-50}$Ti, $^{50,52-54}$Cr, ^{55}Mn, $^{54,56-58}$Fe, $^{58,60-62,64}$Ni, ^{232}Th, ^{235,238}U.

3. Thermal spectrum

ieu-comp-therm-002 (3 cases) Stainless steel clad UO_2 fuel rods in a water filled tank (MATR, Russia, 1970-1973). The fuel rods were arranged in a hexagonal lattice, with gadolinium absorber, cadmium absorber or no absorber. Cases 1, 3 and 5 were at room temperature, case 2 was at T=218.4°C, and cases 4 and 6 were at T=150.8°C. The uranium enrichment was 17% ^{235}U.
The isotopes in these benchmark models are ^{1}H, ^{nat}C, ^{16}O, $^{28-30}$Si, $^{46-50}$Ti, $^{50,52-54}$Cr, ^{55}Mn, $^{54,56-58}$Fe, $^{58,60-62,64}$Ni, and ^{234,235,238}U. Thermal scattering data for H in H_2O are used.
For case 3 ^{27}Al and $^{152,154-158,160}$Gd are also present, for case 5 ^{27}Al and $^{106,108,110-114,116}$Cd.
The temperature for cases 2, 4, and 6 does not match the temperature for which the cross sections were evaluated, and therefore results for these cases are not presented here.

ieu-comp-therm-003 (2 cases) Zirconium hydride fuel rods in water, with a graphite reflector (Triga Mark II reactor, Ljubljana, 1991). The two cases differ only in the position of the 7 outermost fuel elements. The uranium enrichment was 20% ^{235}U.

The isotopes in these benchmark models are ^{1}H, ^{10,11}B, ^{nat}C, ^{14}N, ^{16}O, ^{27}Al, $^{28-30}$Si, ^{31}P, $^{32-34,36}$S, $^{50,52-54}$Cr, ^{55}Mn, $^{54,56-58}$Fe, $^{58,60-62,64}$Ni, $^{90-92,94,96}$Zr, $^{92,94-98,100}$Mo, ^{235,238}U. Thermal scattering data for graphite, for H in ZrH and for H in H_2O are used.

Proteus (1 case) Core 5 of Proteus, a graphite reflected pebble bed reactor, containing uranium-carbon fuel pebbles and graphite moderator pebbles (PSI, 1995-1996) [11]. The uranium enrichment was 16.7% ^{235}U.
The isotopes in these benchmark models are ^{1}H, ^{6,7}Li, ^{10,11}B, ^{nat}C, ^{14}N, ^{16}O, $^{24-26}$Mg, ^{27}Al, $^{28-30}$Si, $^{32-34,36}$S, ^{35,37}Cl, $^{40,42-44,46,48}$Ca, ^{55}Mn, $^{54,56-58}$Fe, ^{63,65}Cu, ^{nat}Zn, ^{nat}Ga, $^{106,108,110-114,116}$Cd, $^{154-158,160}$Gd, $^{144,147-150,152,154}$Sm, ^{234,235,236,238}U. Thermal scattering data for graphite and for H in H_2O are used.

C. Low-enriched uranium (LEU) benchmarks

No LEU benchmark models with a fast or intermediate spectrum are available from the ICSBEP handbook.

1. *Thermal spectrum*

leu-comp-therm-001 (8 cases) Clusters of aluminium clad UO_2 fuel rods in a water filled tank. The clusters were square, with no absorber plates, reflecting walls, dissolved poison or gadolinium impurities. The number of clusters and the separation between them was varied. The uranium enrichment was 2.4% ^{235}U.
The isotopes in these benchmark models are ^{1}H, ^{nat}C, ^{16}O, $^{24-26}$Mg, ^{27}Al, $^{28-30}$Si, $^{46-50}$Ti, $^{50,52-54}$Cr, ^{55}Mn, $^{54,56-58}$Fe, ^{63,65}Cu, ^{nat}Zn, and ^{234,235,236,238}U. Thermal scattering data for H in H_2O and for H in CH_2 are used.

leu-comp-therm-002 (5 cases) Water moderated UO_2 fuel rods, aluminium clad, in square arrays (pitch 2.54 cm, Pacific Northwest Laboratories). The shape of the rod cluster was varied, as well as the distance between clusters (for cases 4 and 5). The uranium enrichment was 4.31% ^{235}U.
The isotopes in these benchmark models are ^{1}H, ^{nat}C, ^{16}O, $^{24-26}$Mg, ^{27}Al, $^{28-30}$Si, $^{32-34,36}$S, $^{40,42-44,46,48}$Ca, $^{46-50}$Ti, $^{50,52-54}$Cr, ^{55}Mn, $^{54,56-58}$Fe, ^{63,65}Cu, ^{234,235,236,238}U. Thermal scattering data for H in H_2O and for H in CH_2 are used.

leu-comp-therm-003 (22 cases) Water moderated UO_2 fuel rods, aluminium clad, in square arrays (pitch 1.684 cm), with gadolinium impurity in water (Pacific Northwest Laboratories). The shape of the rod clusters was varied, as well as the distance between clusters. The uranium enrichment was 2.35% ^{235}U.
The isotopes in these benchmark models are ^{1}H, ^{nat}C, ^{16}O, $^{24-26}$Mg, ^{27}Al, $^{28-30}$Si, $^{46-50}$Ti, $^{50,52-54}$Cr, ^{55}Mn, $^{54,56-58}$Fe, ^{63,65}Cu, $^{152,154-158,160}$Gd, ^{234,235,236,238}U. Thermal scattering data for H in H_2O and for H in CH_2 are used.

leu-comp-therm-005 (16 cases) UO_2 fuel rods, aluminium clad, in water containing dissolved gadolinium (Pacific Northwest Laboratories, early 1980s). The lattice pitch and the gadolinium concentration were varied. The uranium enrichment was 2.35% ^{235}U (cases 1-13) and 4.31% ^{235}U (cases 14-16).
The isotopes in these benchmark models are ^{1}H, ^{nat}C, ^{14}N, ^{16}O, $^{24-26}$Mg, ^{27}Al, $^{28-30}$Si, $^{32-34,36}$S $^{40,42-44,46,48}$Ca, $^{46-50}$Ti, $^{50,52-54}$Cr, ^{55}Mn, $^{54,56-58}$Fe, ^{63,65}Cu, ^{nat}Zn, $^{152,154-158,160}$Gd, ^{234,235,236,238}U. Thermal scattering data for H in H_2O and for H in CH_2 are used.

leu-comp-therm-006 (18 cases) Arrays of UO_2 fuel rods with water-to-fuel ratios from 1.5 to 3.0 in a Tank-type Critical Assembly (TCA, Japan, 1963-1975). The lattice pitch and the number of fuel rods were varied. The uranium enrichment was 2.6% ^{235}U.
The isotopes in these benchmark models are ^{1}H, ^{16}O, ^{27}Al, ^{234,235,238}U. Thermal scattering data for H in H_2O are used.

leu-comp-therm-007 (10 cases) Water moderated UO_2 fuel rod arrays (Valduc, 1978). In four cases the arrays were square, with varying pitch. In the other cases the arrays had a triangular pitch, with either hexagonal pr pseudo-cylindrical section, and with varying pitch. The uranium enrichment was 4.738% ^{235}U.
The isotopes in these benchmark models are ^{1}H, ^{10,11}B, ^{nat}C, ^{14}N, ^{16}O, $^{24-26}$Mg, ^{27}Al, $^{28-30}$Si, ^{31}P, $^{32-34,36}$S, $^{50,52-54}$Cr, ^{55}Mn, $^{54,56-58}$Fe, $^{58,60-62,64}$Ni, ^{nat}Zn, ^{234,235,236,238}U.
Thermal scattering data for H in H_2O are used.

leu-comp-therm-009 (27 cases) Clusters of aluminium-clad UO_2 fuel rods in a large water-filled tank (Pacific Northwest Laboratories, 1977). There were three square-pitched clusters with two absorber plates in between. These plates were stainless steel, borated stainless steel, boral, copper, copper with 1% cadmium, cadmium, aluminium or zircaloy-4. The uranium enrichment was 4.3% ^{235}U.
The isotopes in these benchmark models are ^{1}H, ^{nat}C, ^{16}O, $^{24-26}$Mg, ^{27}Al, $^{28-30}$Si, $^{32-34,36}$S, $^{40,42-44,46,48}$Ca, $^{46-50}$Ti, $^{50,52-54}$Cr, ^{55}Mn, $^{54,56-58}$Fe, ^{63,65}Cu, and ^{234,235,236,238}U. Thermal scattering data for H in H_2O and for H in CH_2 are used.

In some cases ^{23}Na (case $9-13$) is present, in others ^{10,11}B (case $5-9$, 14, 15), $^{106,108,110-114,116}$Cd (case $14-23$), $^{58,60-62,64}$Ni (cases $1-9$, 14, 15), $^{92,94-98,100}$Mo (cases $1-8$), $^{112,114-120,122,124}$Sn (cases 14, 15, 26, 27), and $^{90-92,94,96}$Zr (cases 26, 27).

leu-comp-therm-010 (30 cases) Rectangular clusters of water moderated UO_2 fuel rods, reflected by two lead, uranium or steel walls. Also the pitch and the number of fuel rods were varied. The uranium enrichment was 4.31% ^{235}U.
The isotopes in these benchmark models are ^{1}H, ^{nat}C, ^{16}O, $^{24-26}$Mg, ^{27}Al, $^{28-30}$Si, ^{31}P, $^{32-34,36}$S, $^{40,42-44,46,48}$Ca, $^{46-50}$Ti, $^{50,52-54}$Cr, ^{55}Mn, $^{54,56-58}$Fe, $^{58,60-62,64}$Ni, ^{63,65}Cu, $^{92,94-98,100}$Mo, $^{204,206-208}$Pb, ^{234,235,236,238}U. Thermal scattering data for H in H_2O and for H in CH_2 are used.

leu-comp-therm-016 (32 cases) Low enriched uranium pin assemblies placed in water and separated by absorber plates. The absorber material was steel, borated steel, boral, copper, copper with cadmium, cadmium, aluminium or zircaloy-4. The uranium enrichment was 2.4% ^{235}U.
The isotopes in these benchmark models are ^{1}H, ^{nat}C, ^{16}O, $^{24-26}$Mg, ^{27}Al, $^{28-30}$Si, $^{46-50}$Ti, $^{50,52-54}$Cr, ^{55}Mn, $^{54,56-58}$Fe, ^{63,65}Cu, ^{nat}Zn, and ^{234,235,236,238}U. Thermal scattering data for H in H_2O and for H in CH_2 are used.
In some cases ^{10,11}B is also present (cases $8-14$, 20), in others ^{23}Na (cases $12-19$), $^{32-34,36}$S (cases $12-19$, $28-30$), $^{58,60-62,64}$Ni (cases $1-14$, 20), $^{90-92,94,96}$Zr (cases 31, 32), $^{92,94-98,100}$Mo (cases $1-11$), $^{106,108,110-114,116}$Cd (cases $20-27$), and $^{112,114-120,122,124}$Sn (cases 20, 31, 32).

leu-comp-therm-017 (19 cases) Low enriched uranium pin assemblies placed in water and reflected by steel or lead reflector plates. The separation between the clusters and the distance between the fuel and the reflector were varied. The uranium enrichment was 2.35% ^{235}U.
The isotopes in these benchmark models are ^{1}H, ^{nat}C, ^{16}O, $^{24-26}$Mg, ^{27}Al $^{28-30}$Si, $^{46-50}$Ti, $^{50,52-54}$Cr, ^{55}Mn, $^{54,56-58}$Fe, ^{63,65}Cu ^{nat}Zn, and ^{234,235,236,238}U. Thermal scattering data for H in H_2O and for H in CH_2 are used.
In cases $1-3$, $23-25$ there is also $^{204,206-208}$Pb, in the other cases there ^{31}P, $^{32-34,36}$S, $^{58,60-62,64}$Ni, and $^{92,94-98,100}$Mo.

leu-comp-therm-019 (3 cases) Water-moderated hexagonally pitched lattices with low enriched cylindrical fuel rods with stainless steel cladding (RRC Kurchatov Institute, 1961). The pitch of the lattice was varied. The uranium enrichment was 5% ^{235}U.
The isotopes in these benchmark models are ^{1}H, ^{nat}C, ^{16}O, $^{24-26}$Mg, ^{27}Al, $^{28-30}$Si, $^{46-50}$Ti, $^{50,52-54}$Cr, ^{55}Mn, $^{54,56-58}$Fe, $^{58,60-62,64}$Ni, ^{63,65}Cu, and ^{234,235,236,238}U. Thermal scattering data for H in H_2O are used.

leu-comp-therm-039 (17 cases) Incomplete arrays of water moderated and reflected UO_2 fuel rods (Valduc, 1978). All arrays were square, with a varying number of positions not filled. The uranium enrichment was 4.738% ^{235}U.
The isotopes in these benchmark models are ^{1}H, ^{10,11}B, ^{nat}C, ^{14}N, ^{16}O, $^{24-26}$Mg, ^{27}Al, $^{28-30}$Si, ^{31}P, $^{32-34,36}$S, $^{50,52-54}$Cr, ^{55}Mn, $^{54,56-58}$Fe, $^{58,60-62,64}$Ni, ^{nat}Zn, ^{234,235,236,238}U.
Thermal scattering data for H in H_2O are used.

leu-comp-therm-051 (19 cases) Aluminium-clad uranium oxide in 9 assemblies of 14×14 fuel rods. (Babcock-Wilcox Lynchberg Research Center, 1978-79). The moderator and reflector was borated water, and the absorbers were stainless steel and boron. The loading pattern, water height and boron concentration were varied. The uranium enrichment was 2.5% ^{235}U.
The isotopes in these benchmark models are ^{1}H, ^{10}B, ^{11}B, ^{16}O, $^{24-26}$Mg, ^{27}Al, $^{28-30}$Si, $^{46-50}$Ti, $^{50,52-54}$Cr, ^{55}Mn, $^{54,56-58}$Fe, ^{63,65}Cu, and ^{234,235,236,238}U. Thermal scattering data for H in H_2O are used.
For cases $2-9$ there are also: ^{nat}C, ^{31}P, $^{32-34,36}$S, ^{59}Co, $^{58,60-62,64}$Ni, and $^{92,94-98,100}$Mo.

leu-comp-therm-060 (28 cases) Configurations of UO_2 fuel assemblies in an RBMK-type graphite moderated reactor. Some configurations had empty channels, some had water in the fuel channels, and some had boron or thorium absorber rods. Also the enrichment was varied. The uranium enrichment was 1.8% ^{235}U (cases 1 and 2), 2.4% ^{235}U (cases 5 and 6) or 2.0% ^{235}U (all other cases).
The isotopes in these benchmark models are ^{1}H, ^{10,11}B, ^{nat}C, ^{14}N, ^{16}O, ^{19}F, $^{24-26}$Mg, ^{27}Al, $^{28-30}$Si, ^{31}P, $^{32-34,36}$S, $^{40,42-44,46,48}$Ca, $^{46-50}$Ti, ^{nat}V, $^{50,52-54}$Cr, ^{55}Mn, $^{54,56-58}$Fe, $^{58,60-62,64}$Ni, ^{63,65}Cu, ^{75}As, $^{90-92,94,96}$Zr, ^{93}Nb, $^{92,94-98,100}$Mo, ^{107,109}Ag, $^{106,108,110-114,116}$Cd, $^{112,114-120,122,124}$Sn, $^{174,176-180}$Hf, $^{182-184,186}$W, ^{197}Au, $^{206-208}$Pb, ^{209}Bi, ^{230,232}Th, ^{234,235,236,238}U.
Thermal scattering data for graphite and for H in H_2O are used.

Dimple (1 case) Assembly S01A, a cylindrical arrangement of uranium dioxide fuel pins on a square pitch of 1.32 cm, water moderated and reflected (Winfrith, UK) [12]. The uranium enrichment was 3% ^{235}U.
The isotopes in these benchmark models are ^{1,2}H, ^{nat}C, ^{14}N ^{16}O $^{24-26}$Mg, ^{27}Al, $^{28-30}$Si, ^{31}P $^{32-34,36}$S, ^{35,37}Cl, $^{46-50}$Ti, ^{nat}V, $^{50,52-54}$Cr, ^{55}Mn $^{54,56-58}$Fe, ^{59}Co, $^{58,60-62,64}$Ni, ^{63,65}Cu, ^{nat}Zn, $^{84,86-88}$Sr, ^{93}Nb $^{92,94-98,100}$Mo, $^{112,114-120,122,124}$Sn, ^{234,235,236,238}U. Thermal

scattering data for graphite and for H in H_2O and for H in CH_2 are used.

TRX (2 cases) Light-water moderated UO_2 pins with aluminium cladding in a hexagonal lattice [13]. The pitch was 1.806 cm (case 1) or 2.174 cm (case 2). The uranium enrichment was 1.3% ^{235}U.
The isotopes in these benchmark models are ^{1}H, ^{16}O, ^{27}Al, $^{54,56-58}$Fe, ^{235,238}U. Thermal scattering data for graphite and for H in H_2O are used.

leu-met-therm-001 (1 case) A natural uranium, heavy water moderated critical assembly (Yugoslavia, 1958). The uranium enrichment was 0.72% ^{235}U.
The isotopes in this benchmark model are ^{1,2}H, ^{10,11}B, ^{nat}C, ^{14}N, ^{16}O, $^{24-26}$Mg, ^{27}Al, $^{28-30}$Si, $^{46-50}$Ti, $^{50,52-54}$Cr, ^{55}Mn, $^{54,56-58}$Fe, $^{58,60-62,64}$Ni, ^{63,65}Cu, ^{nat}Zn, $^{106,108,110-114,116}$Cd, ^{234,235,238}U.
Thermal scattering data for D in D_2O and for H in H_2O are used.

leu-sol-therm-001 (1 case, 'Sheba-II') An unreflected UO_2F_2+H_2O cylindrical assembly (LANL). The uranium enrichment was 5% ^{235}U.
The isotopes in this benchmark model are ^{1}H, ^{14}N, ^{16}O, ^{19}F, $^{50,52-54}$Cr, ^{55}Mn, $^{54,56-58}$Fe, $^{58,60-62,64}$Ni, ^{234,235,236,238}U
Thermal scattering data for H in H_2O are used.

leu-sol-therm-003 (9 cases) Full and truncated bare spheres of 10% enriched uranyl nitrate water solutions (Obninsk, 1965). The uranium concentration and the sphere diameters were varied. The uranium enrichment was 10% ^{235}U.
The isotopes in these benchmark models are ^{1}H, ^{14}N, ^{16}O, $^{28-30}$Si, $^{46-50}$Ti, $^{50,52-54}$Cr, ^{55}Mn, $^{54,56-58}$Fe, $^{58,60-62,64}$Ni, ^{234,235,238}U. Thermal scattering data for H in H_2O are used.

leu-sol-therm-004 (7 cases) Water reflected uranyl nitrate solution in a 60 cm cylindrical water tank (STACY, Japan, 1995). The uranium concentration was varied. The uranium enrichment was 10% ^{235}U.
The isotopes in these benchmark models are ^{1}H, ^{nat}C, ^{14}N, ^{16}O, $^{28-30}$Si, ^{31}P, $^{32-34,36}$S, $^{50,52-54}$Cr, ^{55}Mn, $^{54,56-58}$Fe, $^{58,60-62,64}$Ni, ^{234,235,236,238}U.
Thermal scattering data for H in H_2O are used.

leu-sol-therm-007 (5 cases) Unreflected uranyl nitrate solution in a 60 cm cylindrical water tank (STACY, Japan, 1995). The uranium concentration was varied. The uranium enrichment was 10% ^{235}U.
The isotopes in these benchmark models are ^{1}H, ^{nat}C, ^{14}N, ^{16}O, $^{28-30}$Si, ^{31}P, $^{32-34,36}$S, $^{50,52-54}$Cr, ^{55}Mn, $^{54,56-58}$Fe, $^{58,60-62,64}$Ni, ^{234,235,236,238}U.
Thermal scattering data for H in H_2O are used.

leu-sol-therm-016 (7 cases) Water reflected slabs (28 cm) of uranyl nitrate solutions (STACY, Japan, 1997). The uranium concentration was varied. The uranium enrichment was 10% ^{235}U.
The isotopes in these benchmark models are ^{1}H, ^{nat}C, ^{14}N, ^{16}O, $^{28-30}$Si, ^{31}P, $^{32-34,36}$S, $^{50,52-54}$Cr, ^{55}Mn, $^{54,56-58}$Fe, $^{58,60-62,64}$Ni, ^{234,235,236,238}U.
Thermal scattering data for H in H_2O are used.

leu-sol-therm-017 (6 cases) Unreflected slabs (28 cm) of uranyl nitrate solutions (STACY, Japan, 1997). The uranium concentration was varied. The uranium enrichment was 10% ^{235}U.
The isotopes in these benchmark models are ^{1}H, ^{nat}C, ^{14}N, ^{16}O, $^{28-30}$Si, ^{31}P, $^{32-34,36}$S, $^{50,52-54}$Cr, ^{55}Mn, $^{54,56-58}$Fe, $^{58,60-62,64}$Ni, ^{234,235,236,238}U.
Thermal scattering data for H in H_2O are used.

leu-sol-therm-018 (6 cases) Concrete reflected slabs (28 cm) of uranyl nitrate solutions (STACY, Japan, 1997). The thickness of the reflector was varied. The uranium enrichment was 10% ^{235}U.
The isotopes in these benchmark models are ^{1}H, ^{nat}C, ^{14}N, ^{16}O, ^{23}Na, $^{24-26}$Mg, ^{27}Al, $^{28-30}$Si, ^{31}P, $^{32-34,36}$S, ^{35,37}Cl, $^{39-41}$K, $^{40,42-44,46,48}$Ca, $^{50,52-54}$Cr, ^{55}Mn, $^{54,56-58}$Fe, $^{58,60-62,64}$Ni, ^{63,65}Cu, and ^{234,235,236,238}U. Thermal scattering data for H in H_2O are used.

leu-sol-therm-020 (4 cases) Water reflected uranyl nitrate solution in a 80 cm cylindrical water tank (STACY, Japan, 1998-1999). The uranium concentration was varied. The uranium enrichment was 10% ^{235}U.
The isotopes in these benchmark models are ^{1}H, ^{nat}C, ^{14}N, ^{16}O, $^{28-30}$Si, ^{31}P, $^{32-34,36}$S, $^{50,52-54}$Cr, ^{55}Mn, $^{54,56-58}$Fe, $^{58,60-62,64}$Ni, ^{234,235,236,238}U.
Thermal scattering data for H in H_2O are used.

leu-sol-therm-021 (4 cases) Unreflected uranyl nitrate solution in a 80 cm cylindrical water tank (STACY, Japan, 1998-1999). The uranium concentration was varied. The uranium enrichment was 10% ^{235}U.
The isotopes in these benchmark models are ^{1}H, ^{nat}C, ^{14}N, ^{16}O, $^{28-30}$Si, ^{31}P, $^{32-34,36}$S, $^{50,52-54}$Cr, ^{55}Mn, $^{54,56-58}$Fe, $^{58,60-62,64}$Ni, ^{234,235,236,238}U.
Thermal scattering data for H in H_2O are used.

D. Plutonium (PU) benchmarks

1. *Fast spectrum*

pu-met-fast-001 (1 case, 'Jezebel') A bare sphere of plutonium (LANL, 1950s). The plutonium-239 enrichment was 95.2% ^{239}Pu.
The isotopes in this benchmark model are ^{nat}Ga, ^{239,240,241}Pu.

pu-met-fast-002 (1 case, '^{240}Jezebel') A bare sphere of plutonium (LANL, 1964). The plutonium enrichment was 76.4% ^{239}Pu and 20.1% ^{240}Pu.

The isotopes in this benchmark model are ^{nat}Ga, ^{239,240,241,242}Pu.

pu-met-fast-005 (1 case) A critical experiment of a plutonium sphere reflected by tungsten (LANL, 1958).
The isotopes in these benchmark models are $^{58,60-62,64}$Ni, ^{63,65}Cu, ^{nat}Ga, $^{90-92,94,96}$Zr, $^{182-184,186}$W, ^{235,238}U, ^{239,240,241}Pu.

pu-met-fast-006 (1 case, 'Popsy', 'Flattop-Pu') A sphere of plutonium reflected by normal uranium (LANL, 1960s). The plutonium enrichment was 94.9% ^{239}Pu.
The isotopes in this benchmark model are ^{nat}Ga, ^{234,235,238}U, ^{239,240,241}Pu.

pu-met-fast-008 (1 case, 'Thor') A sphere of plutonium reflected by thorium (LANL, 1961). The plutonium enrichment was 94.9% ^{239}Pu.
The isotopes in this benchmark model are ^{nat}Ga, ^{232}Th, ^{239,240,241}Pu.

pu-met-fast-012 (1 case) A cylindrical arrangement of short, close-packed stainless steel clad rods of plutonium metal (97.6 at.%^{239}Pu), reflected on all sides by thick depleted uranium (IPPE, Obninsk, 1956).
The isotopes in these benchmark models are ^{nat}C, $^{28-30}$Si, $^{46-50}$Ti, $^{50,52-54}$Cr, ^{55}Mn, $^{54,56-58}$Fe, $^{58,60-62,64}$Ni, ^{63,65}Cu, ^{nat}Ga, ^{235,238}U, ^{238,239,240,241}Pu.

pu-met-fast-013 (1 case)

A cylindrical arrangement of short, close-packed stainless steel clad rods of plutonium metal (97.6 at.%^{239}Pu), reflected on all sides by thick copper reflector (IPPE, Obninsk, 1960).
The isotopes in these benchmark models are ^{nat}C, $^{28-30}$Si, $^{46-50}$Ti, $^{50,52-54}$Cr, ^{55}Mn, $^{54,56-58}$Fe, $^{58,60-62,64}$Ni, ^{63,65}Cu, ^{nat}Ga, ^{235,238}U, ^{238,239,240,241}Pu.

2. *Intermediate spectrum*

pu-comp-inter-001 (1 case) A k_∞ experiment at the HECTOR reactor (Winfrith, UK, 1960s): a graphite moderated plutonium oxide core (5% ^{240}Pu). The benchmark model is an infinite medium with a material composition appropriate to the interpolated boron/^{239}Pu ratio.
The isotopes in these benchmark models are ^{1}H, ^{10,11}B, ^{nat}C, ^{16}O, $^{40,42-44,46,48}$Ca, ^{235,238}U, ^{239,240,241,242}Pu.
Thermal scattering data for graphite are used.

pu-met-inter-002 (1 case) A cylindrical assembly containing plutonium, carbon and stainless steel, reflected by stainless steel and iron (ANL, ZPR-6 assembly 10, 1981-1982). The plutonium enrichment was 95.3% ^{239}Pu.
The isotopes in these benchmark models are ^{nat}C, ^{27}Al, $^{28-30}$Si, $^{50,52-54}$Cr, ^{nat}Co, ^{55}Mn, $^{54,56-58}$Fe, $^{58,60-62,64}$Ni, ^{63,65}Cu, $^{92,94-98,100}$Mo, $^{238-242}$Pu, ^{241}Am.

3. *Thermal spectrum*

pu-sol-therm-001 (6 cases) Water reflected 11.5 inch diameter spheres of plutonium nitrate solution (Pacific Northwest Laboratories, 1960s). The plutonium concentration was varied. The plutonium enrichment was 95% ^{239}Pu.
The isotopes in these benchmark models are ^{1}H, ^{14}N, ^{16}O, $^{50,52-54}$Cr, ^{55}Mn, $^{54,56-58}$Fe, $^{58,60-62,64}$Ni, ^{238,239,240,241,242}Pu. Thermal scattering data for H in H_2O are used.

pu-sol-therm-002 (7 cases) Water reflected 12 inch diameter spheres of plutonium nitrate solution (Hanford Reservation, 1950s). The plutonium concentration was varied. The plutonium enrichment was 96.9% ^{239}Pu.
The isotopes in these benchmark models are ^{1}H, ^{14}N, ^{16}O, $^{50,52-54}$Cr, $^{54,56-58}$Fe, $^{58,60-62,64}$Ni, ^{239,240}Pu. Thermal scattering data for H in H_2O are used.

pu-sol-therm-003 (8 cases) Water reflected 13 inch diameter spheres of plutonium nitrate solution (Hanford Reservation, 1950s). The plutonium concentration was varied. The plutonium enrichment was 98.3% ^{239}Pu (cases 1 and 2) and 96.9% ^{239}Pu (cases 3-7).
The isotopes in these benchmark models are ^{1}H, ^{14}N, ^{16}O, ^{27}Al, $^{28-30}$Si, $^{50,52-54}$Cr, ^{55}Mn, $^{54,56-58}$Fe, $^{58,60-62,64}$Ni, ^{63,65}Cu, ^{239,240}Pu. Thermal scattering data for H in H_2O are used.

pu-sol-therm-004 (13 cases) Water reflected 14 inch diameter spheres of plutonium nitrate solution (Hanford Reservation, 1950s). The plutonium concentration was varied. The plutonium enrichment was 99.5% ^{239}Pu (cases 1-4), 98.25% ^{239}Pu (case 5), and 96.9% ^{239}Pu (cases 6-13).
The isotopes in these benchmark models are ^{1}H, ^{14}N, ^{16}O, $^{50,52-54}$Cr, $^{54,56-58}$Fe, $^{58,60-62,64}$Ni, ^{239,240}Pu. Thermal scattering data for H in H_2O are used.

pu-sol-therm-005 (9 cases) Water reflected 14 inch diameter spheres of plutonium nitrate solution (Hanford Reservation, 1950s). The plutonium concentration was varied. The plutonium enrichment was 96.0% ^{239}Pu (cases 1-7), and 95.6% ^{239}Pu (cases 8 and 9).
The isotopes in these benchmark models are ^{1}H, ^{14}N, ^{16}O, $^{50,52-54}$Cr, $^{54,56-58}$Fe, $^{58,60-62,64}$Ni,

^{239,240}Pu. Thermal scattering data for H in H_2O are used.

pu-sol-therm-006 (3 cases) Water reflected 15 inch diameter spheres of plutonium nitrate solution (Hanford Reservation, 1950s). The plutonium concentration was varied. The plutonium enrichment was 96.9% ^{239}Pu.
The isotopes in these benchmark models are ^{1}H, ^{14}N, ^{16}O, $^{50,52-54}$Cr, $^{54,56-58}$Fe, $^{58,60-62,64}$Ni, ^{239,240}Pu. Thermal scattering data for H in H_2O are used.

pu-sol-therm-007 (8 cases) Water reflected 11.5 inch diameter spheres partly filled with plutonium nitrate solution (Pacific Northwest Laboratories, 1960s). The plutonium concentration was varied. The plutonium enrichment was 95% ^{239}Pu.
The isotopes in these benchmark models are ^{1}H, ^{14}N, ^{16}O, $^{50,52-54}$Cr, ^{55}Mn, $^{54,56-58}$Fe, $^{58,60-62,64}$Ni, ^{238,239,240,241,242}Pu. Thermal scattering data for H in H_2O are used.

pu-sol-therm-008 (29 cases) Concrete reflected 14 inch diameter spheres of plutonium nitrate solution (Pacific Northwest Laboratories, 1961-2). The geometry and the thickness of the concrete reflector was varied. Some cases had an extra shell of stainless steel outside the solution tank, inside the reflector. some others an extra shell of cadmium at that place. The plutonium enrichment was 95% ^{239}Pu.
The isotopes in these benchmark models are ^{1}H, ^{14}N, ^{16}O, ^{23}Na, $^{24-26}$Mg, ^{27}Al, $^{28-30}$Si, $^{39-41}$K, $^{40,42-44,46,48}$Ca, $^{50,52-54}$Cr, ^{55}Mn, $^{54,56-58}$Fe, $^{58,60-62,64}$Ni, $^{106,108,110-114,116}$Cd, ^{238,239,240,241,242}Pu. Thermal scattering data for H in H_2O are used.

pu-sol-therm-012 (22 cases) Plutonium nitrate solution in a large tank, with and without water reflector (Valduc, 1974). The tank was a right parallelepiped of dimension $130 \times 130 \times 100$ cm^3. The water reflector was either on six sides (cases 2-5), on five sides (cases 6-13), or on no sides (cases 14-23). The plutonium concentration was varied. The plutonium enrichment was 74% ^{239}Pu, and 19% ^{240}Pu.
The isotopes in these benchmark models are ^{1}H, ^{10}B, ^{nat}C, ^{14}N, ^{16}O, ^{27}Al, $^{28-30}$Si, ^{35,37}Cl, $^{40,42-44,46,48}$Ca, $^{50,52-54}$Cr, $^{54,56-58}$Fe, $^{58,60-62,64}$Ni, ^{239,240,241,242}Pu, ^{241}Am. Thermal scattering data for H in H_2O and for H in CH_2 are used.

4. *Mixed spectrum*

pu-met-mixed-001 (6 cases) Heterogeneous configurations of plutonium, silicon dioxide, and polyethylene (IPPE, Obninsk, 1999-2000). The cores were configured to cover a broad range in neutron spectra.
The isotopes in these benchmark models are ^{1}H, ^{6,7}Li, ^{10,11}B, ^{nat}C, ^{14}N, ^{16}O, ^{23}Na, $^{24-26}$Mg, ^{27}Al, $^{28-30}$Si, ^{32}S, ^{39,40,41}K, $^{40,42-44,46,48}$Ca, $^{46-50}$Ti, ^{nat}V, $^{50,52-54}$Cr, ^{55}Mn, $^{54,56-58}$Fe, $^{58,60-62,64}$Ni, ^{63,65}Cu, ^{nat}Ga, $^{92,94-98,100}$Mo, $^{106,108,110-114,116}$Cd, $^{206-208}$Pb, ^{235,238}U, ^{239,240,241}Pu, ^{241}Am.
Thermal scattering data for H in H_2O are used.

E. Mixed uranium plutonium (MIX) benchmarks

1. *Fast spectrum*

mix-met-fast-011 (4 cases) Cylindrical assemblies of mixed fissile plutonium and uranium metal, reflected by graphite (ANL, ZPPR-21 phases B-E, 1990). The ratio of plutonium to uranium was varied.
The isotopes in these benchmark models are ^{1}H, ^{6,7}Li, ^{10,11}B, ^{nat}C, ^{14}N, ^{16}O, ^{23}Na, ^{27}Al, $^{28-30}$Si, $^{50,52-54}$Cr, ^{55}Mn, $^{54,56-58}$Fe, ^{nat}Co, $^{58,60-62,64}$Ni, ^{63,65}Cu, $^{90-92,94,96}$Zr, $^{92,94-98,100}$Mo, ^{234,235,236,238}U, ^{238,239,240,241,242}Pu, ^{241}Am.

2. *Thermal spectrum*

mix-comp-therm-012 (33 cases) Rectangular parallelepipeds of homogeneous plutonium uranium mixed oxide polystyrene (Pacific Northwest Laboratories, 1970-1972). The cores were either unreflected (cases 20-22 and 31-33) or plexiglas reflected (cases 1-19 and 23-30). The amount of plutonium in the MOX, and the plutonium vector were varied.
The isotopes in these benchmark models are ^{1}H, ^{nat}C, ^{16}O, ^{235,238}U, ^{238,239,240,241,242}Pu, ^{241}Am. Thermal scattering data for H in CH_2 are used.

Kritz (2 cases) Core 2:19, consisting of light water moderated and reflected square lattices with mixed oxide fuel rods (Studsvik, Sweden, 1970s) [14]. Criticality was obtained at room temperature and at 235.9°C, by adjusting the boron content of the water and by adjusting the water height. The only differences between the cold and the hot case are the densities, the water level, and some slight dimensional changes of the core components. The plutonium enrichment was 91% ^{239}Pu.
The isotopes in these benchmark models are ^{1}H, ^{10,11}B, ^{14}N, ^{16}O, $^{50,52-54}$Cr, $^{54,56-58}$Fe, $^{58,60-62,64}$Ni, $^{90-92,94,96}$Zr, $^{112,114-120,122,124}$Sn, ^{235,238}U, ^{239,240,241,242}Pu, ^{241}Am. Thermal scattering data for H in H_2O are used.

mix-sol-therm-001 (3 cases) Critical experiments with mixed plutonium and uranium nitrate solutions in a large cylindrical geometry (Pacific Northwest Laboratories, 1980s). The concentration of the solution and the U/Pu ratio was varied.
The isotopes in these benchmark models are ^{1}H, ^{6}Li, ^{10}B, ^{14}N, ^{16}O, $^{50,52-54}$Cr, ^{55}Mn, $^{54,56-58}$Fe, $^{58,60-62,64}$Ni, $^{106,108,110-114,116}$Cd, $^{152,154-158,160}$Gd, ^{234,235,236,238}U, ^{238,239,240,241,242}Pu, ^{241}Am.
Thermal scattering data for H in H_2O are used.

mix-sol-therm-007 (7 cases) Configurations of plutonium-uranyl nitrate solutions containing gadolinium nitrate (Pacific Northwest Laboratories, 1970s). The concentration gadolinium in solution was varied.
The isotopes in this benchmark are $^{234-236,238}$U, $^{238-242}$Pu, ^{241}Am, ^{1}H, ^{14}N, ^{16}O, $^{152,154-158,160}$Gd.
Thermal scattering data for H in H_2O are used.

F. ^{233}U benchmarks

1. *Fast spectrum*

u233-met-fast-001 (1 case, 'Skidoo', '^{233}Jezebel') A bare sphere of highly enriched ^{233}U metal (LANL, 1961). The uranium enrichment was 98% ^{233}U.
The isotopes in these benchmark models are ^{233,234,235,238}U.

u233-met-fast-005 (2 cases) Highly enriched ^{233}U spheres, reflected by beryllium (LANL, 1958). The mass of the uranium-233 core was 10 kg (case 1) and 7.6 kg (case 2). The uranium enrichment was 98% ^{233}U.
The isotopes in these benchmark models are ^{9}Be, ^{16}O, ^{233,234,238}U.

u233-met-fast-006 (1 case, 'Flattop-23') A highly enriched ^{233}U sphere, reflected by normal uranium (LANL, 1964). The uranium enrichment was 98% ^{233}U.
The isotopes in these benchmark models are ^{233,234,235,238}U.

2. *Thermal spectrum*

u233-comp-therm-001 (8 cases) Cores of $^{235}UO_2-ZrO_2$ and cores of $^{233}UO_2-ZrO_2$, with blankets of either $^{233}UO_2$ or ThO_2 (BAPL, 1960s). The moderator was light water. Five assemblies were rectangular (cases 1-5) and three hexagonal (cases 6-8). The uranium enrichment was 97% ^{233}U for cases 2, 3, 4, 7, and 8, and 93% ^{235}U for cases 1, 5, and 6.
The isotopes in these benchmark models are ^{1}H, ^{10}B, ^{nat}C, ^{16}O, $^{50,52-54}$Cr, ^{55}Mn, $^{54,56-58}$Fe, $^{58,60-62,64}$Ni, $^{90-92,94,96}$Zr, $^{112,114-120,122,124}$Sn, $^{152,154-158,160}$Gd, ^{232}Th, ^{233,234,235,238}U. Thermal scattering data for H in H_2O and for H in CH_2 are used.

u233-sol-therm-001 (5 cases) Unreflected spheres of uranium-233 nitrate solutions (ORNL, 1950s). The amount of boron poison and the uranium concentration was varied. The uranium enrichment was 98% ^{233}U.
The isotopes in these benchmark models are ^{1}H, ^{10,11}B, ^{14}N, ^{16}O, ^{27}Al, $^{28-30}$Si, ^{55}Mn, $^{54,56-58}$Fe, ^{63,65}Cu, ^{232}Th, ^{233,234,235,238}U. Thermal scattering data for H in H_2O are used.

G. Occurrence of elements

In Table I are listed those elements that are present in *a* material of a benchmark series, either with more than 1 wt% or with more than 1e-4 atoms per barn-cm. Elements that do not show up in the table are either not at all present in the benchmark models, or only in minor fractions.

TABLE I: The benchmark series in which elements are present in *a* material, either with more than 1 wt% or with more than 1e-4 atoms/barn-cm.

Element	Benchmark series
H in H_2O	(59 benchmark series)
D in D_2O	lmt01, hst04
Be	hcm03
Be in BeO	hcm03
C in graphite	lct60, proteus, ict03, hci04, hmm05, pci01, pmm01
H in ZrH	ict03, hcm03
H in CH_2	(26 benchmark series)
H	(75 benchmark series)
Li	mmf11
Be	hcm03, hst38, hmf05, hmf057, u3mf05
B	(13 benchmark series)
C	(58 benchmark series)
N	(33 benchmark series)
O	(72 benchmark series)
F	hst04, hst09, hst10, hst39, hmf07, lst01
Na	lst18, hmm05, hmt18, hst02, hst38, pmm01, pst08, mcf01
Mg	(30 benchmark series)
Al	(53 benchmark series)
Si	(59 benchmark series)
P	hst02
S	hst02, lct02, lct05, lct09, lct10, lst18
Cl	pst12
K	lst18, hmt18, hmm05, hst02, pmm01, pst08
Ca	(15 benchmark series)
Ti	(14 benchmark series)
Cr	(59 benchmark series)
Mn	(54 benchmark series)
Fe	(77 benchmark series)
Ni	(62 benchmark series)
Co	lct51
Cu	(18 benchmark series)
Ga	pmf01, pmf02, pmf05, pmf06, pmf08, pmf12, pmf13, pmm01
Zr	lct09, lct16, lct60, ict03, hci05, hcm03, pmf05, kritz, mmf11, u3ct01
Nb	lct60, imf07, hcm03
Mo	ict03, hmt16, hst42, hci05, hcm03, hmf05
Cd	lct09, lct16, ict02, hst38, hmt06, hmm05, pst08, pmm01
Sn	lct09, kritz, u3ct01
Gd	ict02, hmt10, hmt16
W	imf14, hmf60, hmf67, hcm03, pmf05
Pb	lct10, lct17, hst38, hmf27, hmf57, hmf64
Th	lct60, ici01, pmf08, u3ct01
U	(87 benchmark series)
Pu	(24 benchmark series)

III. RESULTS OF CRITICALITY CALCULATIONS

In this Section we report all the k_{eff} results of the calculations. All results are given in graphical and tabular form. The columns contain the following items.

1. The benchmark value for k_{eff}, and its uncertainty in pcm between brackets. These values were obtained from Refs [2, 11–14].

2. Results from calculations based on ENDF/B-VI.8.

3. The results of the present work, based on ENDF/B-VII.0 (beta3).

4. The values for the third column divided by the first column (including uncertainty).

5. The benchmark name, abbreviated to fit into the column. For each of the three components of the ICSBEP name we use the first character: LEU → L, COMP → C, THERM → T, which gives LCT-001 for LEU-COMP-THERM-001. Similarly, PU-MET-FAST-001 is abbreviated to PMF-001.

For all benchmark cases a consistent pattern of calculating was used. All these benchmarks are criticality safety benchmarks, and thus require an MCNP calculation in the so-called kcode-mode. For this mode one needs to start with a user specified distribution of source neutrons. In the end all results should be independent of the user choice for this source distribution, and therefore we ran three calculations for each benchmark case. The first, short run used the user specified source distribution, and ran 100 cycles of 100 neutrons. The second run used the source distribution created by the first run subsequently ran 100 cycles of 1000 neutrons. The third run, finally, used the source distribution created by the second run, and subsequently ran 100 cycles of 10000 neutrons, of which the first 10 cycles were skipped. For certain selected benchmarks, such as heu-met-fast-001 and leu-comp-therm-006, the number of neutrons for the last run was chosen to be higher, in order to facilitate in-depth comparisons with results from others [1].

A. High-enriched uranium (HEU) results

1. *Fast spectrum*

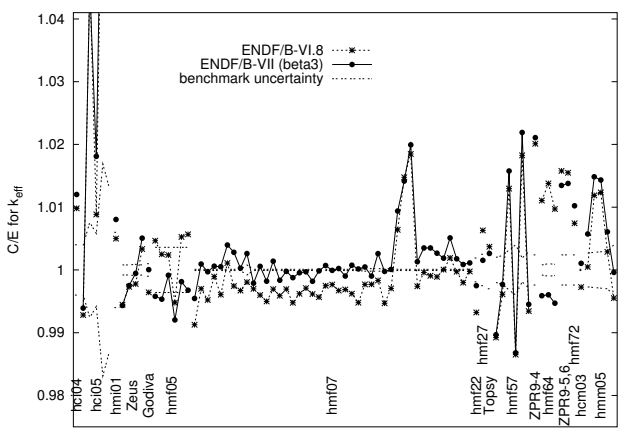

FIG. 1: Results for the HEU benchmarks with a fast or intermediate spectrum.

TABLE II: Results for HEU benchmarks with a fast spectrum.

benchmark	VI.8	VII.0	C/E (VII.0)	name
1.00000(100)	0.99644(40)	1.00005(19)	1.00005(102)	hmf-001_bare
1.00000(360)	1.00466(70)	0.99579(63)	0.99579(366)	hmf-005_1
1.00070(360)	1.00320(60)	0.99604(67)	0.99534(366)	hmf-005_2
0.99960(360)	1.00198(70)	0.99876(77)	0.99916(368)	hmf-005_3
0.99890(360)	0.99368(89)	0.99095(75)	0.99204(368)	hmf-005_4
0.99800(360)	1.00325(90)	0.99614(71)	0.99814(368)	hmf-005_5
0.99870(360)	1.00436(70)	0.99547(68)	0.99677(367)	hmf-005_6
0.99710(10)	0.98840(75)	0.99257(65)	0.99546(66)	hmf-007_1
0.99860(10)	0.99560(71)	0.99954(83)	1.00094(84)	hmf-007_2
1.00120(10)	0.99641(77)	1.00091(68)	0.99971(69)	hmf-007_3
0.99700(10)	0.99594(68)	0.99760(73)	1.00060(74)	hmf-007_4
1.00000(10)	0.99607(68)	1.00052(69)	1.00052(70)	hmf-007_5
1.00280(10)	1.00389(81)	1.00679(78)	1.00398(78)	hmf-007_6

continued on next column

TABLE II: Results for HEU benchmarks with a fast spectrum.

benchmark	VI.8	VII.0	C/E (VII.0)	name
0.99960(10)	0.99704(69)	1.00241(70)	1.00281(71)	hmf-007_7
0.99920(10)	0.99591(77)	0.99948(79)	1.00028(80)	hmf-007_8
1.00170(80)	0.99977(80)	1.00431(83)	1.00261(115)	hmf-007_9
1.00000(10)	0.99699(89)	0.99790(86)	0.99790(87)	hmf-007_10
0.99820(10)	0.99421(89)	0.99877(89)	1.00057(90)	hmf-007_11
0.99510(10)	0.99011(99)	0.99332(91)	0.99821(92)	hmf-007_12
1.00090(10)	0.99784(78)	1.00229(101)	1.00139(101)	hmf-007_13
0.99830(10)	0.99420(87)	0.99666(85)	0.99836(86)	hmf-007_14
0.99780(10)	0.99475(100)	0.99758(90)	0.99978(91)	hmf-007_15
0.99880(10)	0.99359(85)	0.99757(77)	0.99877(78)	hmf-007_16
0.99720(10)	0.99341(84)	0.99675(83)	0.99955(84)	hmf-007_17
0.99910(10)	0.99620(105)	0.99881(76)	0.99971(77)	hmf-007_18
0.99830(10)	0.99448(61)	0.99649(57)	0.99819(58)	hmf-007_19
0.99810(10)	0.99378(76)	0.99795(79)	0.99985(80)	hmf-007_20
0.99870(10)	0.99618(67)	0.99941(83)	1.00071(84)	hmf-007_21
0.99940(10)	0.99707(83)	0.99933(74)	0.99993(75)	hmf-007_22
0.99930(10)	0.99601(75)	0.99953(80)	1.00023(81)	hmf-007_23
1.00010(10)	0.99698(86)	0.99913(101)	0.99903(102)	hmf-007_24
0.99900(10)	0.99522(87)	0.99975(75)	1.00075(76)	hmf-007_25
0.99970(10)	0.99449(78)	0.99986(81)	1.00016(82)	hmf-007_26
0.99650(20)	0.99420(67)	0.99697(58)	1.00047(62)	hmf-007_27
0.99870(20)	0.99641(65)	0.99772(72)	0.99902(75)	hmf-007_28
0.99780(20)	0.99613(86)	1.00039(78)	1.00260(81)	hmf-007_29
0.99810(20)	0.99280(76)	0.99787(95)	0.99977(97)	hmf-007_30
1.00130(20)	0.99836(105)	1.00139(99)	1.00009(101)	hmf-007_31
0.99590(10)	1.00227(71)	1.00525(65)	1.00939(65)	hmf-007_32
0.99950(10)	1.01425(67)	1.01366(73)	1.01417(73)	hmf-007_33
0.99770(10)	1.01614(70)	1.01758(76)	1.01993(75)	hmf-007_34
1.00110(10)	0.99849(77)	1.00241(80)	1.00131(80)	hmf-007_35
0.99990(10)	0.99950(83)	1.00340(92)	1.00350(92)	hmf-007_36
0.99880(10)	0.99787(84)	1.00230(89)	1.00350(89)	hmf-007_37
1.00000(10)	0.99890(83)	1.00267(85)	1.00267(85)	hmf-007_38
1.00180(10)	1.00185(87)	1.00368(84)	1.00188(84)	hmf-007_39
1.00130(10)	1.00322(95)	1.00642(87)	1.00511(87)	hmf-007_40
0.99940(10)	0.99912(86)	1.00118(105)	1.00178(105)	hmf-007_41
1.00160(10)	0.99958(80)	1.00247(84)	1.00087(84)	hmf-007_42
0.99980(10)	0.99957(84)	1.00092(90)	1.00112(90)	hmf-007_43
1.00000(190)	0.99323(41)	0.99750(43)	0.99750(195)	hmf-022
1.00000(250)	1.00630(42)	1.00154(38)	1.00154(253)	hmf-027
1.00000(300)	1.00370(39)	1.00263(45)	1.00263(303)	hmf-028
1.00000(200)	1.00328(69)	0.98967(69)	0.98967(212)	hmf-057_1
1.00000(230)	1.00940(62)	0.99770(68)	0.99770(240)	hmf-057_2
1.00000(320)	1.03062(66)	1.01577(71)	1.01577(328)	hmf-057_3
1.00000(400)	0.99679(71)	0.98680(66)	0.98680(406)	hmf-057_4
1.00000(190)	1.03615(69)	1.02191(73)	1.02191(203)	hmf-057_5
1.00000(290)	1.00991(75)	0.99452(79)	0.99452(301)	hmf-057_6
0.99550(240)	1.01551(30)	1.01650(60)	1.02109(248)	hmf-060
0.99960(80)	1.01066(67)	0.99550(67)	0.99590(105)	hmf-064_1
0.99960(100)	1.01337(77)	0.99564(76)	0.99604(126)	hmf-064_2
0.99960(90)	1.00931(73)	0.99430(81)	0.99470(121)	hmf-064_3
0.99590(240)	1.01162(28)	1.00931(63)	1.01347(249)	hmf-067_1
0.99380(240)	1.00919(24)	1.00749(61)	1.01378(249)	hmf-067_2
0.99910(240)	1.00653(72)	1.00931(67)	1.01022(249)	hmf-072_1

2. *Intermediate spectrum*

TABLE III: Results for HEU benchmarks with an intermediate spectrum.

benchmark	VI.8	VII.0	C/E (VII.0)	name
1.00000(400)	1.00981(45)	1.01203(46)	1.01203(403)	hci-004
1.03200(400)	1.02459(40)	1.02574(40)	0.99393(390)	hci-005_1
1.05000(800)	1.09871(36)	1.09768(41)	1.04541(763)	hci-005_2
1.03000(600)	1.03912(42)	1.04864(34)	1.01810(583)	hci-005_3
1.06400(1800)	1.14568(42)	1.14568(44)	1.07677(1692)	hci-005_4
0.99700(1300)	0.94167(40)	0.94792(43)	0.95077(1305)	hci-005_5
1.00100(600)	1.00600(49)	1.00905(79)	1.00804(604)	hmi-001_1
0.99770(80)	0.99217(66)	0.99205(86)	0.99434(118)	hmi-006_1
1.00010(80)	0.99741(91)	0.99761(80)	0.99751(113)	hmi-006_2
1.00150(90)	0.99927(77)	1.00095(74)	0.99945(116)	hmi-006_3
1.00160(80)	1.00494(87)	1.00668(76)	1.00507(110)	hmi-006_4

3. *Thermal spectrum*

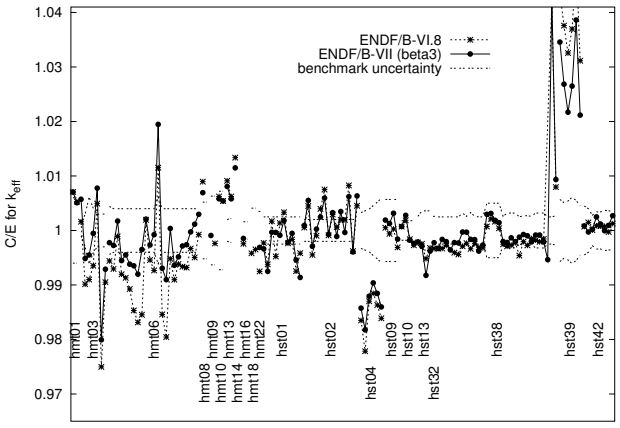

FIG. 2: Results for the HEU benchmarks with a thermal spectrum.

TABLE IV: Results for HEU benchmarks with a thermal spectrum.

benchmark	VI.8	VII.0	C/E (VII.0)	name
1.00100(600)	1.00808(91)	1.00806(93)	1.00705(606)	hmt-001_detail
1.00100(600)	1.00629(92)	1.00610(102)	1.00509(608)	hmt-001_simple
1.00000(100)	1.00162(95)	1.00573(79)	1.00573(127)	hmt-003_1
0.99100(300)	0.98125(79)	0.98590(82)	0.99485(314)	hmt-003_2
0.98260(600)	0.97377(93)	0.97819(88)	0.99551(617)	hmt-003_3
0.98760(400)	0.98122(92)	0.98707(94)	0.99946(416)	hmt-003_4
0.99300(300)	0.99790(98)	1.00072(86)	1.00777(314)	hmt-003_5
0.98890(300)	0.96416(89)	0.96905(98)	0.97993(320)	hmt-003_6
0.99190(300)	0.98249(93)	0.98486(90)	0.99290(316)	hmt-003_7
1.00000(440)	0.99441(99)	0.99776(95)	0.99776(450)	hmt-006_1
1.00000(400)	0.99295(89)	0.99725(101)	0.99725(413)	hmt-006_2
1.00000(400)	0.99891(80)	1.00173(87)	1.00173(409)	hmt-006_3
1.00000(400)	0.99196(79)	0.99448(85)	0.99448(409)	hmt-006_4
1.00000(400)	0.99132(89)	0.99553(82)	0.99553(408)	hmt-006_5
1.00000(400)	0.98925(89)	0.99381(78)	0.99381(408)	hmt-006_6
1.00000(400)	0.98533(79)	0.99352(77)	0.99352(407)	hmt-006_7
1.00000(400)	0.98313(79)	0.99199(77)	0.99199(407)	hmt-006_8
1.00000(400)	0.98454(79)	0.99651(83)	0.99651(409)	hmt-006_9
1.00000(400)	1.00195(80)	1.00209(108)	1.00209(414)	hmt-006_10
1.00000(400)	0.99458(90)	0.99733(86)	0.99733(409)	hmt-006_11
1.00000(400)	0.99266(79)	0.99923(88)	0.99923(410)	hmt-006_12
1.00000(610)	1.01152(91)	1.01947(91)	1.01947(616)	hmt-006_13
1.00000(400)	0.98461(79)	0.99306(80)	0.99306(408)	hmt-006_14
1.00000(400)	0.98044(78)	0.99097(72)	0.99097(407)	hmt-006_15
1.00000(400)	0.99480(90)	1.00037(84)	1.00037(409)	hmt-006_16
1.00000(400)	0.99097(99)	0.99361(89)	0.99361(410)	hmt-006_17
1.00000(400)	0.99384(89)	0.99517(97)	0.99517(412)	hmt-006_18
1.00000(400)	0.99335(70)	0.99716(72)	0.99716(406)	hmt-006_19
1.00000(400)	0.99319(89)	0.99739(75)	0.99739(407)	hmt-006_20
1.00000(400)	0.99668(90)	0.99973(80)	0.99973(408)	hmt-006_21
1.00000(400)	0.99505(90)	1.00115(84)	1.00115(409)	hmt-006_22
1.00000(400)	0.99925(90)	1.00296(90)	1.00296(410)	hmt-006_23
1.00090(520)	1.00986(87)	1.00785(80)	1.00694(526)	hmt-008_detail
1.00320(630)	1.00082(95)	1.00228(94)	0.99908(635)	hmt-009_simple
1.00260(720)	1.00886(91)	1.00842(83)	1.00580(723)	hmt-010_15mil
1.00300(720)	1.00844(86)	1.00844(92)	1.00542(724)	hmt-010_7.5mil
0.99830(200)	1.00738(94)	1.00636(97)	1.00807(222)	hmt-013_15mil
1.00210(220)	1.00834(82)	1.00792(94)	1.00581(239)	hmt-013_625in
0.99390(150)	1.00719(108)	1.00531(102)	1.01148(182)	hmt-014_simple
1.00170(160)	0.99926(89)	1.00025(90)	0.99855(183)	hmt-016_detail
1.00380(410)	0.99959(94)			hmt-018_detail
1.00380(410)	1.00031(84)			hmt-018_simple
1.00180(350)	0.99427(82)	0.99868(84)	0.99689(359)	hmt-022
1.00040(600)	0.99811(105)	0.99703(118)	0.99663(611)	hst-001_1
1.00210(720)	0.99589(111)	0.99458(117)	0.99250(728)	hst-001_2
1.00030(350)	1.00201(99)	0.99997(131)	0.99967(374)	hst-001_3
1.00080(530)	0.99603(118)	1.00043(115)	0.99963(542)	hst-001_4

continued on next column

TABLE IV: Results for HEU benchmarks with a thermal spectrum.

benchmark	VI.8	VII.0	C/E (VII.0)	name
1.00010(490)	1.00146(91)	0.99922(98)	0.99912(500)	hst-001_5
1.00020(460)	1.00355(110)	1.00203(87)	1.00183(468)	hst-001_6
1.00080(400)	0.99845(104)	0.99865(100)	0.99785(412)	hst-001_7
0.99980(380)	0.99815(108)	0.99928(97)	0.99948(392)	hst-001_8
1.00080(540)	0.99332(113)	0.99539(102)	0.99459(549)	hst-001_9
0.99930(540)	0.99514(104)	0.99069(104)	0.99138(550)	hst-001_10
1.00250(580)	1.00303(100)	1.00343(110)	1.00093(589)	hst-002_1
1.00280(580)	1.00731(111)	1.00834(104)	1.00552(588)	hst-002_2
1.00330(680)	0.99882(110)	1.00038(122)	0.99709(689)	hst-002_3
1.00340(690)	1.00243(110)	1.00366(120)	1.00026(698)	hst-002_4
1.00180(440)	1.00578(101)	1.00427(114)	1.00247(454)	hst-002_5
1.00230(410)	1.00983(101)	1.00827(113)	1.00596(424)	hst-002_6
1.00250(500)	1.00160(110)	1.00179(106)	0.99929(510)	hst-002_7
1.00300(550)	1.00594(111)	1.00628(112)	1.00327(560)	hst-002_8
1.00120(460)	1.00183(100)	1.00010(73)	0.99890(465)	hst-002_9
1.00240(500)	1.00434(90)	1.00588(105)	1.00347(510)	hst-002_10
1.00170(380)	1.00365(110)	1.00133(94)	0.99963(391)	hst-002_11
1.00270(500)	1.01100(101)	1.00893(117)	1.00621(512)	hst-002_12
1.00250(550)	0.99870(110)	0.99856(106)	0.99607(559)	hst-002_13
1.00310(660)	1.00765(91)	1.00947(103)	1.00635(666)	hst-002_14
1.00000(330)	0.98350(94)	0.98575(42)	0.98575(333)	hst-004_1
1.00000(360)	0.97785(108)	0.98176(50)	0.98176(364)	hst-004_2
1.00000(390)	0.98702(101)	0.98794(49)	0.98794(393)	hst-004_3
1.00000(460)	0.98847(98)	0.99038(49)	0.99038(463)	hst-004_4
1.00000(520)	0.98631(102)	0.98845(55)	0.98845(523)	hst-004_5
1.00000(590)	0.98388(102)	0.98598(53)	0.98598(592)	hst-004_6
0.99900(430)	0.99950(102)	1.00091(100)	1.00191(442)	hst-009_1
1.00000(390)	0.99938(102)	1.00129(105)	1.00129(404)	hst-009_2
1.00000(360)	1.00028(108)	1.00317(103)	1.00317(374)	hst-009_3
0.99860(350)	0.99550(99)	0.99702(109)	0.99842(367)	hst-009_4
1.00000(290)	1.00071(99)	1.00073(101)	1.00073(307)	hst-010_1
1.00000(290)	1.00187(89)	1.00279(111)	1.00279(310)	hst-010_2
1.00000(290)	0.99839(94)	0.99821(98)	0.99821(306)	hst-010_3
0.99920(290)	0.99649(96)	0.99684(101)	0.99764(307)	hst-010_4
1.00120(260)	0.99899(60)	0.99910(62)	0.99790(267)	hst-013_1
1.00070(360)	0.99824(70)	0.99781(68)	0.99711(366)	hst-013_2
1.00090(360)	0.99573(80)	0.99266(74)	0.99177(367)	hst-013_3
1.00030(360)	0.99708(60)	0.99651(74)	0.99621(367)	hst-013_4
1.00150(260)	0.99815(44)	0.99926(36)	0.99776(262)	hst-032_1
1.00000(250)	0.99668(47)	0.99674(61)	0.99674(257)	hst-038_1
1.00000(250)	0.99670(53)	0.99837(54)	0.99837(256)	hst-038_2
1.00000(250)	0.99726(52)	0.99795(49)	0.99795(255)	hst-038_3
1.00000(250)		0.99643(56)	0.99643(256)	hst-038_4
1.00000(250)	0.99593(50)	0.99778(54)	0.99778(256)	hst-038_5
1.00000(250)	0.99561(45)	0.99771(50)	0.99771(255)	hst-038_6
1.00000(320)	0.99711(58)	0.99972(53)	0.99972(324)	hst-038_7
1.00000(260)	0.99767(54)	0.99968(55)	0.99968(266)	hst-038_8
1.00000(330)	0.99664(48)	0.99837(52)	0.99837(334)	hst-038_9
1.00000(260)	0.99758(48)	0.99833(59)	0.99833(267)	hst-038_10
1.00000(250)	0.99691(53)	0.99621(49)	0.99621(255)	hst-038_11
1.00000(250)	0.99682(58)	0.99732(52)	0.99732(255)	hst-038_12
1.00000(500)	1.00073(51)	1.00296(57)	1.00296(503)	hst-038_13
1.00000(500)	1.00214(53)	1.00313(48)	1.00313(502)	hst-038_14
1.00000(500)	1.00161(50)	1.00188(48)	1.00188(502)	hst-038_15
1.00000(500)	1.00041(59)	1.00143(58)	1.00143(503)	hst-038_16
1.00000(260)	0.99746(49)	0.99798(54)	0.99798(266)	hst-038_17
1.00000(320)	0.99709(54)	0.99780(50)	0.99780(324)	hst-038_18
1.00000(320)	0.99732(56)	0.99866(51)	0.99866(324)	hst-038_19
1.00000(320)	0.99776(57)	0.99796(58)	0.99796(325)	hst-038_20
1.00000(250)	0.99540(50)	0.99877(54)	0.99877(256)	hst-038_21
1.00000(270)	0.99796(53)	0.99927(50)	0.99927(275)	hst-038_22
1.00000(270)	0.99727(47)	0.99903(48)	0.99903(274)	hst-038_23
1.00000(260)	0.99852(56)	0.99790(50)	0.99790(265)	hst-038_24
1.00000(320)	0.99821(50)	0.99917(54)	0.99917(325)	hst-038_25
1.00000(320)	0.99793(48)	0.99917(48)	0.99917(324)	hst-038_26
1.00000(320)	0.99845(50)	0.99789(53)	0.99789(324)	hst-038_27
1.00000(250)		0.99464(56)	0.99464(256)	hst-038_28
1.00000(250)	1.04209(53)	1.04215(50)	1.04215(255)	hst-038_29
1.00000(270)	1.00797(52)	1.00935(53)	1.00935(275)	hst-038_30
1.00000(570)	1.04370(104)	1.03457(93)	1.03457(577)	hst-039_1
1.00000(510)	1.03759(102)	1.02684(85)	1.02684(517)	hst-039_2
1.00120(540)	1.03380(100)	1.02294(86)	1.02171(546)	hst-039_3
1.00180(610)	1.03884(91)	1.02834(103)	1.02649(617)	hst-039_4
1.00180(550)	1.05134(114)	1.04048(112)	1.03861(559)	hst-039_5
1.00250(450)	1.03372(109)	1.02371(100)	1.02116(459)	hst-039_6
0.99570(390)	0.99641(53)	0.99654(49)	1.00084(395)	hst-042_1
0.99650(360)	0.99798(41)	0.99622(42)	0.99972(364)	hst-042_2
0.99940(280)	0.99947(39)	0.99963(40)	1.00023(283)	hst-042_3
1.00000(340)	1.00088(38)	1.00249(33)	1.00249(342)	hst-042_4
1.00000(340)	1.00081(29)	1.00118(36)	1.00118(342)	hst-042_5

continued on next column

TABLE IV: Results for HEU benchmarks with a thermal spectrum.

benchmark	VI.8	VII.0	C/E (VII.0)	name
1.00000(370)	1.00076(29)	0.99994(35)	0.99994(372)	hst-042_6
1.00000(360)	0.99972(23)	1.00095(32)	1.00095(361)	hst-042_7
1.00000(350)	1.00127(27)	1.00271(29)	1.00271(351)	hst-042_8

4. *Mixed spectrum*

TABLE V: Results for HEU benchmarks with a mixed spectrum.

benchmark	VI.8	VII.0	C/E (VII.0)	name
1.00000(10)	0.99727(91)	1.00105(44)	1.00105(45)	hcm-003_5
1.00070(270)	1.00118(84)	1.00643(79)	1.00573(281)	hmm-005_1
1.00030(280)	1.01218(88)	1.01514(86)	1.01484(292)	hmm-005_2
1.00120(290)	1.01356(76)	1.01556(80)	1.01434(300)	hmm-005_3
1.00160(300)	1.00448(84)	1.00768(90)	1.00607(313)	hmm-005_4
1.00050(400)	0.99601(87)	1.00011(71)	0.99961(406)	hmm-005_5

B. Intermediate-enriched uranium (IEU) results

1. *Fast spectrum*

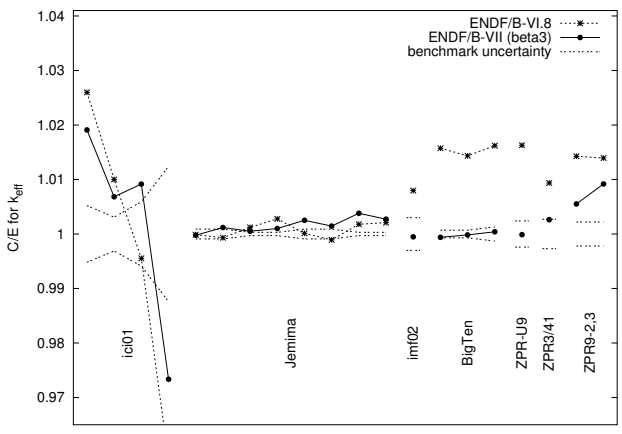

FIG. 3: Results for the IEU benchmarks with a fast or intermediate spectrum.

TABLE VI: Results for IEU benchmarks with a fast spectrum.

benchmark	VI.8	VII.0	C/E (VII.0)	name
0.99880(90)	0.99869(68)	0.99857(61)	0.99977(109)	imf-001_1
0.99880(90)	0.99811(56)	0.99998(60)	1.00118(108)	imf-001_2
0.99900(30)	1.00022(72)	0.99951(68)	1.00051(74)	imf-001_3
0.99900(30)	1.00177(66)	1.00001(73)	1.00101(79)	imf-001_4
0.99890(90)	0.99903(67)	1.00141(63)	1.00251(110)	imf-001_1i
0.99970(90)	0.99862(78)	1.00115(73)	1.00145(116)	imf-001_2i
0.99930(30)	1.00110(73)	1.00310(56)	1.00380(63)	imf-001_3i
1.00020(30)	1.00228(65)	1.00293(74)	1.00273(80)	imf-001_4i
1.00000(300)	1.00796(71)	0.99948(29)	0.99948(301)	imf-002_1
1.00450(70)	1.02031(30)	1.00389(30)	0.99939(76)	imf-007_detail
1.00450(70)	1.01890(57)	1.00433(28)	0.99983(75)	imf-007_simple
0.99480(130)	1.01093(62)	0.99520(28)	1.00040(134)	imf-007_twozone
0.99540(240)	1.01162(35)	0.99528(57)	0.99988(248)	imf-010_1
1.00070(270)	1.01007(50)	1.00333(56)	1.00263(276)	imf-012_1
0.99580(220)	1.01001(25)	1.00129(51)	1.00551(227)	imf-014_1
0.99270(220)	1.00653(26)	1.00182(51)	1.00919(227)	imf-014_2

2. *Intermediate spectrum*

TABLE VII: Results for IEU benchmarks with an intermediate spectrum.

benchmark	VI.8	VII.0	C/E (VII.0)	name
0.96900(500)	0.99418(30)	0.98751(33)	1.01910(517)	ici-001_1
0.98000(300)	0.98980(43)	0.98669(40)	1.00683(309)	ici-001_2
1.01400(600)	1.00948(57)	1.02328(54)	1.00915(594)	ici-001_3
0.96400(1200)	0.92401(60)	0.93830(62)	0.97334(1247)	ici-001_4

3. *Thermal spectrum*

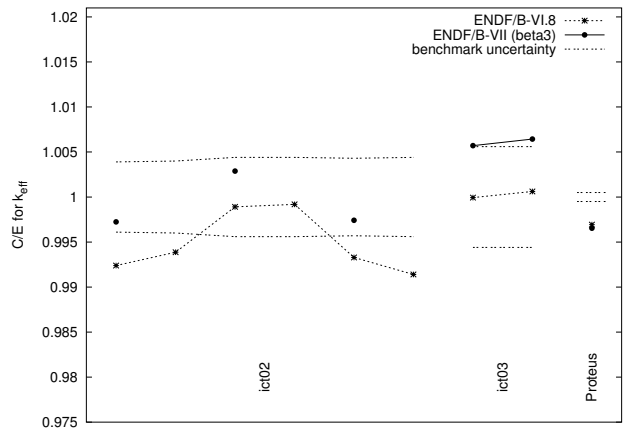

FIG. 4: Results for the IEU benchmarks with a thermal spectrum.

TABLE VIII: Results for IEU benchmarks with a thermal spectrum.

benchmark	VI.8	VII.0	C/E (VII.0)	name
1.00140(390)	0.99378(80)	0.99864(82)	0.99724(398)	ict-002_1
1.00190(400)	0.99576(80)			ict-002_2
1.00170(440)	1.00061(70)	1.00458(91)	1.00288(448)	ict-002_3
1.00190(440)	1.00109(80)			ict-002_4
1.00140(430)	0.99468(80)	0.99882(75)	0.99742(436)	ict-002_5
1.00160(440)	0.99299(70)			ict-002_6
1.00060(560)	1.00054(84)	1.00631(70)	1.00571(564)	ict-003_132
1.00460(560)	1.00522(103)	1.01107(91)	1.00644(565)	ict-003_133
1.01120(50)	1.00810(90)	1.00770(39)	0.99654(63)	proteus

C. Low-enriched uranium (LEU) results

1. *Thermal spectrum*

TABLE IX: Results for LEU benchmarks with a thermal spectrum.

benchmark	VI.8	VII.0	C/E (VII.0)	name
1.00000(310)	0.99746(80)	0.99976(66)	0.99976(317)	lct-001_1
0.99980(300)	0.99275(70)	0.99887(73)	0.99907(309)	lct-001_2
0.99980(300)	0.99155(69)	0.99938(68)	0.99958(308)	lct-001_3
0.99980(300)	0.99603(60)	0.99898(65)	0.99918(307)	lct-001_4
0.99980(300)	0.99170(69)	0.99789(66)	0.99809(307)	lct-001_5
0.99980(300)	0.99286(79)	0.99942(68)	0.99962(308)	lct-001_6
0.99980(310)	0.99393(60)	0.99965(58)	0.99985(315)	lct-001_7

continued on next column

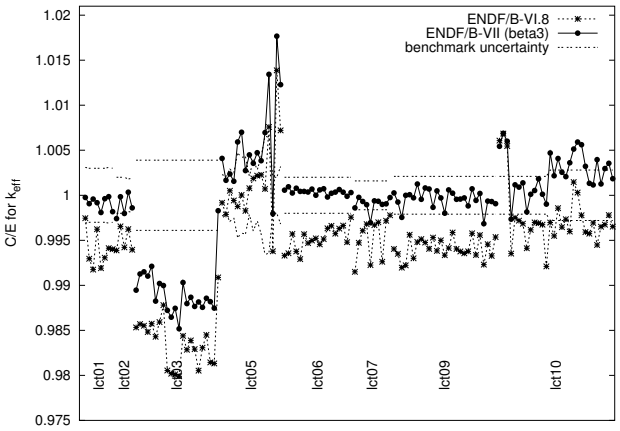

FIG. 5: Results for the LEU benchmarks with a thermal spectrum.

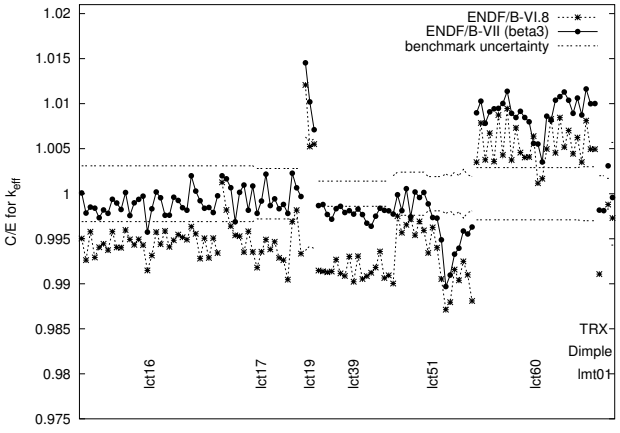

FIG. 6: Results for the LEU benchmarks with a thermal spectrum (continued).

TABLE IX: Results for LEU benchmarks with a thermal spectrum.

benchmark	VI.8	VII.0	C/E (VII.0)	name
0.99980(300)	0.99382(70)	0.99798(69)	0.99818(308)	lct-001_8
0.99970(200)	0.99358(84)	0.99711(79)	0.99741(215)	lct-002_1
0.99970(200)	0.99625(69)	0.99954(85)	0.99984(217)	lct-002_2
0.99970(200)	0.99392(90)	0.99768(73)	0.99798(213)	lct-002_3
0.99970(180)	0.99594(92)	1.00004(75)	1.00034(195)	lct-002_4
0.99970(190)	0.99365(70)	0.99830(82)	0.99860(207)	lct-002_5
1.00000(390)	0.98532(80)	0.98946(78)	0.98946(398)	lct-003_1
1.00000(390)	0.98570(69)	0.99126(80)	0.99126(398)	lct-003_2
1.00000(390)	0.98551(81)	0.99150(72)	0.99150(397)	lct-003_3
1.00000(390)	0.98481(79)	0.99102(73)	0.99102(397)	lct-003_4
1.00000(390)	0.98574(80)	0.99211(75)	0.99211(397)	lct-003_5
1.00000(390)	0.98429(68)	0.98825(81)	0.98825(399)	lct-003_6
1.00000(390)	0.98592(74)	0.99020(67)	0.99020(396)	lct-003_7
1.00000(390)	0.98780(73)	0.98998(74)	0.98998(397)	lct-003_8
1.00000(390)	0.98054(73)	0.98722(73)	0.98722(397)	lct-003_9
1.00000(390)	0.98019(68)	0.98646(71)	0.98646(397)	lct-003_10
1.00000(390)	0.98012(68)	0.98745(68)	0.98745(396)	lct-003_11
1.00000(390)	0.97990(59)	0.98518(71)	0.98518(397)	lct-003_12
1.00000(390)	0.98439(71)	0.99031(71)	0.99031(397)	lct-003_13
1.00000(390)	0.98284(74)	0.98797(61)	0.98797(395)	lct-003_14
1.00000(390)	0.98388(78)	0.98867(75)	0.98867(397)	lct-003_15
1.00000(390)	0.98291(66)	0.98766(68)	0.98766(396)	lct-003_16
1.00000(390)	0.98052(76)	0.98815(70)	0.98815(396)	lct-003_17
1.00000(390)	0.98307(77)	0.98756(64)	0.98756(395)	lct-003_18

continued on next column

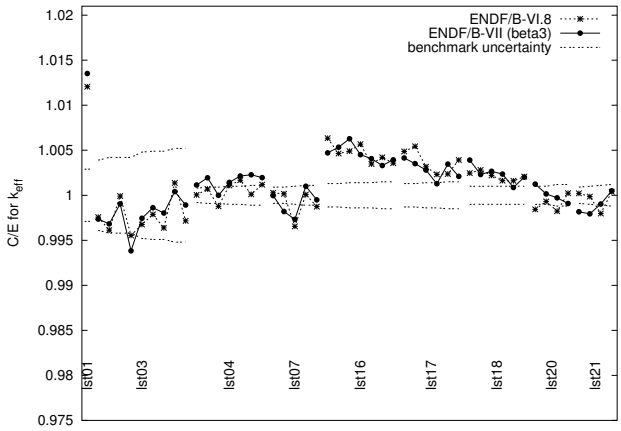

FIG. 7: Results for the LEU benchmarks with a thermal spectrum (continued).

TABLE IX: Results for LEU benchmarks with a thermal spectrum.

benchmark	VI.8	VII.0	C/E (VII.0)	name
1.00000(390)	0.98449(76)	0.98856(81)	0.98856(399)	lct-003_19
1.00000(390)	0.98144(76)	0.98819(75)	0.98819(397)	lct-003_20
1.00000(390)	0.98132(83)	0.98747(73)	0.98747(397)	lct-003_21
1.00000(390)	0.99088(75)	0.99829(70)	0.99829(396)	lct-003_22
1.00000(230)	0.99917(24)	1.00410(76)	1.00410(242)	lct-005_1
1.00000(210)	0.99786(25)	1.00167(82)	1.00167(225)	lct-005_2
1.00000(290)	1.00050(25)	1.00237(81)	1.00237(301)	lct-005_3
1.00000(250)	0.99942(25)	1.00156(72)	1.00156(260)	lct-005_4
1.00000(470)	0.99876(24)	1.00592(68)	1.00592(475)	lct-005_5
1.00000(420)	1.00004(25)	1.00700(80)	1.00700(427)	lct-005_6
1.00000(430)	0.99827(23)	1.00274(84)	1.00274(438)	lct-005_7
1.00000(210)	1.00079(26)	1.00449(89)	1.00449(228)	lct-005_8
1.00000(400)	1.00187(24)	1.00355(73)	1.00355(407)	lct-005_9
1.00000(280)	1.00218(24)	1.00473(77)	1.00473(290)	lct-005_10
1.00000(430)	1.00227(25)	1.00384(71)	1.00384(436)	lct-005_11
1.00000(660)	1.00071(24)	1.00696(73)	1.00696(664)	lct-005_12
1.00000(640)	1.00758(23)	1.01343(70)	1.01343(644)	lct-005_13
1.00000(200)	0.99378(23)	0.99796(75)	0.99796(214)	lct-005_14
1.00000(200)	1.01388(22)	1.01767(75)	1.01767(213)	lct-005_15
1.00000(320)	1.00721(24)	1.01229(83)	1.01229(330)	lct-005_16
1.00000(200)	0.99330(76)	1.00057(26)	1.00057(202)	lct-006_1
1.00000(200)	0.99356(84)	1.00094(28)	1.00094(202)	lct-006_2
1.00000(200)	0.99571(81)	1.00025(25)	1.00025(202)	lct-006_3
1.00000(200)	0.99377(72)	1.00079(24)	1.00079(201)	lct-006_4
1.00000(200)	0.99291(92)	1.00043(24)	1.00043(201)	lct-006_5
1.00000(200)	0.99568(85)	1.00043(26)	1.00043(202)	lct-006_6
1.00000(200)	0.99469(76)	1.00036(22)	1.00036(201)	lct-006_7
1.00000(200)	0.99498(76)	1.00069(22)	1.00069(201)	lct-006_8
1.00000(200)	0.99521(75)	1.00001(26)	1.00001(202)	lct-006_9
1.00000(200)	0.99455(68)	1.00060(25)	1.00060(202)	lct-006_10
1.00000(200)	0.99513(71)	1.00073(22)	1.00073(201)	lct-006_11
1.00000(200)	0.99633(79)	0.99981(26)	0.99981(202)	lct-006_12
1.00000(200)	0.99661(73)	1.00022(23)	1.00022(201)	lct-006_13
1.00000(200)	0.99574(77)	1.00035(26)	1.00035(202)	lct-006_14
1.00000(200)	0.99630(61)	1.00064(20)	1.00064(201)	lct-006_15
1.00000(200)	0.99664(64)	1.00034(21)	1.00034(201)	lct-006_16
1.00000(200)	0.99479(65)	0.99989(23)	0.99989(201)	lct-006_17
1.00000(200)	0.99757(76)	1.00030(24)	1.00030(201)	lct-006_18
1.00000(160)	0.99150(83)	0.99860(42)	0.99860(165)	lct-007_1
1.00000(160)	0.99472(94)	0.99977(43)	0.99977(166)	lct-007_2
1.00000(160)	0.99606(78)	0.99931(43)	0.99931(166)	lct-007_3
1.00000(160)	0.99679(71)	0.99896(38)	0.99896(164)	lct-007_4
1.00000(160)	0.99225(83)	0.99695(42)	0.99695(165)	lct-007_5
1.00000(160)	0.99669(87)	0.99938(42)	0.99938(165)	lct-007_6
1.00000(160)	0.99700(75)	0.99933(35)	0.99933(164)	lct-007_7
1.00000(160)	0.99262(93)	0.99899(42)	0.99899(165)	lct-007_8
1.00000(160)	0.99717(96)	0.99905(37)	0.99905(164)	lct-007_9
1.00000(160)	0.99778(70)	0.99975(33)	0.99975(163)	lct-007_10
1.00000(210)	0.99404(80)	1.00026(82)	1.00026(225)	lct-009_1
1.00000(210)	0.99349(70)	0.99924(78)	0.99924(224)	lct-009_2
1.00000(210)	0.99196(79)	0.99755(72)	0.99755(222)	lct-009_3

continued on next column

TABLE IX: Results for LEU benchmarks with a thermal spectrum.

benchmark	VI.8	VII.0	C/E (VII.0)	name
1.00000(210)	0.99222(89)	1.00000(84)	1.00000(226)	lct-009_4
1.00000(210)	0.99562(80)	1.00006(80)	1.00006(225)	lct-009_5
1.00000(210)	0.99300(79)	0.99972(84)	0.99972(226)	lct-009_6
1.00000(210)	0.99481(70)	1.00125(80)	1.00125(225)	lct-009_7
1.00000(210)	0.99513(80)	0.99955(81)	0.99955(225)	lct-009_8
1.00000(210)	0.99475(77)	1.00082(78)	1.00082(224)	lct-009_9
1.00000(210)	0.99405(80)	1.00070(88)	1.00070(228)	lct-009_10
1.00000(210)	0.99530(70)	0.99866(75)	0.99866(223)	lct-009_11
1.00000(210)	0.99382(80)	1.00049(78)	1.00049(224)	lct-009_12
1.00000(210)	0.99500(80)	0.99971(78)	0.99971(224)	lct-009_13
1.00000(210)	0.99335(89)	0.99801(87)	0.99801(227)	lct-009_14
1.00000(210)	0.99414(80)	1.00060(77)	1.00060(224)	lct-009_15
1.00000(210)	0.99587(80)	1.00023(74)	1.00023(223)	lct-009_16
1.00000(210)	0.99404(90)	0.99955(74)	0.99955(223)	lct-009_17
1.00000(210)	0.99376(80)	0.99958(88)	0.99958(228)	lct-009_18
1.00000(210)	0.99355(80)	0.99971(70)	0.99971(221)	lct-009_19
1.00000(210)	0.99377(80)	0.99882(78)	0.99882(224)	lct-009_20
1.00000(210)	0.99578(80)	1.00072(82)	1.00072(225)	lct-009_21
1.00000(210)	0.99337(70)	0.99943(88)	0.99943(228)	lct-009_22
1.00000(210)	0.99558(70)	1.00020(82)	1.00020(225)	lct-009_23
1.00000(210)	0.99230(70)	0.99684(87)	0.99684(227)	lct-009_24
1.00000(210)	0.99457(80)	0.99935(72)	0.99935(222)	lct-009_25
1.00000(210)	0.99327(80)	0.99930(84)	0.99930(226)	lct-009_26
1.00000(210)	0.99536(90)	0.99907(68)	0.99907(221)	lct-009_27
1.00000(210)	1.00607(76)	1.00544(85)	1.00544(226)	lct-010_1
1.00000(210)	1.00685(92)	1.00688(79)	1.00688(224)	lct-010_2
1.00000(210)	1.00547(74)	1.00600(89)	1.00600(228)	lct-010_3
1.00000(210)	0.99352(80)	0.99735(77)	0.99735(224)	lct-010_4
1.00000(210)	0.99751(64)	1.00116(81)	1.00116(225)	lct-010_5
1.00000(210)	0.99718(75)	1.00090(80)	1.00090(225)	lct-010_6
1.00000(210)	0.99684(76)	1.00138(70)	1.00138(221)	lct-010_7
1.00000(210)	0.99412(84)	0.99815(73)	0.99815(222)	lct-010_8
1.00000(210)	0.99616(77)	1.00011(76)	1.00011(223)	lct-010_9
1.00000(210)	0.99698(77)	1.00053(69)	1.00053(221)	lct-010_10
1.00000(210)	0.99691(87)	1.00182(82)	1.00182(225)	lct-010_11
1.00000(210)	0.99674(78)	1.00011(83)	1.00011(226)	lct-010_12
1.00000(210)	0.99210(72)	0.99902(82)	0.99902(225)	lct-010_13
1.00000(280)	0.99697(89)	1.00470(86)	1.00470(293)	lct-010_14
1.00000(280)	0.99549(85)	1.00217(77)	1.00217(290)	lct-010_15
1.00000(280)	0.99857(94)	1.00409(75)	1.00409(290)	lct-010_16
1.00000(280)	0.99646(75)	1.00255(84)	1.00255(292)	lct-010_17
1.00000(280)	0.99734(91)	1.00207(84)	1.00207(292)	lct-010_18
1.00000(280)	0.99597(84)	1.00361(80)	1.00361(291)	lct-010_19
1.00000(280)	1.00147(85)	1.00513(70)	1.00513(289)	lct-010_20
1.00000(280)	1.00030(74)	1.00591(89)	1.00591(294)	lct-010_21
1.00000(280)	0.99778(93)	1.00562(72)	1.00562(289)	lct-010_22
1.00000(280)	0.99592(91)	1.00322(70)	1.00322(289)	lct-010_23
1.00000(280)	0.99574(78)	1.00133(82)	1.00133(292)	lct-010_24
1.00000(280)	0.99693(73)	1.00115(74)	1.00115(290)	lct-010_25
1.00000(280)	0.99448(70)	1.00396(73)	1.00396(289)	lct-010_26
1.00000(280)	0.99651(79)	1.00126(70)	1.00126(289)	lct-010_27
1.00000(280)	0.99674(76)	1.00297(81)	1.00297(291)	lct-010_28
1.00000(280)	0.99780(78)	1.00355(69)	1.00355(288)	lct-010_29
1.00000(280)	0.99652(77)	1.00184(72)	1.00184(289)	lct-010_30
1.00000(310)	0.99503(70)	1.00008(69)	1.00008(318)	lct-016_1
1.00000(310)	0.99263(60)	0.99785(69)	0.99785(318)	lct-016_2
1.00000(310)	0.99578(60)	0.99851(72)	0.99851(318)	lct-016_3
1.00000(310)	0.99292(60)	0.99840(73)	0.99840(319)	lct-016_4
1.00000(310)	0.99406(70)	0.99733(69)	0.99733(318)	lct-016_5
1.00000(310)	0.99443(60)	0.99820(68)	0.99820(317)	lct-016_6
1.00000(310)	0.99373(70)	0.99782(69)	0.99782(318)	lct-016_7
1.00000(310)	0.99579(70)	0.99938(67)	0.99938(317)	lct-016_8
1.00000(310)	0.99404(70)	0.99897(68)	0.99897(317)	lct-016_9
1.00000(310)	0.99400(70)	0.99825(67)	0.99825(317)	lct-016_10
1.00000(310)	0.99597(70)	1.00013(68)	1.00013(317)	lct-016_11
1.00000(310)	0.99493(70)	0.99758(80)	0.99758(320)	lct-016_12
1.00000(310)	0.99432(70)	0.99899(70)	0.99899(318)	lct-016_13
1.00000(310)	0.99494(70)	0.99937(58)	0.99937(315)	lct-016_14
1.00000(310)	0.99430(70)	0.99973(70)	0.99973(318)	lct-016_15
1.00000(310)	0.99148(69)	0.99574(81)	0.99574(320)	lct-016_16
1.00000(310)	0.99314(70)	0.99833(77)	0.99833(319)	lct-016_17
1.00000(310)	0.99575(80)	1.00019(67)	1.00019(317)	lct-016_18
1.00000(310)	0.99439(70)	0.99955(61)	0.99955(316)	lct-016_19
1.00000(310)	0.99587(60)	0.99760(68)	0.99760(317)	lct-016_20
1.00000(310)	0.99410(70)	0.99761(70)	0.99761(318)	lct-016_21
1.00000(310)	0.99483(70)	0.99961(68)	0.99961(317)	lct-016_22
1.00000(310)	0.99546(60)	0.99925(57)	0.99925(315)	lct-016_23
1.00000(310)	0.99516(70)	0.99844(70)	0.99844(318)	lct-016_24
1.00000(310)	0.99490(60)	0.99817(66)	0.99817(317)	lct-016_25
1.00000(310)	0.99634(60)	1.00199(65)	1.00199(317)	lct-016_26

continued on next column

TABLE IX: Results for LEU benchmarks with a thermal spectrum.

benchmark	VI.8	VII.0	C/E (VII.0)	name
1.00000(310)	0.99555(70)	1.00029(73)	1.00029(318)	lct-016_27
1.00000(310)	0.99279(70)	0.99923(63)	0.99923(316)	lct-016_28
1.00000(310)	0.99506(70)	0.99839(65)	0.99839(317)	lct-016_29
1.00000(310)	0.99287(60)	0.99847(63)	0.99847(316)	lct-016_30
1.00000(310)	0.99507(60)	0.99791(75)	0.99791(319)	lct-016_31
1.00000(310)	0.99342(70)	0.99977(71)	0.99977(318)	lct-016_32
1.00000(310)	1.00127(70)	1.00199(61)	1.00199(316)	lct-017_1
1.00000(310)	0.99820(80)	1.00166(78)	1.00166(320)	lct-017_2
1.00000(310)	0.99640(70)	1.00067(68)	1.00067(317)	lct-017_3
1.00000(310)	0.99538(80)	0.99688(69)	0.99688(318)	lct-017_10
1.00000(310)	0.99528(70)	1.00015(72)	1.00015(318)	lct-017_11
1.00000(310)	0.99351(70)	1.00096(70)	1.00096(318)	lct-017_12
1.00000(310)	0.99583(70)	0.99817(64)	0.99817(317)	lct-017_13
1.00000(310)	0.99354(80)	1.00086(67)	1.00086(317)	lct-017_14
1.00000(280)	0.99180(79)	0.99782(78)	0.99782(291)	lct-017_15
1.00000(280)	0.99355(70)	0.99919(70)	0.99919(289)	lct-017_16
1.00000(280)	0.99491(70)	1.00217(71)	1.00217(289)	lct-017_17
1.00000(280)	0.99382(70)	0.99868(76)	0.99868(290)	lct-017_18
1.00000(280)	0.99466(70)	0.99943(65)	0.99943(287)	lct-017_19
1.00000(280)	0.99287(70)	0.99834(68)	0.99834(288)	lct-017_20
1.00000(280)	0.99263(79)	0.99881(75)	0.99881(290)	lct-017_21
1.00000(280)	0.99045(69)	0.99781(64)	0.99781(287)	lct-017_22
1.00000(280)	0.99690(70)	1.00228(77)	1.00228(290)	lct-017_23
1.00000(280)	0.99818(70)	1.00066(76)	1.00066(290)	lct-017_24
1.00000(280)	0.99335(70)	0.99969(75)	0.99969(290)	lct-017_25
1.00000(630)	1.01208(81)	1.01454(67)	1.01454(633)	lct-019_1
1.00000(580)	1.00524(70)	1.01020(84)	1.01020(586)	lct-019_2
1.00000(610)	1.00551(70)	1.00711(68)	1.00711(614)	lct-019_3
1.00000(140)	0.99147(77)	0.99868(42)	0.99868(146)	lct-039_1
1.00000(140)	0.99138(68)	0.99880(42)	0.99880(146)	lct-039_2
1.00000(140)	0.99128(91)	0.99769(42)	0.99769(146)	lct-039_3
1.00000(140)	0.99136(88)	0.99717(40)	0.99717(146)	lct-039_4
1.00000(140)	0.99268(94)	0.99834(48)	0.99834(148)	lct-039_5
1.00000(140)	0.99115(83)	0.99860(42)	0.99860(146)	lct-039_6
1.00000(140)	0.99087(74)	0.99791(39)	0.99791(145)	lct-039_7
1.00000(140)	0.99303(98)	0.99812(47)	0.99812(148)	lct-039_8
1.00000(140)	0.99022(77)	0.99773(41)	0.99773(146)	lct-039_9
1.00000(140)	0.99306(81)	0.99830(43)	0.99830(146)	lct-039_10
1.00000(140)	0.99053(83)	0.99768(39)	0.99768(145)	lct-039_11
1.00000(140)	0.99085(84)	0.99673(37)	0.99673(145)	lct-039_12
1.00000(140)	0.99122(88)	0.99639(46)	0.99639(147)	lct-039_13
1.00000(140)	0.99181(73)	0.99751(43)	0.99751(146)	lct-039_14
1.00000(140)	0.99358(91)	0.99839(42)	0.99839(146)	lct-039_15
1.00000(140)	0.99064(85)	0.99816(46)	0.99816(147)	lct-039_16
1.00000(140)	0.99094(80)	0.99810(40)	0.99810(146)	lct-039_17
1.00100(200)	0.99102(69)	0.99874(63)	0.99774(210)	lct-051_1
1.00100(240)	0.99851(80)	1.00089(71)	0.99989(250)	lct-051_2
1.00100(240)	0.99667(70)	0.99912(70)	0.99812(250)	lct-051_3
1.00100(240)	0.99755(70)	1.00156(73)	1.00056(251)	lct-051_4
1.00100(240)	0.99818(70)	0.99844(73)	0.99744(251)	lct-051_5
1.00100(240)	0.99639(80)	1.00119(70)	1.00019(250)	lct-051_6
1.00100(240)	0.99792(70)	1.00058(78)	0.99958(252)	lct-051_7
1.00100(240)	0.99693(70)	1.00114(62)	1.00014(248)	lct-051_8
1.00100(190)	0.99442(70)	0.99987(76)	0.99887(204)	lct-051_9
1.00100(190)	0.99726(80)	0.99836(77)	0.99736(205)	lct-051_10
1.00100(190)	0.99500(70)	0.99829(76)	0.99729(205)	lct-051_11
1.00100(190)	0.99152(79)	0.99587(75)	0.99488(204)	lct-051_12
1.00100(220)	0.98811(79)	0.99068(72)	0.98969(231)	lct-051_13
1.00100(190)	0.98894(79)	0.99196(79)	0.99097(206)	lct-051_14
1.00100(240)	0.99257(70)	0.99428(77)	0.99329(252)	lct-051_15
1.00100(200)	0.99137(79)	0.99494(77)	0.99395(214)	lct-051_16
1.00100(270)	0.99348(80)	0.99686(70)	0.99586(279)	lct-051_17
1.00100(210)	0.99199(69)	0.99653(76)	0.99553(223)	lct-051_18
1.00100(190)	0.98908(69)	0.99730(75)	0.99630(204)	lct-051_19
0.99900(260)	1.00250(59)	1.00798(67)	1.00899(269)	lct-060_1
0.99770(260)	1.00554(78)	1.00796(79)	1.01028(272)	lct-060_2
1.00010(260)	1.00387(65)	1.00792(70)	1.00782(269)	lct-060_3
1.00170(260)	1.00843(67)	1.01081(70)	1.00909(269)	lct-060_4
1.00090(260)	1.00447(66)	1.01034(61)	1.00943(267)	lct-060_5
0.98940(270)	0.99805(66)	0.99878(74)	1.00948(283)	lct-060_6
1.00280(260)	1.00712(72)	1.01285(68)	1.01002(268)	lct-060_7
1.00390(260)	1.01340(70)	1.01532(69)	1.01138(268)	lct-060_8
1.00430(260)	1.00807(59)	1.01327(61)	1.00893(266)	lct-060_9
1.00140(260)	1.00873(83)	1.00987(69)	1.00846(268)	lct-060_10
1.00010(260)	1.00467(65)	1.00925(70)	1.00915(269)	lct-060_11
1.00090(260)	1.00493(77)	1.00937(74)	1.00846(270)	lct-060_12
1.00100(260)	1.00508(69)	1.00900(70)	1.00799(269)	lct-060_13
1.00150(260)	1.00791(74)	1.00710(70)	1.00559(269)	lct-060_14
1.00120(260)	1.00237(67)	1.00673(84)	1.00552(273)	lct-060_15
1.00070(260)	1.00237(81)	1.00422(73)	1.00352(270)	lct-060_16

continued on next column

TABLE IX: Results for LEU benchmarks with a thermal spectrum.

benchmark	VI.8	VII.0	C/E (VII.0)	name
1.00120(260)	1.00618(65)	1.00982(56)	1.00861(266)	lct-060_17
1.00060(260)	1.00889(69)	1.00877(65)	1.00817(268)	lct-060_18
1.00070(260)	1.00524(66)	1.01110(74)	1.01039(270)	lct-060_19
1.00390(260)	1.01238(67)	1.01472(69)	1.01078(268)	lct-060_20
1.00030(260)	1.00547(54)	1.01160(61)	1.01130(267)	lct-060_21
1.00360(260)	1.01065(64)	1.01402(73)	1.01038(269)	lct-060_22
1.00170(260)	1.00614(77)	1.01065(69)	1.00893(268)	lct-060_23
1.00250(260)	1.00876(79)	1.01316(68)	1.01063(268)	lct-060_24
1.00160(260)	1.00512(72)	1.01035(55)	1.00874(265)	lct-060_25
0.99960(260)	1.00772(79)	1.01123(71)	1.01163(269)	lct-060_26
1.00310(260)	1.00807(79)	1.01312(69)	1.00999(268)	lct-060_27
1.00280(260)	1.00776(74)	1.01284(73)	1.01001(269)	lct-060_28
1.00000(200)	0.99107(19)	0.99818(21)	0.99818(201)	trx_1_3d
1.00000(200)		0.99812(20)	0.99812(201)	trx_2_3d
0.99830(170)	0.99710(50)	1.00139(34)	1.00310(174)	dimple
0.99900(570)	0.99630(60)	0.99858(53)	0.99958(573)	lmt-001_1
0.99910(290)	1.01115(89)	1.01261(89)	1.01352(303)	lst-001
0.99970(390)	0.99728(73)	0.99706(68)	0.99736(396)	lst-003_1
0.99930(420)	0.99543(65)	0.99612(71)	0.99682(426)	lst-003_2
0.99950(420)	0.99942(68)	0.99855(67)	0.99905(426)	lst-003_3
0.99950(420)	0.99504(77)	0.99333(62)	0.99383(425)	lst-003_4
0.99970(480)	0.99646(56)	0.99715(54)	0.99745(483)	lst-003_5
0.99990(490)	0.99778(55)	0.99852(60)	0.99862(494)	lst-003_6
0.99940(490)	0.99578(62)	0.99743(57)	0.99803(494)	lst-003_7
0.99930(520)	1.00067(42)	0.99971(42)	1.00041(522)	lst-003_8
0.99960(520)	0.99676(52)	0.99852(43)	0.99892(522)	lst-003_9
0.99940(80)	0.99945(59)	1.00054(61)	1.00114(101)	lst-004_001
0.99990(90)	1.00060(72)	1.00184(63)	1.00194(110)	lst-004_029
0.99990(90)	0.99867(72)	0.99990(67)	1.00000(112)	lst-004_033
0.99990(100)	1.00099(62)	1.00133(64)	1.00143(119)	lst-004_034
0.99990(100)	1.00158(53)	1.00204(58)	1.00214(116)	lst-004_046
0.99940(110)	0.99951(68)	1.00168(61)	1.00228(126)	lst-004_051
0.99960(110)	1.00078(57)	1.00156(60)	1.00196(125)	lst-004_054
0.99610(90)	0.99637(75)	0.99607(68)	0.99997(113)	lst-007_14
0.99730(90)	0.99746(75)	0.99550(67)	0.99820(113)	lst-007_30
0.99850(100)	0.99506(76)	0.99583(63)	0.99733(118)	lst-007_32
0.99880(110)	0.99888(70)	0.99980(59)	1.00100(125)	lst-007_36
0.99830(110)	0.99704(56)	0.99779(60)	0.99949(126)	lst-007_49
0.99960(130)	1.00594(86)	1.00431(90)	1.00471(158)	lst-016_105
0.99990(130)	1.00454(89)	1.00524(71)	1.00534(148)	lst-016_113
0.99940(140)	1.00431(77)	1.00568(85)	1.00628(164)	lst-016_125
0.99960(140)	1.00528(82)	1.00411(68)	1.00451(156)	lst-016_129
0.99950(140)	1.00297(74)	1.00357(74)	1.00407(158)	lst-016_131
0.99920(150)	1.00341(64)	1.00251(67)	1.00331(164)	lst-016_140
0.99940(150)	1.00297(75)	1.00334(69)	1.00394(165)	lst-016_196
0.99810(130)	1.00296(91)	1.00224(82)	1.00415(154)	lst-017_104
0.99860(130)	1.00403(72)	1.00211(75)	1.00351(150)	lst-017_122
0.99890(140)	1.00207(72)	1.00170(81)	1.00280(162)	lst-017_123
0.99920(140)	1.00152(72)	1.00048(82)	1.00128(162)	lst-017_126
0.99870(150)	1.00107(71)	1.00216(77)	1.00346(169)	lst-017_130
0.99960(150)	1.00352(66)	1.00170(70)	1.00210(166)	lst-017_147
0.99920(100)	1.00167(70)	1.00311(66)	1.00391(120)	lst-018_1
0.99960(100)	1.00241(70)	1.00191(59)	1.00231(116)	lst-018_2
0.99960(100)	1.00181(70)	1.00226(65)	1.00266(119)	lst-018_3
0.99970(100)	1.00133(60)	1.00206(76)	1.00236(126)	lst-018_4
0.99920(100)	1.00081(70)	1.00007(69)	1.00087(122)	lst-018_5
0.99960(100)	1.00167(70)	1.00161(74)	1.00201(124)	lst-018_6
0.99950(100)	0.99793(53)	1.00074(67)	1.00124(120)	lst-020_216
0.99960(100)	0.99891(58)	0.99975(58)	1.00015(116)	lst-020_217
0.99970(120)	0.99794(62)	0.99942(52)	0.99972(131)	lst-020_220
0.99980(120)	1.00003(49)	0.99889(43)	0.99909(128)	lst-020_226
0.99830(90)	0.99851(70)	0.99647(69)	0.99817(114)	lst-021_215
0.99850(100)	0.99836(54)	0.99644(60)	0.99794(117)	lst-021_218
0.99890(110)	0.99688(59)	0.99793(57)	0.99903(124)	lst-021_221
0.99930(120)	0.99969(49)	0.99980(54)	1.00050(132)	lst-021_223

D. Plutonium (PU) results

1. Fast spectrum

TABLE X: Results for PU benchmarks with a fast spectrum.

benchmark	VI.8	VII.0	C/E (VII.0)	name
1.00000(200)	0.99811(40)	1.00016(19)	1.00016(201)	pmf-001_bare
1.00000(200)	1.00067(63)	1.00019(65)	1.00019(210)	pmf-002
1.00000(130)	1.00638(74)	1.00825(74)	1.00825(149)	pmf-005

continued on next column

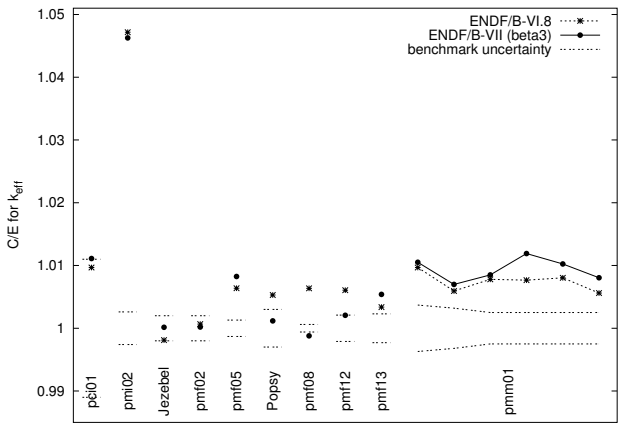

FIG. 8: Results for the PU benchmarks with a fast, intermediate, or mixed spectrum.

TABLE X: Results for PU benchmarks with a fast spectrum.

benchmark	VI.8	VII.0	C/E (VII.0)	name
1.00000(300)	1.00530(44)	1.00118(45)	1.00118(303)	pmf-006
1.00000(60)	1.00636(43)	0.99879(37)	0.99879(71)	pmf-008_1
1.00090(210)	1.00698(65)	1.00297(78)	1.00207(224)	pmf-012
1.00340(230)	1.00678(64)	1.00882(72)	1.00540(240)	pmf-013

2. Intermediate spectrum

TABLE XI: Results for PU benchmarks with an intermediate spectrum.

benchmark	VI.8	VII.0	C/E (VII.0)	name
1.00000(1100)	1.00968(56)	1.01111(58)	1.01111(1101)	pci-001
0.98690(260)	1.03345(48)	1.03255(84)	1.04626(276)	pmi-002_1

3. Thermal spectrum

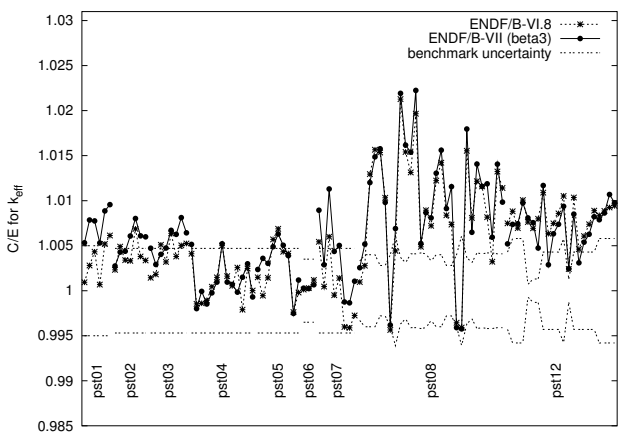

FIG. 9: Results for the PU benchmarks with a thermal spectrum.

TABLE XII: Results for PU benchmarks with a thermal spectrum.

benchmark	VI.8	VII.0	C/E (VII.0)	name
1.00000(500)	1.00094(104)	1.00532(100)	1.00532(510)	pst-001_1
1.00000(500)	1.00280(100)	1.00785(97)	1.00785(509)	pst-001_2
1.00000(500)	1.00432(117)	1.00775(87)	1.00775(507)	pst-001_3
1.00000(500)	1.00068(103)	1.00530(92)	1.00530(508)	pst-001_4
1.00000(500)	1.00519(109)	1.00886(108)	1.00886(511)	pst-001_5
1.00000(500)	1.00613(97)	1.00956(98)	1.00956(509)	pst-001_6
1.00000(470)	1.00232(93)	1.00274(84)	1.00274(477)	pst-002_1
1.00000(470)	1.00490(93)	1.00429(92)	1.00429(479)	pst-002_2
1.00000(470)	1.00340(104)	1.00438(100)	1.00438(480)	pst-002_3
1.00000(470)	1.00332(89)	1.00607(94)	1.00607(479)	pst-002_4
1.00000(470)	1.00686(100)	1.00802(91)	1.00802(479)	pst-002_5
1.00000(470)	1.00380(97)	1.00609(90)	1.00609(478)	pst-002_6
1.00000(470)	1.00337(101)	1.00598(87)	1.00598(478)	pst-002_7
1.00000(470)	1.00144(84)	1.00472(86)	1.00472(478)	pst-003_1
1.00000(470)	1.00182(81)	1.00291(84)	1.00291(477)	pst-003_2
1.00000(470)	1.00510(91)	1.00404(82)	1.00404(477)	pst-003_3
1.00000(470)	1.00320(95)	1.00474(94)	1.00474(479)	pst-003_4
1.00000(470)	1.00637(89)	1.00671(93)	1.00671(479)	pst-003_5
1.00000(470)	1.00380(88)	1.00626(87)	1.00626(478)	pst-003_6
1.00000(470)	1.00504(99)	1.00812(105)	1.00812(481)	pst-003_7
1.00000(470)	1.00524(83)	1.00643(81)	1.00643(477)	pst-003_8
1.00000(470)	1.00411(89)	1.00514(77)	1.00514(476)	pst-004_1
1.00000(470)	0.99854(84)	0.99801(88)	0.99801(478)	pst-004_2
1.00000(470)	0.99860(86)	0.99993(81)	0.99993(477)	pst-004_3
1.00000(470)	0.99893(76)	0.99853(77)	0.99853(476)	pst-004_4
1.00000(470)	1.00044(72)	0.99976(82)	0.99976(477)	pst-004_5
1.00000(470)	1.00148(90)	1.00096(83)	1.00096(477)	pst-004_6
1.00000(470)	1.00501(91)	1.00521(88)	1.00521(478)	pst-004_7
1.00000(470)	1.00162(87)	1.00096(84)	1.00096(477)	pst-004_8
1.00000(470)	1.00054(89)	1.00070(92)	1.00070(479)	pst-004_9
1.00000(470)	1.00257(87)	0.99984(76)	0.99984(476)	pst-004_10
1.00000(470)	0.99789(76)	1.00150(70)	1.00150(475)	pst-004_11
1.00000(470)	1.00247(85)	1.00299(80)	1.00299(477)	pst-004_12
1.00000(470)	1.00002(81)	0.99931(85)	0.99931(478)	pst-004_13
1.00000(470)	1.00149(82)	1.00236(77)	1.00236(476)	pst-005_1
1.00000(470)	0.99945(75)	1.00359(93)	1.00359(479)	pst-005_2
1.00000(470)	1.00143(86)	1.00304(83)	1.00304(477)	pst-005_3
1.00000(470)	1.00570(90)	1.00489(81)	1.00489(477)	pst-005_4
1.00000(470)	1.00687(92)	1.00630(96)	1.00630(480)	pst-005_5
1.00000(470)	1.00432(86)	1.00505(92)	1.00505(479)	pst-005_6
1.00000(470)	1.00414(90)	1.00389(90)	1.00389(478)	pst-005_7
1.00000(470)	0.99763(88)	0.99748(79)	0.99748(477)	pst-005_8
1.00000(470)	0.99980(78)	1.00118(90)	1.00118(479)	pst-005_9
1.00000(350)	1.00013(85)	1.00028(71)	1.00028(357)	pst-006_1
1.00000(350)	1.00029(76)	1.00023(83)	1.00023(360)	pst-006_2
1.00000(350)	1.00119(89)	1.00066(80)	1.00066(359)	pst-006_3
1.00000(470)	1.00543(94)	1.00894(100)	1.00894(480)	pst-007_2
1.00000(470)	1.00046(109)	1.00288(110)	1.00288(483)	pst-007_3
1.00000(470)	1.00599(93)	1.01130(96)	1.01130(479)	pst-007_5
1.00000(470)	0.99950(102)	1.00436(89)	1.00436(478)	pst-007_6
1.00000(470)	1.00141(87)	1.00503(97)	1.00503(480)	pst-007_7
1.00000(470)	0.99598(112)	0.99875(92)	0.99875(479)	pst-007_8
1.00000(470)	0.99588(98)	0.99865(97)	0.99865(480)	pst-007_9
1.00000(470)	0.99725(97)	1.00105(100)	1.00105(480)	pst-007_10
1.00000(330)	1.00097(82)	1.00256(82)	1.00256(340)	pst-008_1
1.00000(400)	1.00278(91)	1.00517(87)	1.00517(409)	pst-008_2
1.00000(400)	1.01295(99)	1.01201(83)	1.01201(408)	pst-008_3
1.00000(400)	1.01566(89)	1.01487(83)	1.01487(408)	pst-008_4
1.00000(280)	1.01535(88)	1.01577(90)	1.01577(294)	pst-008_5
1.00000(280)	1.01032(80)	1.00981(78)	1.00981(290)	pst-008_7
1.00000(400)	0.99564(90)	0.99618(95)	0.99618(411)	pst-008_8
1.00000(610)	1.00442(111)	1.00690(92)	1.00690(617)	pst-008_9
1.00000(370)	1.02128(91)	1.02192(100)	1.02192(383)	pst-008_10
1.00000(310)	1.01541(95)	1.01617(80)	1.01617(320)	pst-008_11
1.00000(410)	1.01314(99)	1.01538(100)	1.01538(422)	pst-008_12
1.00000(410)	1.01966(95)	1.02225(102)	1.02225(422)	pst-008_13
1.00000(420)	1.00488(96)	1.00524(99)	1.00524(431)	pst-008_14
1.00000(410)	1.00894(95)	1.00866(80)	1.00866(418)	pst-008_15
1.00000(330)	1.00721(89)	1.00809(96)	1.00809(343)	pst-008_16
1.00000(400)	1.01223(87)	1.01305(91)	1.01305(410)	pst-008_17
1.00000(400)	1.01421(90)	1.01561(89)	1.01561(409)	pst-008_18
1.00000(280)	1.00839(90)	1.00913(82)	1.00913(292)	pst-008_19
1.00000(280)	1.00735(94)	1.01156(83)	1.01156(292)	pst-008_20
1.00000(400)	0.99644(83)	0.99590(93)	0.99590(411)	pst-008_21
1.00000(610)	0.99591(99)	0.99576(84)	0.99576(616)	pst-008_22
1.00000(370)	1.01554(97)	1.01796(81)	1.01796(378)	pst-008_23
1.00000(310)	1.00809(82)	1.00649(103)	1.00649(326)	pst-008_24
1.00000(420)	1.01216(92)	1.01407(111)	1.01407(434)	pst-008_25
1.00000(410)	1.01159(106)	1.01159(106)	1.01159(423)	pst-008_26
1.00000(420)	1.00817(104)	1.01187(95)	1.01187(430)	pst-008_27

continued on next column

TABLE XII: Results for PU benchmarks with a thermal spectrum.

benchmark	VI.8	VII.0	C/E (VII.0)	name
1.00000(420)	1.00322(96)	1.00594(103)	1.00594(432)	pst-008_28
1.00000(410)	1.01324(97)	1.01406(100)	1.01406(422)	pst-008_29
1.00000(410)	1.01141(92)	1.00984(96)	1.00984(421)	pst-008_30
1.00000(430)	1.00749(66)	1.00520(59)	1.00520(434)	pst-012_2
1.00000(580)	1.00882(59)	1.00737(55)	1.00737(583)	pst-012_3
1.00000(580)	1.00695(57)	1.00744(58)	1.00744(583)	pst-012_4
1.00000(580)	1.01006(48)	1.00975(49)	1.00975(582)	pst-012_5
1.00000(70)	1.00762(96)	1.00809(106)	1.00809(126)	pst-012_6
1.00000(130)	1.00693(96)	1.00756(100)	1.00756(164)	pst-012_7
1.00000(130)	1.00798(93)	1.00474(95)	1.00474(161)	pst-012_8
1.00000(430)	1.01089(83)	1.01169(84)	1.01169(438)	pst-012_9
1.00000(430)	1.00633(69)	1.00288(78)	1.00288(437)	pst-012_10
1.00000(430)	1.00748(68)	1.00632(82)	1.00632(438)	pst-012_11
1.00000(430)	1.00858(58)	1.00738(59)	1.00738(434)	pst-012_12
1.00000(580)	1.01052(51)	1.00937(53)	1.00937(582)	pst-012_13
1.00000(130)	1.00242(92)	1.00245(82)	1.00245(154)	pst-012_14
1.00000(430)	1.01035(83)	1.00850(76)	1.00850(437)	pst-012_15
1.00000(430)	1.00462(83)	1.00310(78)	1.00310(437)	pst-012_16
1.00000(430)	1.00606(69)	1.00539(66)	1.00539(435)	pst-012_17
1.00000(430)	1.00738(56)	1.00627(73)	1.00627(436)	pst-012_18
1.00000(430)	1.00889(67)	1.00822(66)	1.00822(435)	pst-012_19
1.00000(580)	1.00838(66)	1.00788(68)	1.00788(584)	pst-012_20
1.00000(580)	1.00886(52)	1.00863(56)	1.00863(583)	pst-012_21
1.00000(580)	1.00924(45)	1.01069(50)	1.01069(582)	pst-012_22
1.00000(580)	1.00942(48)	1.00977(49)	1.00977(582)	pst-012_23

4. *Mixed spectrum*

TABLE XIII: Results for PU benchmarks with a mixed spectrum.

benchmark	VI.8	VII.0	C/E (VII.0)	name
1.00020(370)	1.00988(87)	1.01071(78)	1.01051(378)	pmm-001_1
1.00020(320)	1.00613(85)	1.00719(85)	1.00699(331)	pmm-001_2
1.00050(250)	1.00830(92)	1.00900(93)	1.00850(266)	pmm-001_3
1.00000(250)	1.00766(100)	1.01191(92)	1.01191(266)	pmm-001_4
1.00010(250)	1.00814(82)	1.01034(80)	1.01024(262)	pmm-001_5
1.00030(250)	1.00591(89)	1.00835(80)	1.00805(262)	pmm-001_6

E. Mixed uranium plutonium (MIX) results

1. *Fast spectrum*

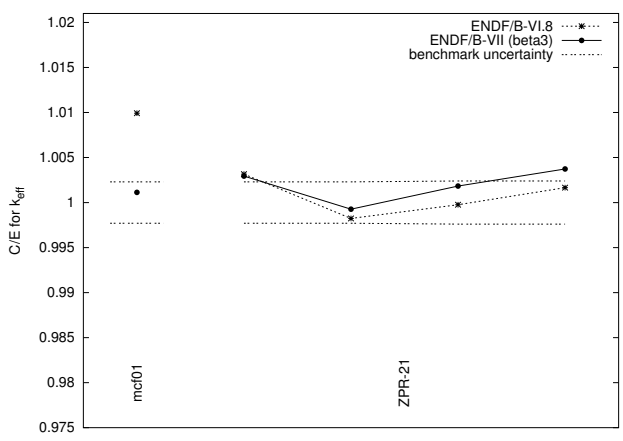

FIG. 10: Results for the MIX benchmarks with a fast spectrum.

TABLE XIV: Results for MIX benchmarks with a fast spectrum.

benchmark	VI.8	VII.0	C/E (VII.0)	name
0.98660(230)	0.99639(58)	0.98771(18)	1.00113(234)	mcf-001
0.98970(230)	0.99283(49)	0.99261(35)	1.00294(235)	mmf-011_1
0.99980(230)	0.99804(46)	0.99906(11)	0.99926(230)	mmf-011_2
1.00180(240)	1.00156(48)	1.00363(31)	1.00183(242)	mmf-011_3
1.00120(240)	1.00286(54)	1.00493(40)	1.00373(243)	mmf-011_4

2. *Thermal spectrum*

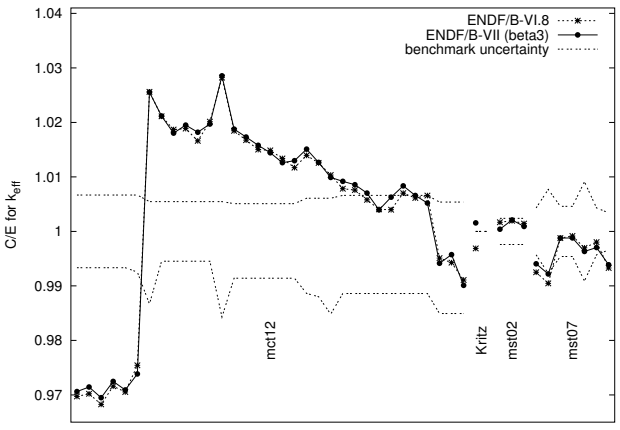

FIG. 11: Results for the MIX benchmarks with a thermal spectrum.

TABLE XV: Results for MIX benchmarks with a thermal spectrum. The benchmark value and its uncertainty is still under investigation for Kritz.

benchmark	VI.8	VII.0	C/E (VII.0)	name
1.00520(670)	0.97476(54)	0.97567(61)	0.97062(669)	mct-012_1
1.00520(670)	0.97526(52)	0.97650(55)	0.97145(669)	mct-012_2
1.00520(670)	0.97329(61)	0.97453(53)	0.96949(669)	mct-012_3
1.00520(670)	0.97665(51)	0.97754(63)	0.97248(670)	mct-012_4
1.00520(670)	0.97559(50)	0.97596(54)	0.97091(669)	mct-012_5
1.00520(750)	0.98050(60)	0.97890(53)	0.97384(748)	mct-012_6
1.00530(1340)	1.03104(55)	1.03098(47)	1.02554(1334)	mct-012_7
1.00530(550)	1.02653(48)	1.02657(61)	1.02116(550)	mct-012_8
1.00530(550)	1.02408(58)	1.02343(44)	1.01803(549)	mct-012_9
1.00530(550)	1.02427(54)	1.02490(49)	1.01950(549)	mct-012_10
1.00530(550)	1.02200(58)	1.02359(40)	1.01819(548)	mct-012_11
1.00530(550)	1.02555(57)	1.02510(57)	1.01970(550)	mct-012_12
1.00530(1580)	1.03367(54)	1.03399(62)	1.02854(1573)	mct-012_13
1.00120(860)	1.01967(67)	1.01998(62)	1.01876(861)	mct-012_14
1.00120(860)	1.01797(59)	1.01853(55)	1.01731(861)	mct-012_15
1.00120(860)	1.01623(53)	1.01702(60)	1.01580(861)	mct-012_16
1.00120(860)	1.01609(55)	1.01565(57)	1.01443(861)	mct-012_17
1.00120(860)	1.01460(59)	1.01384(61)	1.01262(861)	mct-012_18
1.00120(860)	1.01291(63)	1.01420(60)	1.01298(861)	mct-012_19
1.00140(1140)	1.01538(70)	1.01652(68)	1.01510(1140)	mct-012_20
1.00140(1200)	1.01398(62)	1.01408(58)	1.01266(1200)	mct-012_21
1.00140(1520)	1.01175(65)	1.01132(66)	1.00991(1519)	mct-012_22
1.00070(1140)	1.00854(67)	1.00990(60)	1.00919(1141)	mct-012_23
1.00070(1140)	1.00829(58)	1.00928(66)	1.00857(1141)	mct-012_24
1.00070(1140)	1.00649(57)	1.00773(60)	1.00703(1141)	mct-012_25
1.00070(1140)	1.00475(53)	1.00464(56)	1.00394(1141)	mct-012_26
1.00070(1140)	1.00468(66)	1.00698(60)	1.00628(1141)	mct-012_27
1.00070(1140)	1.00772(57)	1.00907(58)	1.00836(1141)	mct-012_28
1.00070(1140)	1.00683(63)	1.00729(59)	1.00659(1141)	mct-012_29
1.00070(1140)	1.00727(57)	1.00591(55)	1.00521(1141)	mct-012_30
1.00170(1510)	0.99679(56)	0.99584(74)	0.99415(1509)	mct-012_31
1.00170(1510)	0.99596(73)	0.99743(60)	0.99574(1509)	mct-012_32

continued on next column

TABLE XV: Results for MIX benchmarks with a thermal spectrum. The benchmark value and its uncertainty is still under investigation for Kritz.

benchmark	VI.8	VII.0	C/E (VII.0)	name
1.00170(1510)	0.99276(70)	0.99179(62)	0.99011(1509)	mct-012_33
1.00000( )	0.99688(20)	1.00157(23)	1.00157(23)	kritz_2.19c
1.00000( )	0.99343(22)			kritz_2.19h
1.00000(240)	1.00167(49)	1.00041(49)	1.00041(245)	mst-002_58
1.00000(240)	1.00196(53)	1.00210(46)	1.00210(244)	mst-002_59
1.00000(240)	1.00143(51)	1.00091(54)	1.00091(246)	mst-002_61
1.00000(430)	0.99250(79)	0.99405(44)	0.99405(432)	mst-007_1
1.00000(770)	0.99046(84)	0.99219(50)	0.99219(772)	mst-007_2
1.00000(460)	0.99878(96)	0.99877(43)	0.99877(462)	mst-007_3
1.00000(460)	0.99917(75)	0.99881(42)	0.99881(462)	mst-007_4
1.00000(910)	0.99697(81)	0.99633(46)	0.99633(911)	mst-007_5
1.00000(430)	0.99803(80)	0.99705(42)	0.99705(432)	mst-007_6
1.00000(340)	0.99329(87)	0.99388(38)	0.99388(342)	mst-007_7

F. ^{233}U results

1. *Fast spectrum*

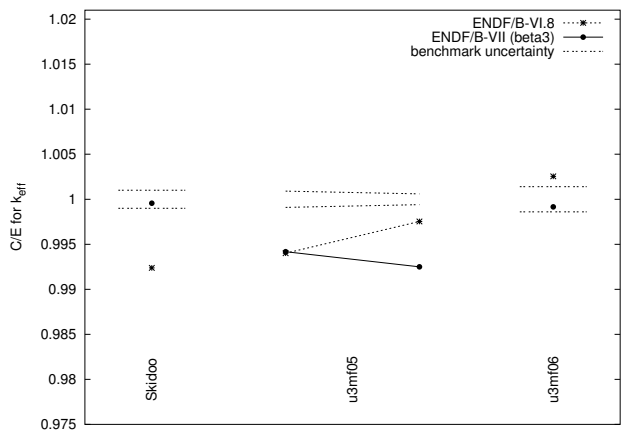

FIG. 12: Results for the U233 benchmarks with a fast spectrum.

TABLE XVI: Results for ^{233}U benchmarks with a fast spectrum.

benchmark	VI.8	VII.0	C/E (VII.0)	name
1.00000(100)	0.99238(35)	0.99956(18)	0.99956(102)	umf-001
1.00000(90)	0.99401(43)	0.99418(10)	0.99418(91)	umf-005_1
1.00000(60)	0.99754(46)	0.99250(10)	0.99250(61)	umf-005_2
1.00000(140)	1.00254(48)	0.99916(22)	0.99916(142)	umf-006

2. *Thermal spectrum*

TABLE XVII: Results for ^{233}U benchmarks with a thermal spectrum.

benchmark	VI.8	VII.0	C/E (VII.0)	name
1.00060(270)	0.99734(107)	1.00228(49)	1.00168(274)	uct-001_1
1.00150(250)	0.99857(116)	1.00439(49)	1.00289(254)	uct-001_2
1.00000(240)	0.99630(118)	1.00437(60)	1.00437(247)	uct-001_3
1.00070(250)	0.99415(85)	1.00142(41)	1.00072(253)	uct-001_4

continued on next column

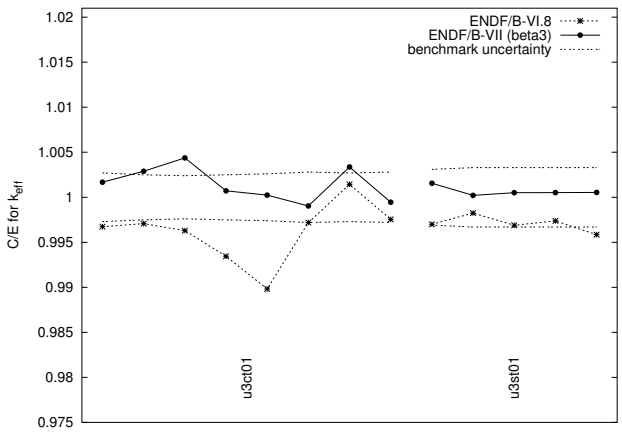

FIG. 13: Results for the U233 benchmarks with a thermal spectrum.

TABLE XVII: Results for ^{233}U benchmarks with a thermal spectrum.

benchmark	VI.8	VII.0	C/E (VII.0)	name
1.00150(260)	0.99130(85)	1.00174(38)	1.00024(262)	uct-001_5
1.00150(280)	0.99869(92)	1.00054(46)	0.99904(283)	uct-001_6
0.99950(270)	1.00094(118)	1.00286(53)	1.00336(275)	uct-001_7
1.00040(280)	0.99795(97)	0.99985(51)	0.99945(284)	uct-001_8
1.00000(310)	0.99700(63)	1.00156(29)	1.00156(311)	ust-001_1
1.00050(330)	0.99875(57)	1.00071(32)	1.00021(331)	ust-001_2
1.00060(330)	0.99749(61)	1.00111(34)	1.00051(332)	ust-001_3
0.99980(330)	0.99718(63)	1.00032(32)	1.00052(332)	ust-001_4
0.99990(330)	0.99575(68)	1.00044(30)	1.00054(331)	ust-001_5

G. Summary

Results for many benchmarks have been presented in the preceding pages. The number of benchmarks in each of the ICSBEP main categories is summarized in Table XVIII. For a specific situation, it can be useful to compute averages of those benchmark cases that are most applicable to that situation. Here, however, we only give average values for $C/E - 1$ for the main ICSBEP categories, see Table XIX.

These numbers can be compared e.g. to those based in ENDF/B-VI.8, see Table XX. The shift going from ENDF/B-VI.8 to ENDF/B-VII.0 is listed in Table XXI. It is clear that in particular for LEU-COMP-THERM benchmarks, the results have improved dramatically. For most of the other categories, there are also improvements. It is interesting to note that that whereas for almost all categories the numbers have gone up, for IEU-MET-FAST and PU-MET-FAST benchmarks the numbers have gone down, which again is, on average, an improvement. The results for solution benchmarks have not changed by much, which means that, on the whole, the numbers for solution benchmarks are still slightly on the high side, and for plutonium solution 0.6% on the high side.

For a more detailed discussion of subsets of these results we refer to Ref. [1].

TABLE XVIII: The number of benchmarks per main ICSBEP category for thermal/intermediate/fast/mixed neutron spectrum.

	COMP				MET				SOL	total
	therm	inter	fast	mixed	therm	inter	fast	mixed	therm	
LEU	257				1				49	307
IEU	6	4					16			26
HEU		6		1	41	5	66	5	87	211
MIX	34		1				4		10	49
PU		1				1	7	6	105	120
U233	8						4		5	17
total	305	11	1	1	42	6	97	11	256	730

TABLE XIX: The average values for $C/E-1$ (in pcm) for ENDF/B-VII.0 per main ICSBEP benchmark category.

	COMP				MET				SOL
	therm	inter	fast	mixed	therm	inter	fast	mixed	therm
LEU	17				−41				123
IEU	103	219					182		
HEU		1744		104	−51	88	147	812	108
MIX	428		110				193		−254
PU		1110				4565	229	936	620
U233	146						−364		66

TABLE XX: The average values for $C/E-1$ (in pcm) for ENDF/B-VI.8 per main ICSBEP benchmark category.

	COMP				MET				SOL
	therm	inter	fast	mixed	therm	inter	fast	mixed	therm
LEU	−452	/	/		−270	/	/		107
IEU	−299	−238	/		/	/	712		
HEU	/	1442	/	−273	−411	−42	186	462	142
MIX	377	/	978		/	/	69		−257
PU	/	967	/		/	4654	375	745	531
U233	−380	/	/		/	/	−338		−292

TABLE XXI: The shift in the average values for $C/E-1$ (in pcm) going from ENDF/B-VI.8 to ENDF/B-VII.0 (beta3) per main ICSBEP benchmark category.

	COMP				MET				SOL
	therm	inter	fast	mixed	therm	inter	fast	mixed	therm
LEU	469	/	/		229	/	/		16
IEU	402	457	/		/	/	−530		
HEU	/	302	/	377	360	130	−39	350	−34
MIX	51	/	−868		/	/	124		3
PU	/	143	/		/	−89	−146	191	89
U233	526	/	/		/	/	−26		358

IV. BRIEF DESCRIPTION OF THE SHIELDING BENCHMARKS

A. Oktavian

The Oktavian benchmark specifications are given on the IAEA web site [3]. The measured quantity was the leakage current spectrum from the outer surface of a spherical pile of a material. At the center of a pile a 14 MeV D-T neutron source was located. The leakage spectrum is given in units of neutrons per MeV per source neutron.

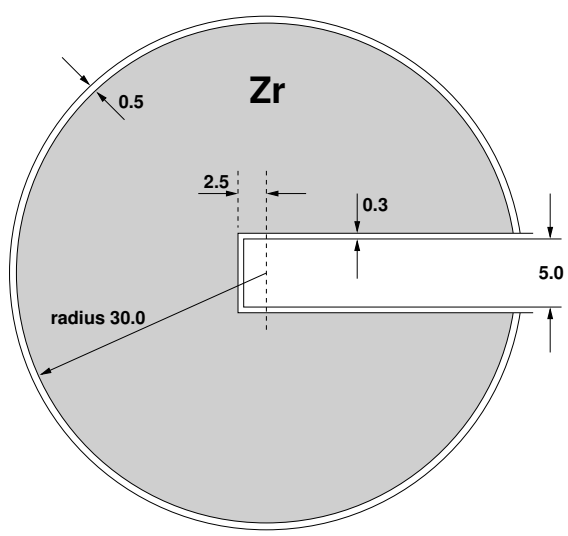

FIG. 14: Schematic drawing of the Oktavian geometry for the Zr benchmark (not to scale). All dimensions are in cm.

The materials for which benchmark calculations have been performed are listed in Table XXII. A schematic drawing of one of the models is given in Fig. 14 (see Ref. [16]).

TABLE XXII: The materials used in the Oktavian shielding benchmarks.

material		outer diameter
aluminum	Al	40 cm
cobalt	Co	40 cm
chromium	Cr	40 cm
copper	Cu	61 cm
lithium fluoride	LiF	61 cm
molybdenum	Mo	61 cm
manganese	Mn	61 cm
silicon	Si	60 cm
titanium	Ti	40 cm
tungsten	W	40 cm
zirconium	Zr	61 cm

B. Fusion Neutronics Source (FNS)

The Fusion Neutronics Source (FNS) Time-of-Flight benchmark specifications are given on the IAEA web site [4]. The neutron spectrum emerging from slabs of material of varying thickness, was measured at five different angles. The slabs were placed at 20 cm distance from a 14 MeV D-T neutron source. The materials for

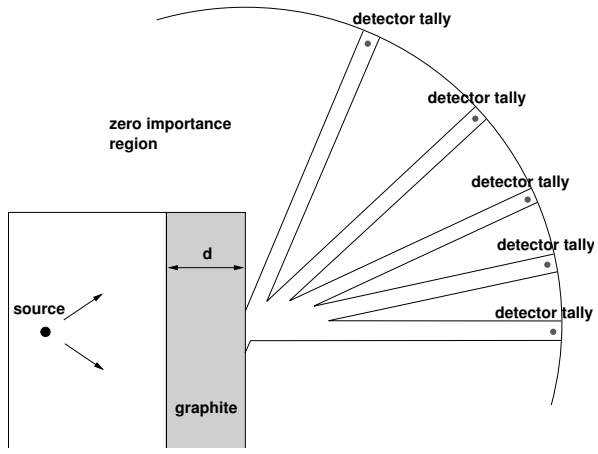

FIG. 15: Schematic drawing of the MCNP model for the FNS benchmark for graphite (not to scale).

which benchmark calculations have been performed are listed in Table XXIII. A schematic drawing of the MCNP model for this benchmark is given in Fig. 15 [17].

TABLE XXIII: The materials used in the FNS shielding benchmarks.

material		slab thickness	angles
beryllium	Be	5 cm	0°, 24.9°, 42.8°, 66.8°
		15 cm	0°, 12.2°, 24.9°, 42.8°, 66.8°
graphite	C	5 cm	0°, 24.9°, 42.8°, 66.8°
		20 cm	0°, 12.2°, 24.9°, 42.8°, 66.8°
		40 cm	0°, 12.2°, 24.9°, 42.8°, 66.8°
nitrogen	N	20 cm	0°, 12.2°, 24.9°, 42.8°, 66.8°
oxygen	O	20 cm	0°, 12.2°, 24.9°, 42.8°, 66.8°
iron	Fe	5 cm	0°, 24.9°, 42.8°, 66.8°
		20 cm	0°, 12.2°, 24.9°, 42.8°, 66.8°
		40 cm	0°, 12.2°, 24.9°, 42.8°, 66.8°
		60 cm	0°, 12.2°, 24.9°, 42.8°
lead	Pb	5 cm	0°, 24.9°, 42.8°, 66.8°
		20 cm	0°, 12.2°, 24.9°, 42.8°, 66.8°
		40 cm	0°, 12.2°, 24.9°, 42.8°, 66.8°

C. LLNL Pulsed Spheres

The description of the experiments performed in the Livermore Pulsed Sphere Program is given in Ref. [5]. Time-of-flight measurements were performed for neutrons passing through spherical shells of varying thickness, containing different materials. The source was a 14 MeV D-T neutron source.

Calculations were performed for many cases, see Table XXIV. For almost all these cases, the measurement was performed at an angle of 39° with respect to the source. For the cases with concrete, the angle was 117°.

TABLE XXIV: The materials used in the LLNL pulsed sphere benchmarks. The thickness of the material is given in units of the mean free path.

material	thickness [mfp]
^{6}Li	0.5, 1.1, 1.6
^{7}Li	0.5, 1.1, 1.6
Be	0.8
C	0.5, 1.3, 2.9
N	1.1, 3.1
O	0.7
Mg	0.7, 1.2, 1.9
Al	0.9, 1.6, 2.6
Ti	1.2, 2.2, 3.5
Fe	0.9, 2.9, 4.8
Pb	1.4
D_2O	1.2, 2.1
H_2O	1.1, 1.9
Concrete	2.0, 3.8
Polyethylene	0.8, 1.8, 3.5
Teflon	0.9, 1.8, 2.9

For the H_2O 1.9 mfp case, and the Teflon 2.9 mfp case, results for both angles are presented.

The geometry of the sample materials for these cases varies; one for concrete is depicted schematically in Fig. 16. The composition of the concrete is given in Table XXV; the density of the concrete was 2.35 g/cm^3. The MCNP model used in the present work was taken over from Ref. [18].

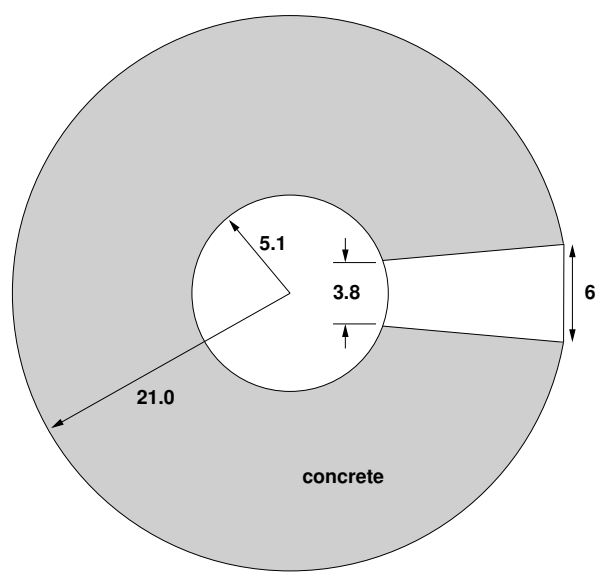

FIG. 16: Schematic drawing of the MCNP model for the LLNL benchmark for concrete (not to scale). All dimensions are in cm.

TABLE XXV: The composition of the concrete used in the LLNL Pulsed Sphere experiments.

Material	at%
O	55.7
H	15.1
Si	14.9
Ca	3.6
Al	3.2
C	3.1
Mg	1.8
Na	1.3
other	< 1.0 each

D. NIST Water Spheres

A description of the experiments performed at NIST with water and cadmium shielding is given in Ref. [6]. A Cf source was placed at the center of the experiment, and fission foils were placed at two, diametrically opposed positions. Between the source and the fission foils were several combinations of shielding materials, see Table XXVI. The fission foils used were ^{235}U, ^{239}Pu, ^{238}U, ^{237}Np.

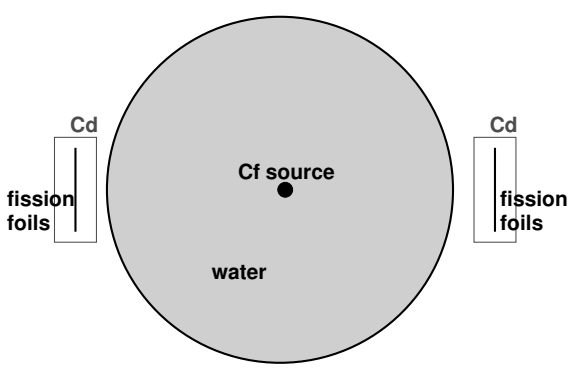

FIG. 17: Schematic drawing of the MCNP model for the NIST benchmark (not to scale).

V. RESULTS OF SHIELDING CALCULATIONS

In this section we report on the results of our calculations. These results are reported as graphs of the neutron spectra, and in some cases also the photon spectrum, as well as in tables of calculated over experimental values of the neutron spectra.

TABLE XXVI: NIST water spheres: the radius and material combinations for which experiments have been performed.

radius (inch)	sphere content	detector shield
1.5	air	–
2.0	air	–
1.5	air	Cd
2.0	air	Cd
1.5	H_2O	–
2.0	H_2O	–
2.5	H_2O	–
1.5	H_2O	Cd
2.0	H_2O	Cd
2.5	H_2O	Cd

A. Oktavian

1. *Oktavian, Al*

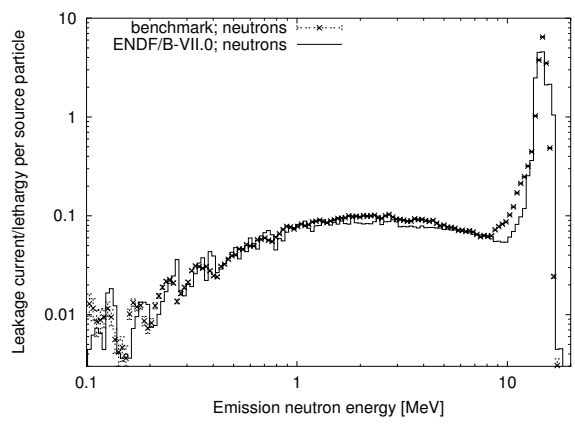

FIG. 18: Result for the neutron leakage spectrum for the Oktavian Al benchmark.

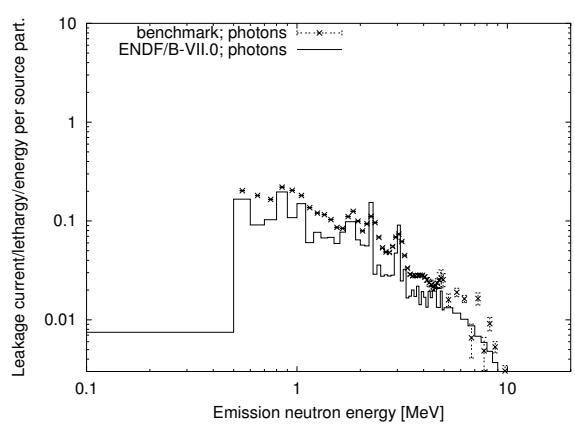

FIG. 19: Result for the photon leakage spectrum for the Oktavian Al benchmark.

TABLE XXVII: C/E values for the neutron spectrum of the Oktavian Al benchmark.

	energy range [MeV]	C/E
Al	0.1−1.0	1.00 ± 0.01
Al	1.0−5.0	0.90 ± 0.01
Al	5.0−10.0	0.92 ± 0.01
Al	10.0−20.0	1.06 ± 0.01

TABLE XXVIII: C/E values for the neutron spectrum of the Oktavian Co benchmark.

	energy range [MeV]	C/E
Co	0.1−1.0	0.64 ± 0.01
Co	1.0−5.0	0.66 ± 0.01
Co	5.0−10.0	0.55 ± 0.01
Co	10.0−20.0	0.98 ± 0.01

2. *Oktavian, Co*

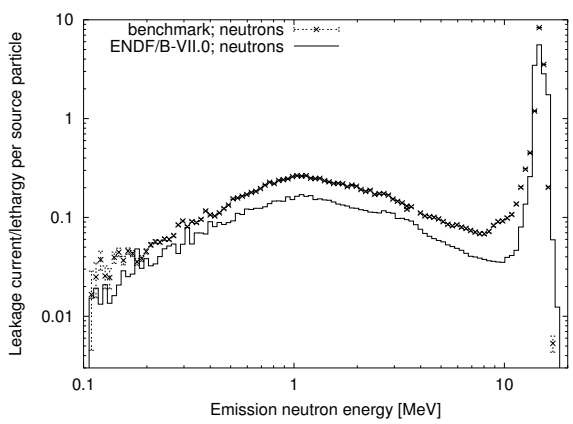

FIG. 20: Result for the neutron leakage spectrum for the Oktavian Co benchmark.

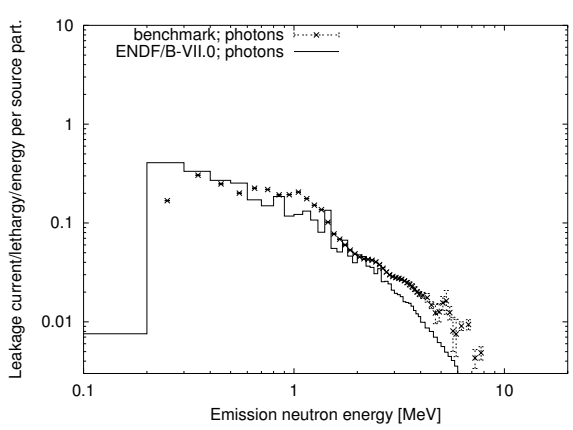

FIG. 21: Result for the photon leakage spectrum for the Oktavian Co benchmark.

3. *Oktavian, Cr*

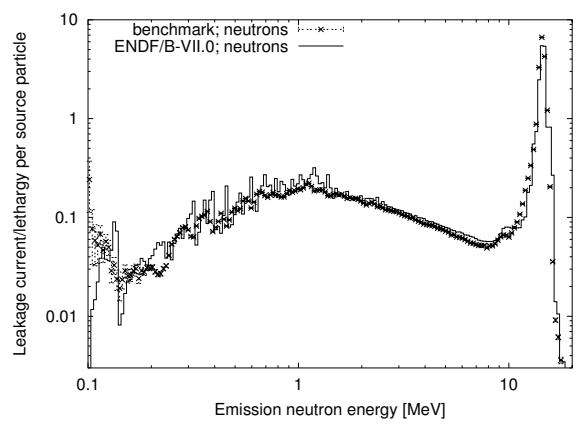

FIG. 22: Result for the neutron leakage spectrum for the Oktavian Cr benchmark.

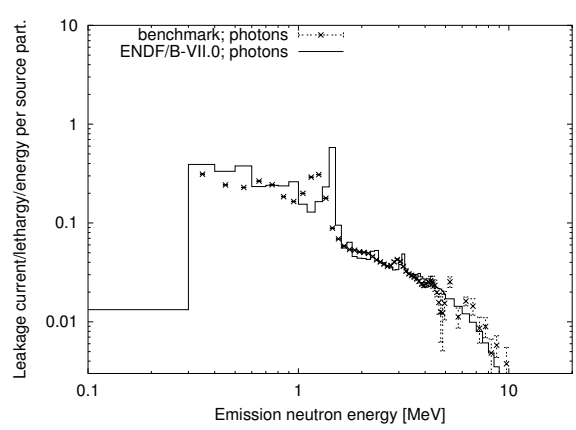

FIG. 23: Result for the photon leakage spectrum for the Oktavian Cr benchmark.

TABLE XXIX: C/E values for the neutron spectrum of the Oktavian Cr benchmark.

	energy range [MeV]	C/E
Cr	0.1−1.0	1.10 ± 0.02
Cr	1.0−5.0	1.14 ± 0.01
Cr	5.0−10.0	1.12 ± 0.01
Cr	10.0−20.0	0.96 ± 0.01

TABLE XXX: C/E values for the neutron spectrum of the Oktavian Cu benchmark.

	energy range [MeV]	C/E
Cu	0.1−1.0	1.07 ± 0.01
Cu	1.0−5.0	1.11 ± 0.01
Cu	5.0−10.0	1.37 ± 0.02
Cu	10.0−20.0	1.12 ± 0.01

4. Oktavian, Cu

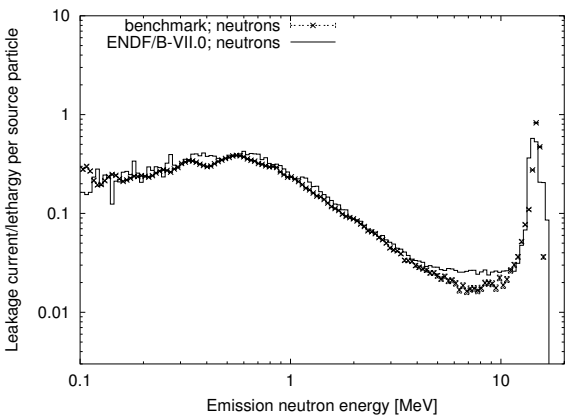

FIG. 24: Result for the neutron leakage spectrum for the Oktavian Cu benchmark.

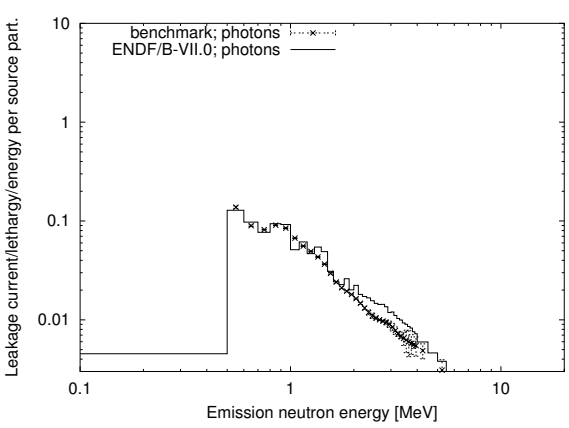

FIG. 25: Result for the photon leakage spectrum for the Oktavian Cu benchmark.

5. Oktavian, LiF

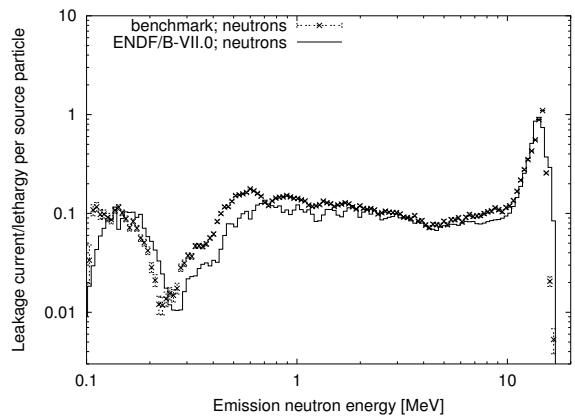

FIG. 26: Result for the neutron leakage spectrum for the Oktavian LiF benchmark.

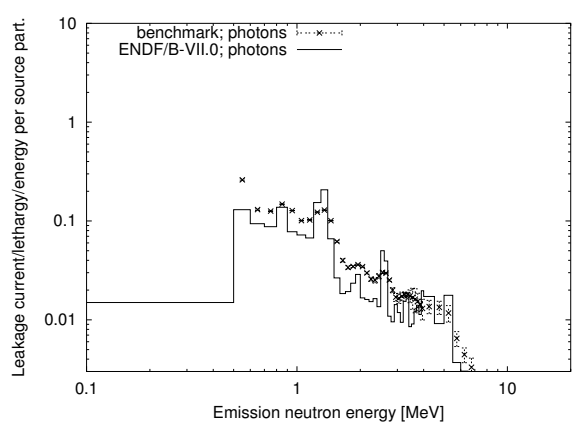

FIG. 27: Result for the photon leakage spectrum for the Oktavian LiF benchmark.

TABLE XXXI: C/E values for the neutron spectrum of the Oktavian LiF benchmark.

	energy range [MeV]	C/E
LiF	0.1−1.0	0.76 ± 0.01
LiF	1.0−5.0	0.88 ± 0.01
LiF	5.0−10.0	0.85 ± 0.01
LiF	10.0−20.0	1.09 ± 0.01

6. *Oktavian, Mn*

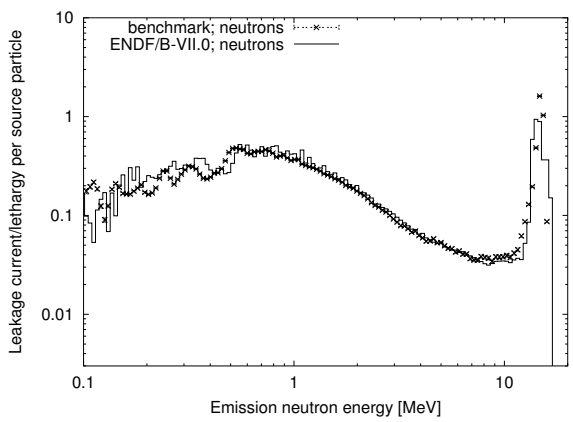

FIG. 28: Result for the neutron leakage spectrum for the Oktavian Mn benchmark.

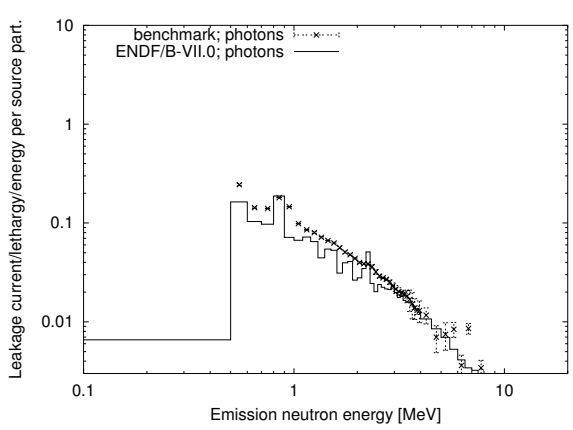

FIG. 29: Result for the photon leakage spectrum for the Oktavian Mn benchmark.

TABLE XXXII: C/E values for the neutron spectrum of the Oktavian Mn benchmark.

	energy range [MeV]	C/E
Mn	0.1−1.0	1.06 ± 0.01
Mn	1.0−5.0	1.10 ± 0.01
Mn	5.0−10.0	0.98 ± 0.01
Mn	10.0−20.0	0.94 ± 0.01

7. *Oktavian, Mo*

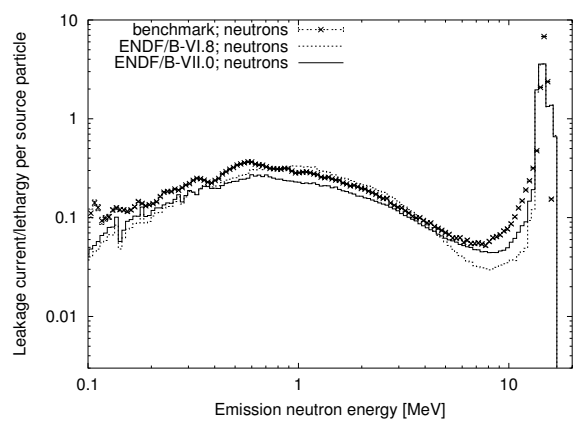

FIG. 30: Result for the neutron leakage spectrum for the Oktavian Mo benchmark.

TABLE XXXIII: C/E values for the neutron spectrum of the Oktavian Mo benchmark.

	energy range [MeV]	C/E
Mo	0.1−1.0	0.76 ± 0.01
Mo	1.0−5.0	0.84 ± 0.01
Mo	5.0−10.0	0.82 ± 0.01
Mo	10.0−20.0	1.01 ± 0.01

8. *Oktavian, Si*

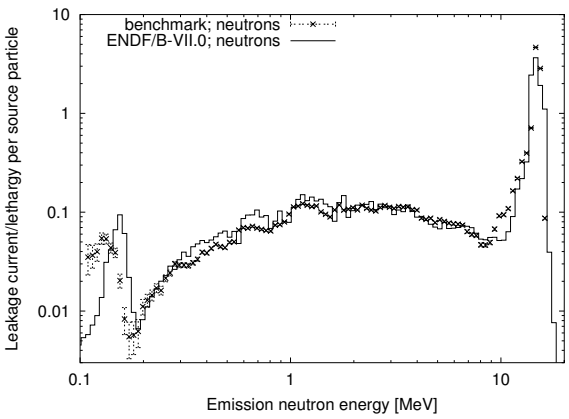

FIG. 31: Result for the neutron leakage spectrum for the Oktavian Si benchmark.

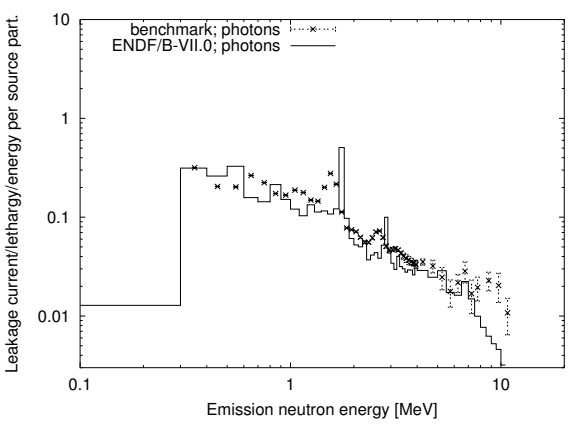

FIG. 32: Result for the photon leakage spectrum for the Oktavian Si benchmark.

TABLE XXXIV: C/E values for the neutron spectrum of the Oktavian Si benchmark.

	energy range [MeV]	C/E
Si	0.1−1.0	1.13 ± 0.02
Si	1.0−5.0	1.05 ± 0.01
Si	5.0−10.0	0.98 ± 0.01
Si	10.0−20.0	1.05 ± 0.01

9. *Oktavian, Ti*

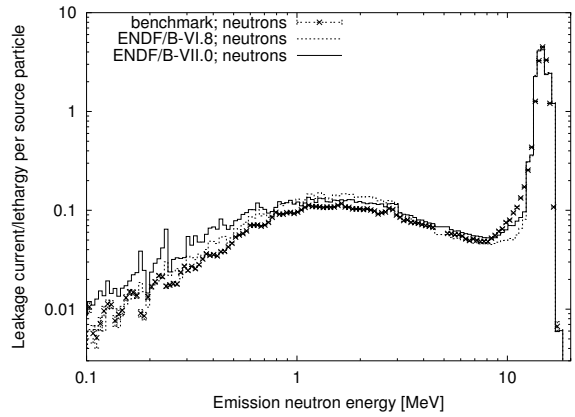

FIG. 33: Result for the neutron leakage spectrum for the Oktavian Ti benchmark.

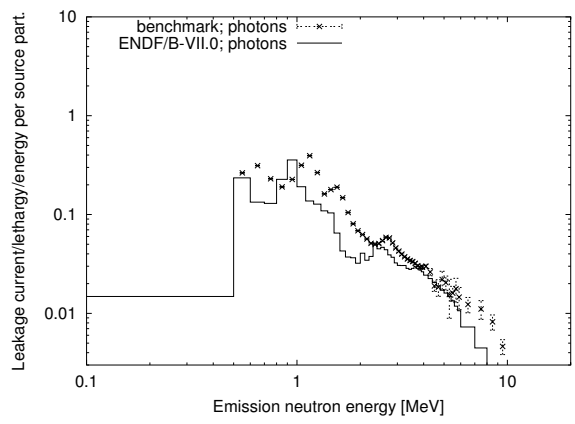

FIG. 34: Result for the photon leakage spectrum for the Oktavian Ti benchmark.

TABLE XXXV: C/E values for the neutron spectrum of the Oktavian Ti benchmark.

	energy range [MeV]	C/E
Ti	0.0−0.1	1.16 ± 0.11
Ti	0.1−1.0	1.51 ± 0.01
Ti	1.0−5.0	1.16 ± 0.01
Ti	5.0−10.0	1.07 ± 0.01
Ti	10.0−20.0	1.18 ± 0.01

10. Oktavian, W

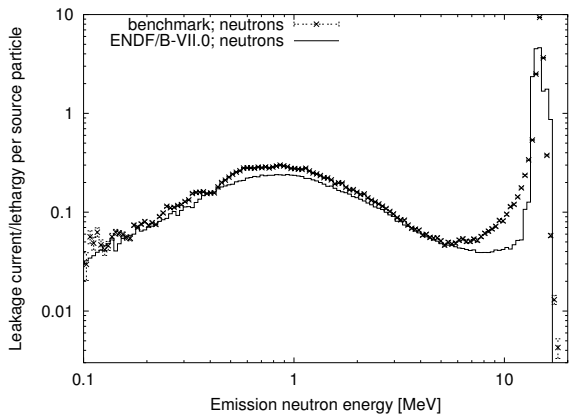

FIG. 35: Result for the neutron leakage spectrum for the Oktavian W benchmark.

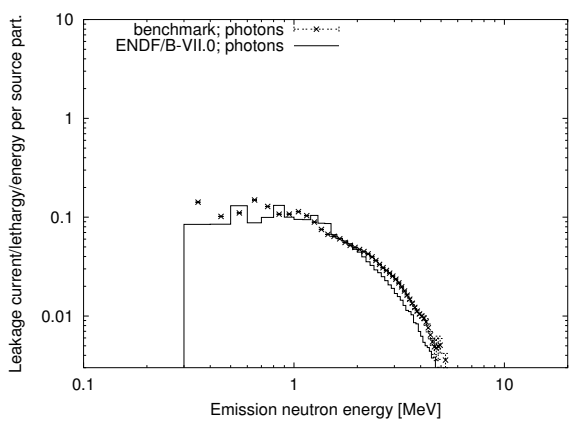

FIG. 36: Result for the photon leakage spectrum for the Oktavian W benchmark.

TABLE XXXVI: C/E values for the neutron spectrum of the Oktavian W benchmark.

	energy range [MeV]	C/E
W	0.1−1.0	0.85 ± 0.01
W	1.0−5.0	0.88 ± 0.01
W	5.0−10.0	0.75 ± 0.01
W	10.0−20.0	0.91 ± 0.01

11. Oktavian, Zr

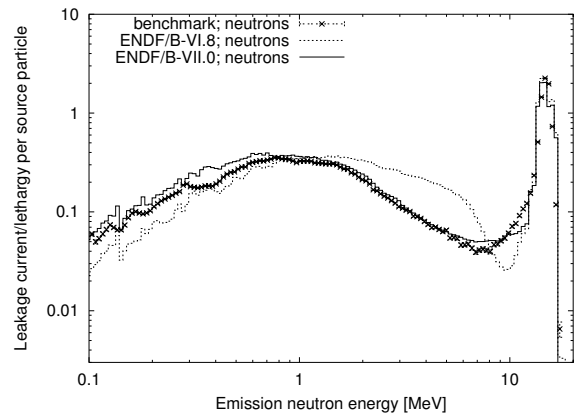

FIG. 37: Result for the neutron leakage spectrum for the Oktavian Zr benchmark.

TABLE XXXVII: C/E values for the neutron spectrum of the Oktavian Zr benchmark.

	energy range [MeV]	C/E
Zr	0.0−0.1	0.95 ± 0.04
Zr	0.1−1.0	1.21 ± 0.01
Zr	1.0−5.0	1.09 ± 0.01
Zr	5.0−10.0	1.12 ± 0.01
Zr	10.0−20.0	1.12 ± 0.01

B. Fusion Neutronics Source (FNS)

1. Calculational methods

For each of the experiments mentioned in Section IV the neutron source spectrum was taken from the underlying reference. Hence, in Oktavian and FNS analyses an isotropic neutron distribution was assumed. However, it is known that the neutron source has a peak energy of 14.8 MeV in the forward direction, and a peak at 13.3 MeV in the backward direction (see Ref. [19]).

The assumption of isotropy will slightly influence the calculated angular spectra for the FNS benchmarks. This influence is expected to be of the order of several percent only.

2. FNS, Be, 5 cm and 15 cm

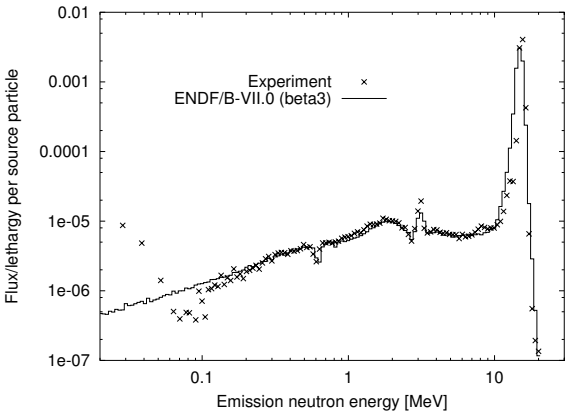

FIG. 38: Neutron spectrum for the FNS, Be, d=5cm benchmark at 0° angle.

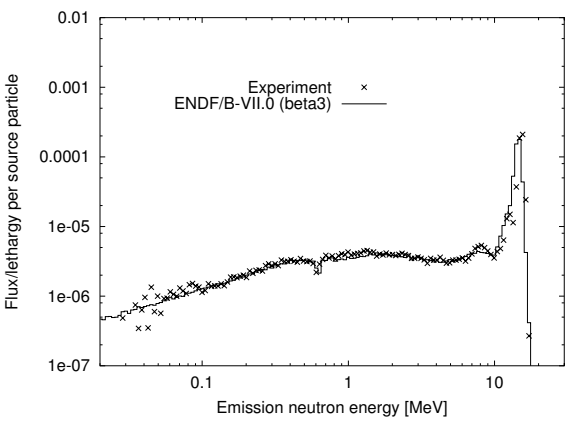

FIG. 39: Neutron spectrum for the FNS, Be, d=5cm benchmark at 24.9° angle.

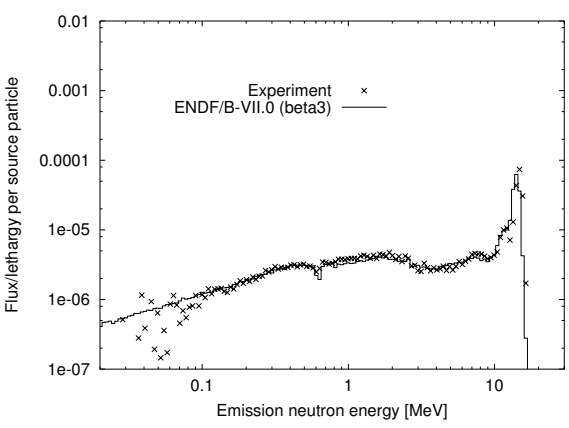

FIG. 40: Neutron spectrum for the FNS, Be, d=5cm benchmark at 42.8° angle.

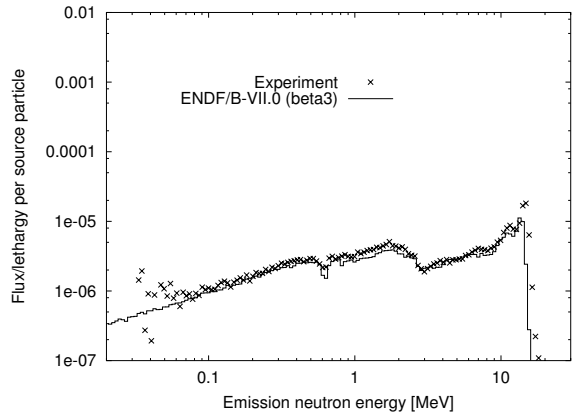

FIG. 41: Neutron spectrum for the FNS, Be, d=5cm benchmark at 66.8° angle.

TABLE XXXVIII: C/E values for the spectrum of the FNS Be 5cm benchmark.

energy [MeV]	0°	12.2°	24.9°	42.8°	66.8°
0.1−1.0	0.97±0.01	n.a.	0.93±0.01	0.95±0.01	0.87±0.01
1.0−5.0	0.91±0.01	n.a.	0.96±0.01	0.95±0.01	0.86±0.01
5.0−10.0	0.92±0.01	n.a.	0.94±0.01	0.94±0.01	0.86±0.01
10.0−20.0	0.95±0.01	n.a.	0.96±0.01	0.95±0.01	0.68±0.01

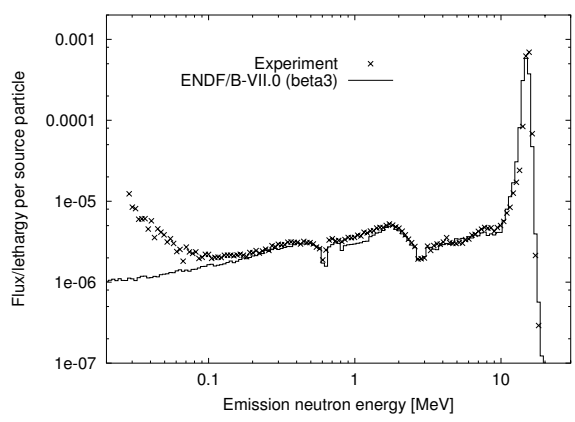

FIG. 42: Neutron spectrum for the FNS, Be, d=15cm benchmark at 0° angle.

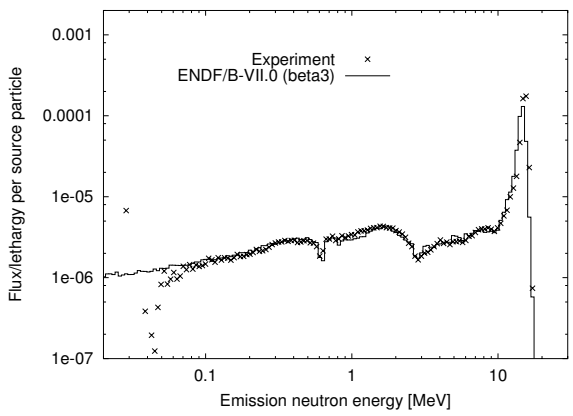

FIG. 43: Neutron spectrum for the FNS, Be, d=15cm benchmark at 12.2° angle.

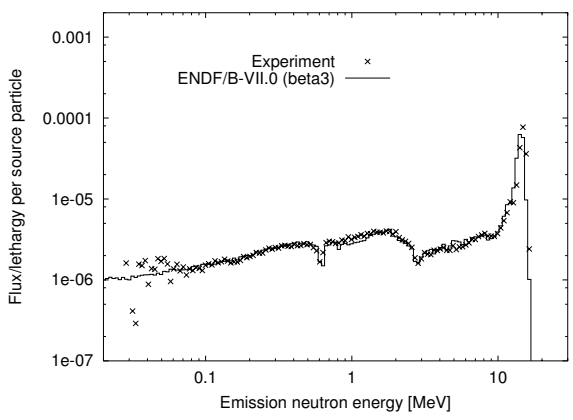

FIG. 44: Neutron spectrum for the FNS, Be, d=15cm benchmark at 24.9° angle.

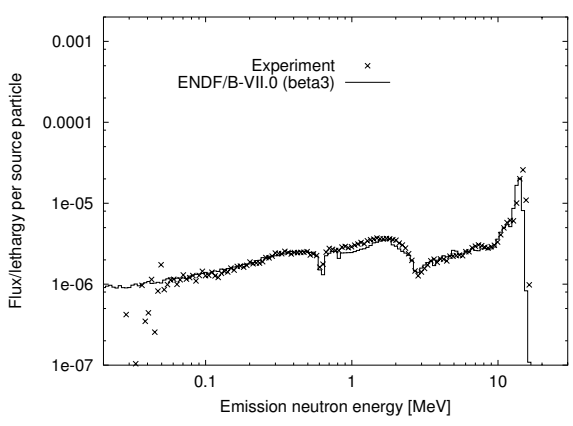

FIG. 45: Neutron spectrum for the FNS, Be, d=15cm benchmark at 42.8° angle.

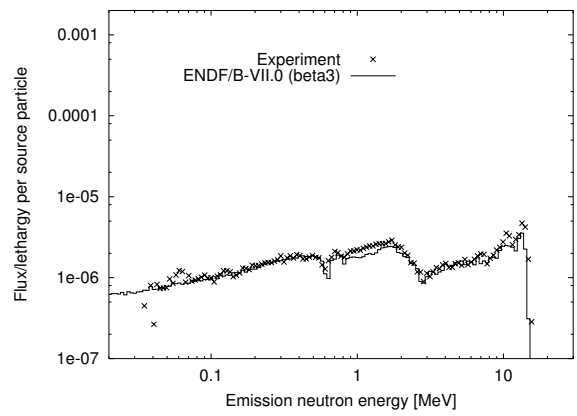

FIG. 46: Neutron spectrum for the FNS, Be, d=15cm benchmark at 66.8° angle.

TABLE XXXIX: C/E values for the spectrum of the FNS Be 15cm benchmark.

energy [MeV]	0°	12.2°	24.9°	42.8°	66.8°
0.1−1.0	0.88±0.01	1.00±0.01	0.98±0.01	0.97±0.01	0.93±0.01
1.0−5.0	0.92±0.01	0.97±0.01	0.97±0.01	0.93±0.01	0.89±0.01
5.0−10.0	0.91±0.01	0.99±0.01	1.01±0.01	0.95±0.01	0.89±0.02
10.0−20.0	0.96±0.01	0.80±0.01	1.00±0.01	0.82±0.01	0.79±0.02

3. FNS, C, 5 cm, 20 cm and 40 cm

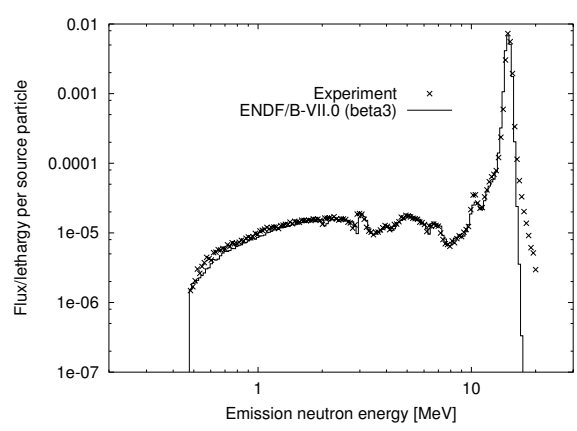

FIG. 47: Neutron spectrum for the FNS, C, d=5cm benchmark at 0° angle.

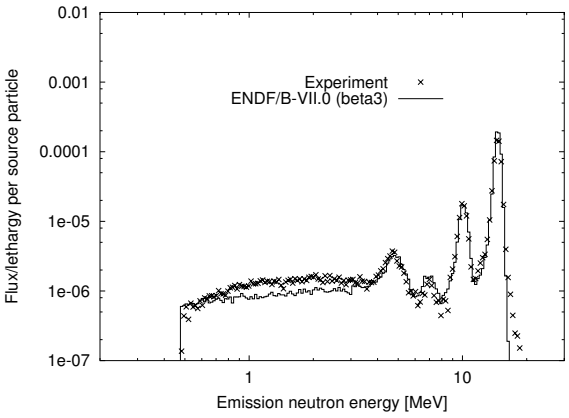

FIG. 48: Neutron spectrum for the FNS, C, d=5cm benchmark at 24.9° angle.

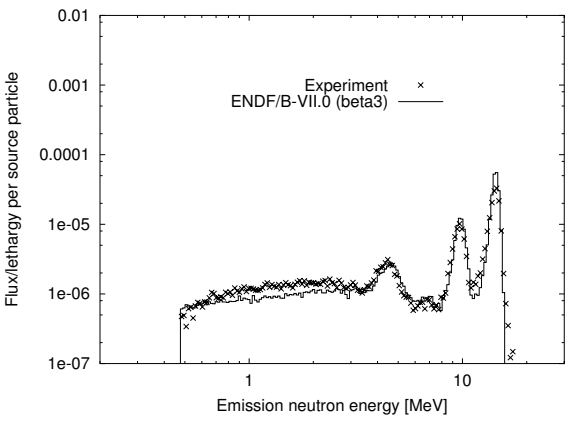

FIG. 49: Neutron spectrum for the FNS, C, d=5cm benchmark at 42.8° angle.

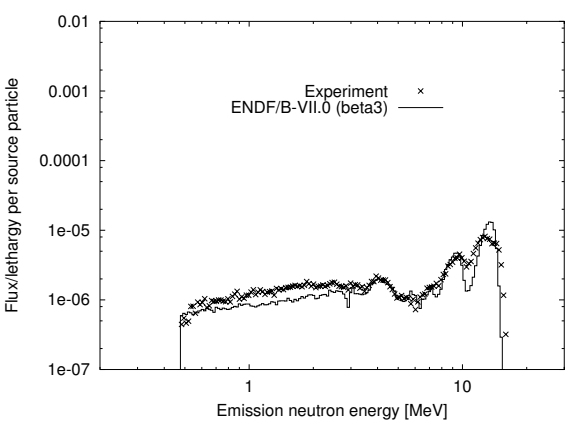

FIG. 50: Neutron spectrum for the FNS, C, d=5cm benchmark at 66.8° angle.

TABLE XL: C/E values for the spectrum of the FNS C 5cm benchmark.

energy [MeV]	0°	12.2°	24.9°	42.8°	66.8°
0.1−1.0	0.81±0.01	n.a.	0.84±0.01	0.83±0.01	0.77±0.01
1.0−5.0	0.94±0.01	n.a.	0.73±0.01	0.79±0.01	0.76±0.01
5.0−10.0	1.01±0.01	n.a.	0.83±0.01	0.93±0.01	0.95±0.01
10.0−20.0	1.01±0.01	n.a.	1.23±0.01	1.39±0.01	1.01±0.01

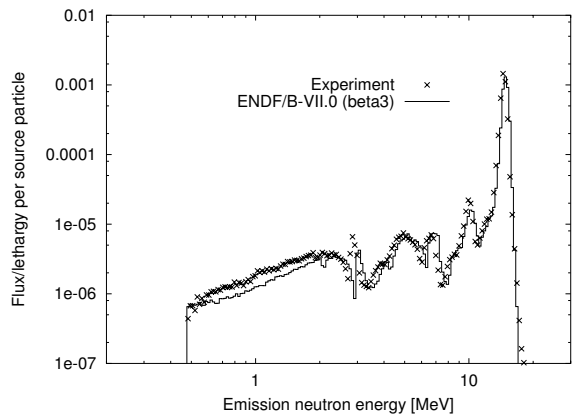

FIG. 51: Neutron spectrum for the FNS, C, d=20cm benchmark at 0° angle.

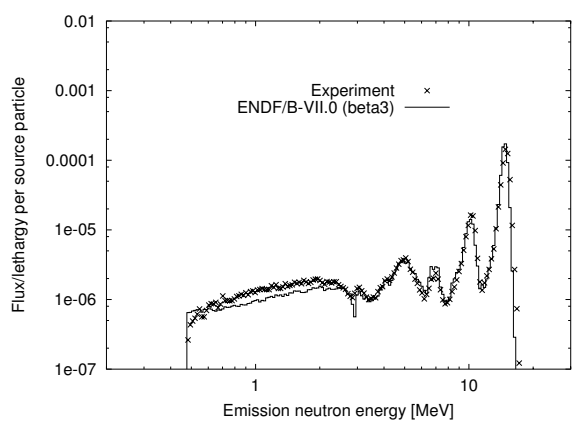

FIG. 52: Neutron spectrum for the FNS, C, d=20cm benchmark at 12.2° angle.

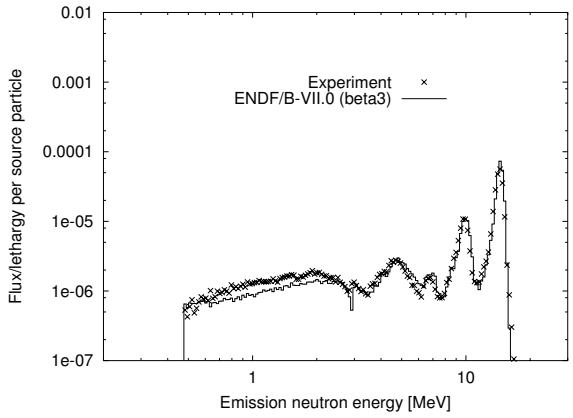

FIG. 53: Neutron spectrum for the FNS, C, d=20cm benchmark at 24.9° angle.

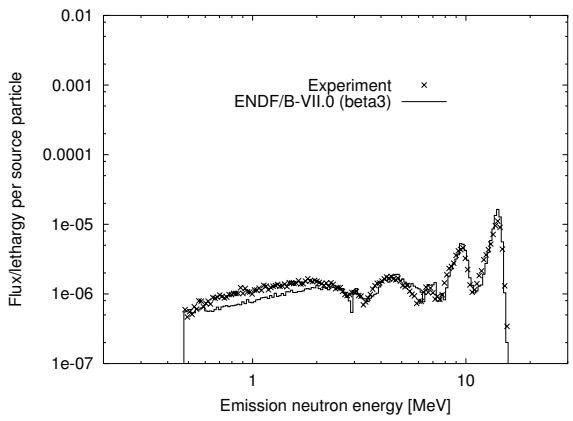

FIG. 54: Neutron spectrum for the FNS, C, d=20cm benchmark at 42.8° angle.

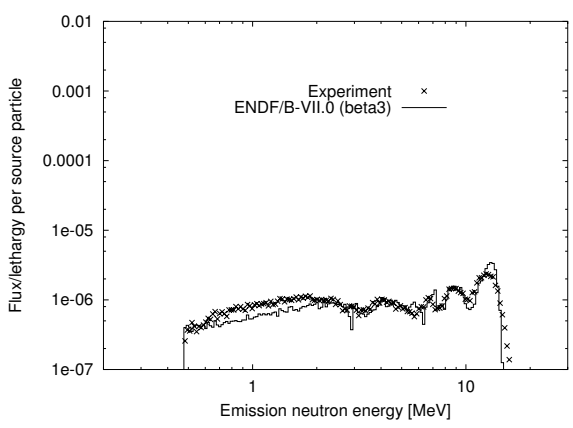

FIG. 55: Neutron spectrum for the FNS, C, d=20cm benchmark at 66.8° angle.

TABLE XLI: C/E values for the spectrum of the FNS C 20cm benchmark.

energy [MeV]	0°	12.2°	24.9°	42.8°	66.8°
0.1−1.0	0.72±0.01	0.82±0.01	0.76±0.01	0.72±0.01	0.75±0.01
1.0−5.0	0.77±0.01	0.81±0.01	0.81±0.01	0.84±0.01	0.83±0.01
5.0−10.0	0.90±0.01	1.01±0.01	0.89±0.01	1.01±0.01	1.04±0.01
10.0−20.0	0.98±0.01	1.07±0.01	1.20±0.01	1.24±0.01	1.07±0.01

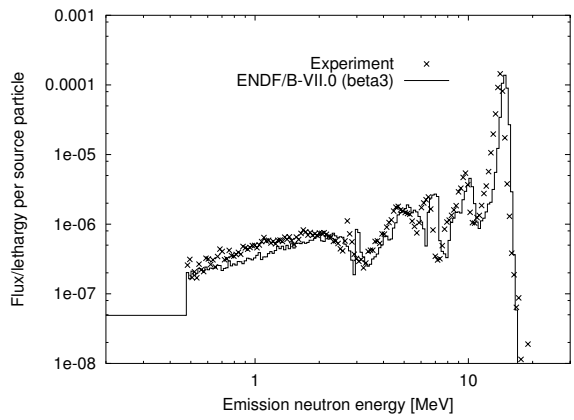

FIG. 56: Neutron spectrum for the FNS, C, d=40cm benchmark at 0° angle.

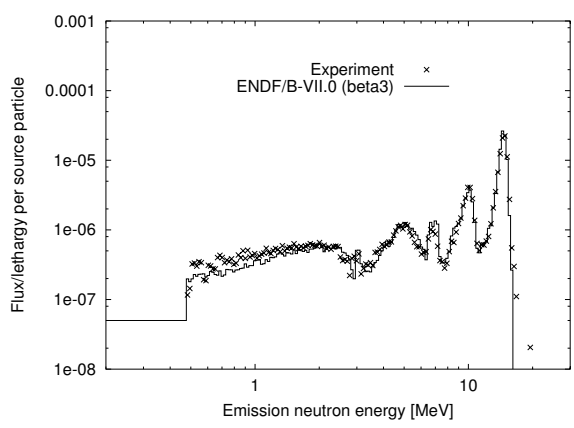

FIG. 57: Neutron spectrum for the FNS, C, d=40cm benchmark at 12.2° angle.

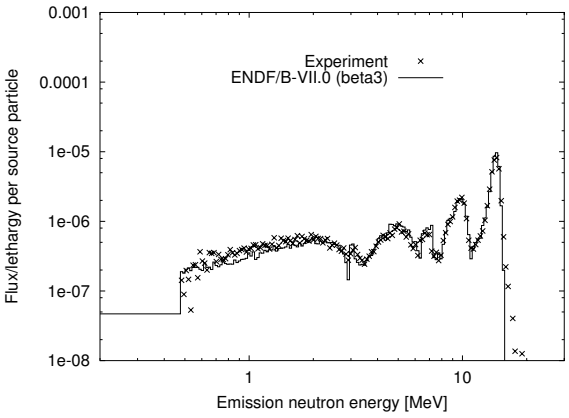

FIG. 58: Neutron spectrum for the FNS, C, d=40cm benchmark at 24.9° angle.

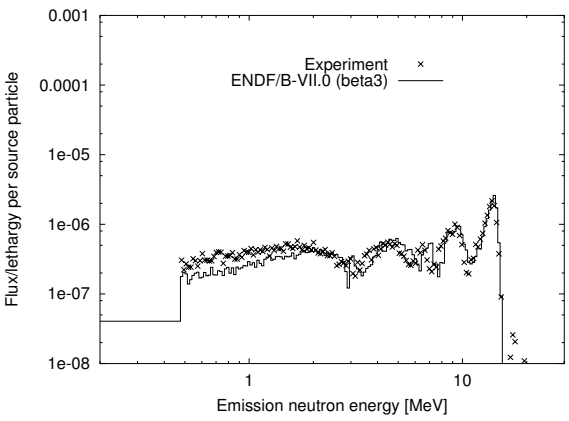

FIG. 59: Neutron spectrum for the FNS, C, d=40cm benchmark at 42.8° angle.

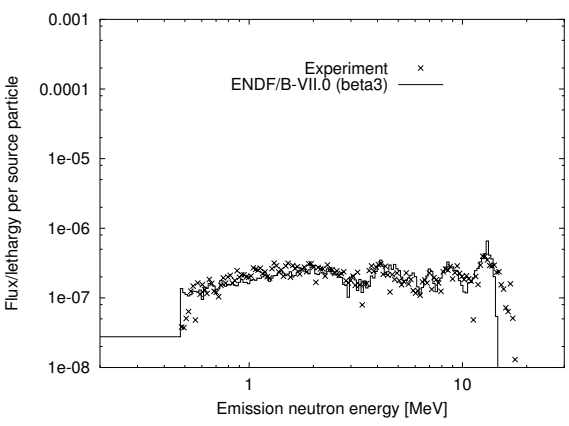

FIG. 60: Neutron spectrum for the FNS, C, d=40cm benchmark at 66.8° angle.

TABLE XLII: C/E values for the spectrum of the FNS C 40cm benchmark.

energy [MeV]	0°	12.2°	24.9°	42.8°	66.8°
0.1−1.0	0.71±0.01	0.70±0.01	0.80±0.01	0.60±0.02	0.94±0.02
1.0−5.0	0.78±0.01	0.90±0.01	0.91±0.01	0.86±0.01	0.91±0.01
5.0−10.0	0.85±0.01	1.02±0.01	1.01±0.01	1.05±0.02	1.12±0.02
10.0−20.0	1.03±0.01	1.08±0.01	1.09±0.01	1.14±0.02	0.94±0.04

4. FNS, N, 20 cm

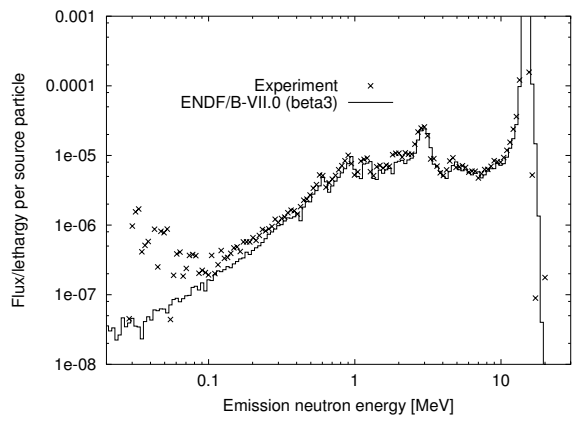

FIG. 61: Neutron spectrum for the FNS, N, d=20cm benchmark at 0° angle.

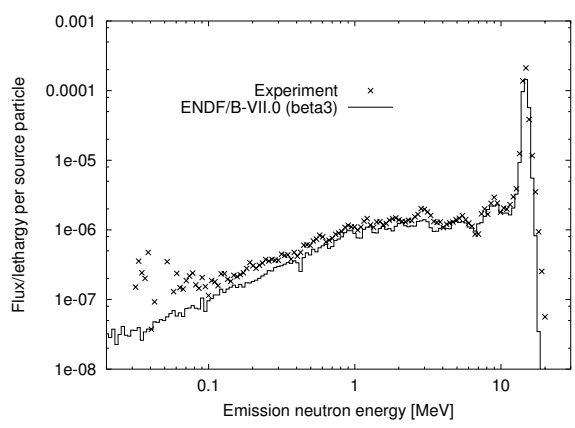

FIG. 62: Neutron spectrum for the FNS, N, d=20cm benchmark at 12.2° angle.

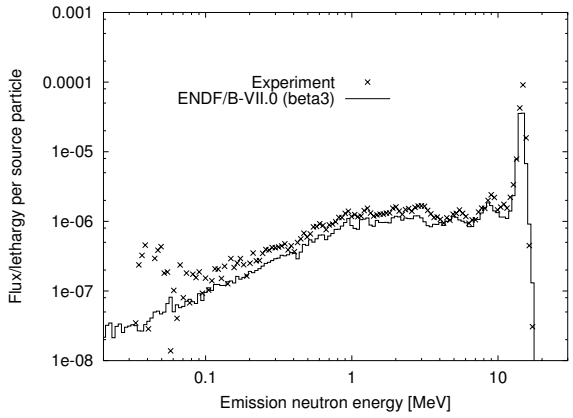

FIG. 63: Neutron spectrum for the FNS, N, d=20cm benchmark at 24.9° angle.

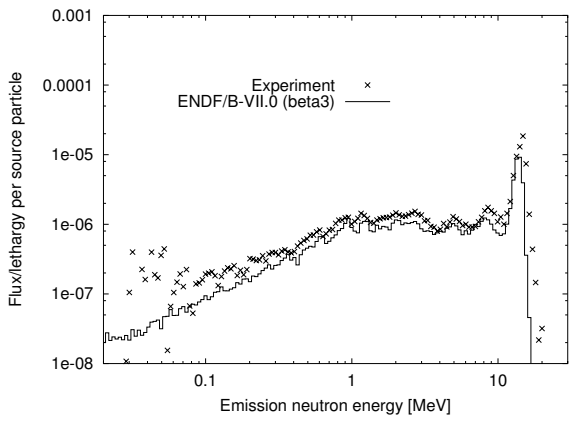

FIG. 64: Neutron spectrum for the FNS, N, d=20cm benchmark at 42.8° angle.

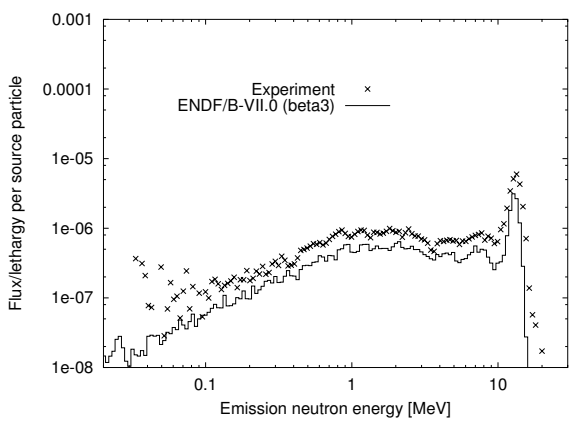

FIG. 65: Neutron spectrum for the FNS, N, d=20cm benchmark at 66.8° angle.

TABLE XLIII: C/E values for the spectrum of the FNS N 20cm benchmark.

energy [MeV]	0°	12.2°	24.9°	42.8°	66.8°
0.1−1.0	0.80±0.01	0.72±0.01	0.68±0.01	0.70±0.01	0.56±0.01
1.0−5.0	0.86±0.01	0.79±0.01	0.75±0.01	0.77±0.01	0.63±0.01
5.0−10.0	0.92±0.01	0.89±0.01	0.82±0.01	0.78±0.01	0.57±0.02
10.0−20.0	0.85±0.01	0.76±0.01	0.57±0.01	0.51±0.01	0.42±0.01

5. *FNS, O, 20 cm*

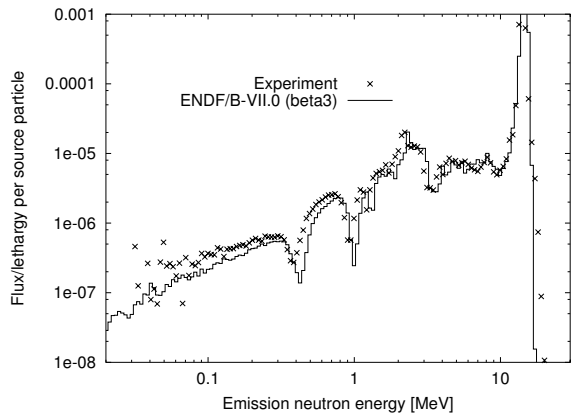

FIG. 66: Neutron spectrum for the FNS, O, d=20cm benchmark at 0° angle.

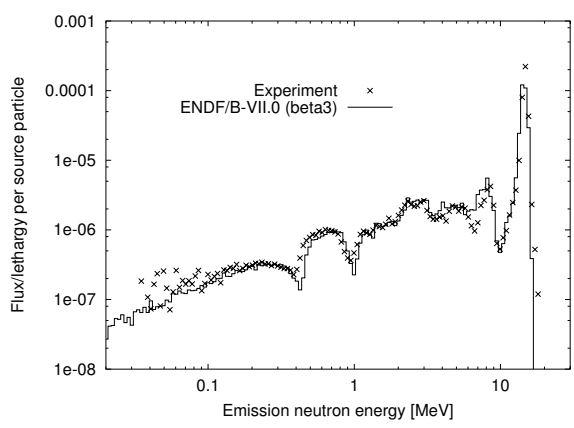

FIG. 67: Neutron spectrum for the FNS, O, d=20cm benchmark at 12.2° angle.

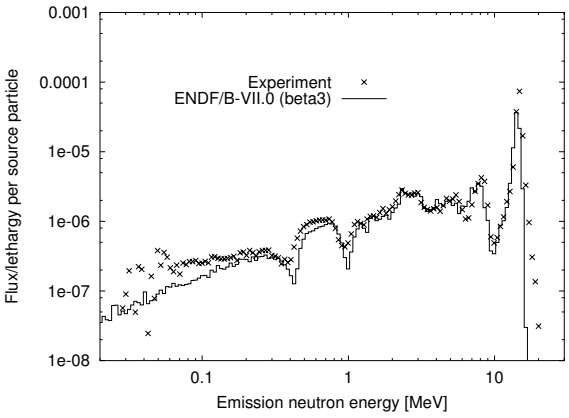

FIG. 68: Neutron spectrum for the FNS, O, d=20cm benchmark at 24.9° angle.

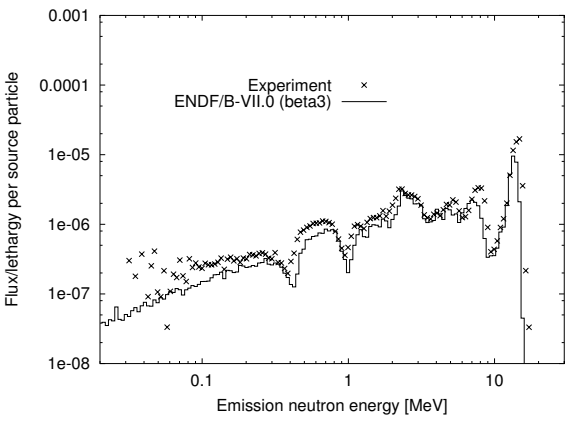

FIG. 69: Neutron spectrum for the FNS, O, d=20cm benchmark at 42.8° angle.

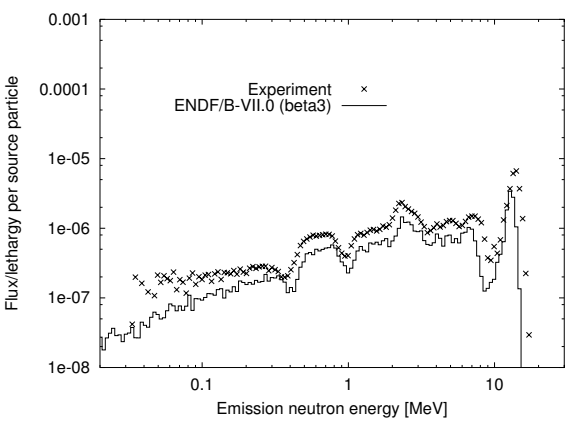

FIG. 70: Neutron spectrum for the FNS, O, d=20cm benchmark at 66.8° angle.

TABLE XLIV: C/E values for the spectrum of the FNS O 20cm benchmark.

energy [MeV]	0°	12.2°	24.9°	42.8°	66.8°
0.1−1.0	0.79±0.01	0.89±0.01	0.78±0.01	0.70±0.01	0.62±0.01
1.0−5.0	0.84±0.01	1.03±0.01	0.91±0.01	0.78±0.01	0.58±0.01
5.0−10.0	1.07±0.01	1.32±0.01	0.95±0.01	0.74±0.01	0.55±0.01
10.0−20.0	0.89±0.01	0.81±0.01	0.55±0.01	0.51±0.01	0.41±0.01

6. *FNS, Fe, 5 cm, 20 cm, 40 cm, 60 cm*

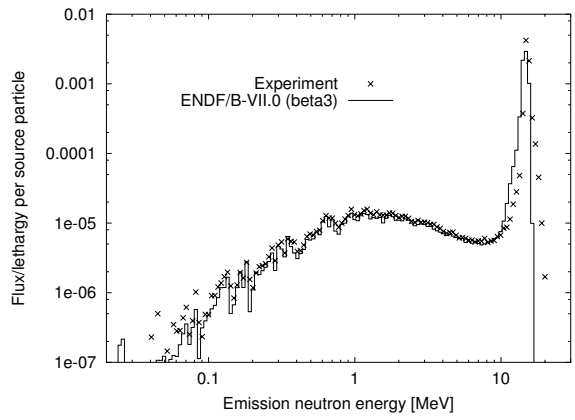

FIG. 71: Neutron spectrum for the FNS, Fe, d=5cm benchmark at 0° angle.

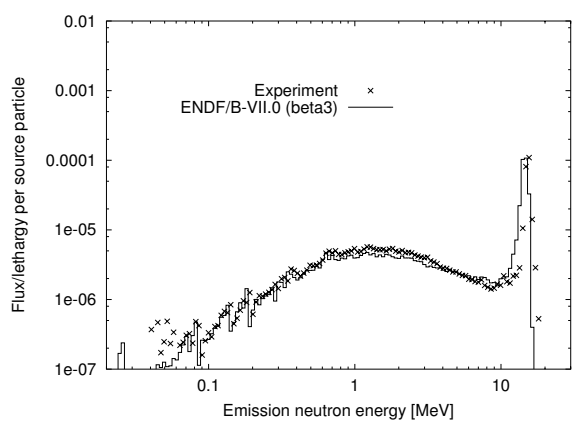

FIG. 72: Neutron spectrum for the FNS, Fe, d=5cm benchmark at 24.9° angle.

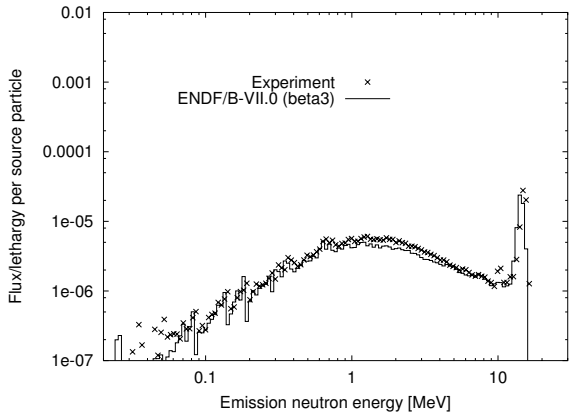

FIG. 73: Neutron spectrum for the FNS, Fe, d=5cm benchmark at 42.8° angle.

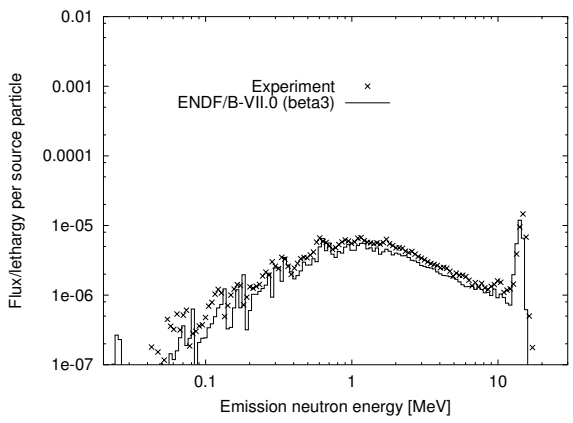

FIG. 74: Neutron spectrum for the FNS, Fe, d=5cm benchmark at 66.8° angle.

TABLE XLV: C/E values for the spectrum of the FNS Fe 5cm benchmark.

energy [MeV]	0°	12.2°	24.9°	42.8°	66.8°
0.1−1.0	0.83±0.01	n.a.	0.85±0.01	0.84±0.01	0.76±0.01
1.0−5.0	0.90±0.01	n.a.	0.85±0.01	0.83±0.01	0.82±0.01
5.0−10.0	0.95±0.01	n.a.	1.13±0.02	0.97±0.02	0.85±0.02
10.0−20.0	0.91±0.01	n.a.	1.24±0.01	0.92±0.01	0.73±0.01

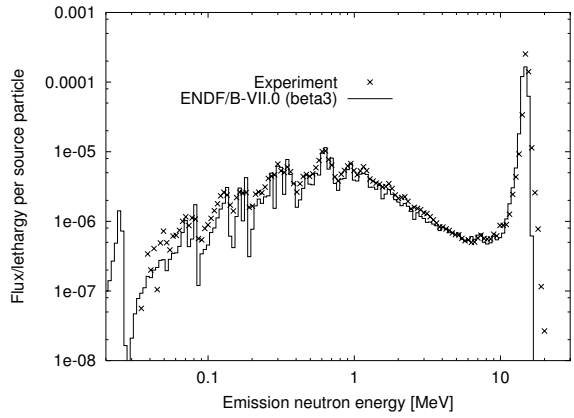

FIG. 75: Neutron spectrum for the FNS, Fe, d=20cm benchmark at 0° angle.

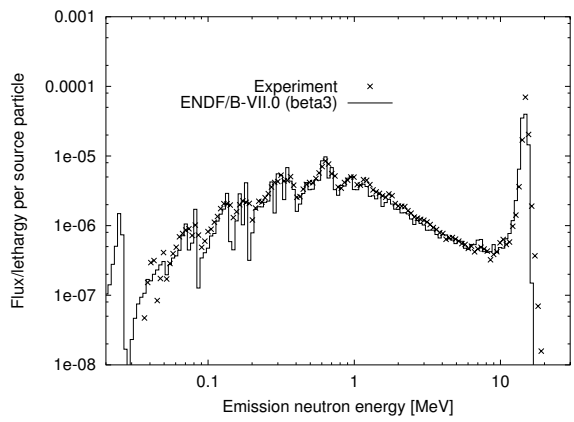

FIG. 76: Neutron spectrum for the FNS, Fe, d=20cm benchmark at 12.2° angle.

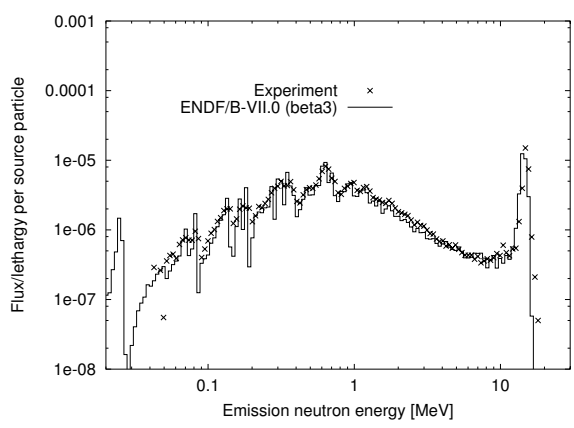

FIG. 77: Neutron spectrum for the FNS, Fe, d=20cm benchmark at 24.9° angle.

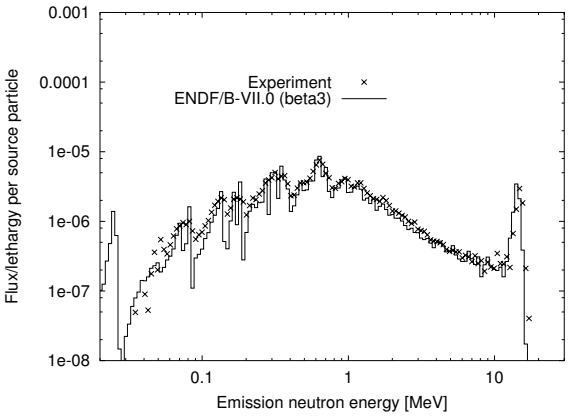

FIG. 78: Neutron spectrum for the FNS, Fe, d=20cm benchmark at 42.8° angle.

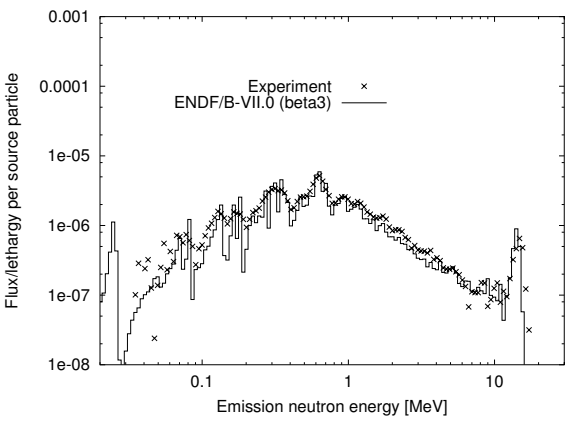

FIG. 79: Neutron spectrum for the FNS, Fe, d=20cm benchmark at 66.8° angle.

TABLE XLVI: C/E values for the spectrum of the FNS Fe 20cm benchmark.

energy [MeV]	0°	12.2°	24.9°	42.8°	66.8°
0.1−1.0	0.82±0.01	0.89±0.01	0.89±0.01	0.85±0.01	0.85±0.01
1.0−5.0	0.88±0.01	0.88±0.01	0.88±0.01	0.87±0.01	0.83±0.01
5.0−10.0	0.96±0.03	1.09±0.03	1.01±0.03	1.02±0.04	1.11±0.06
10.0−20.0	0.82±0.01	0.87±0.01	1.03±0.02	1.04±0.03	0.95±0.05

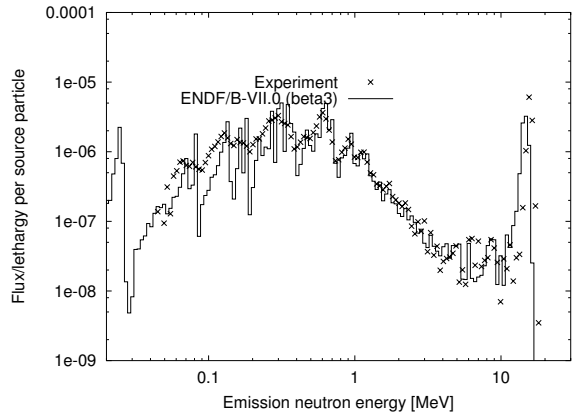

FIG. 80: Neutron spectrum for the FNS, Fe, d=40cm benchmark at 0° angle.

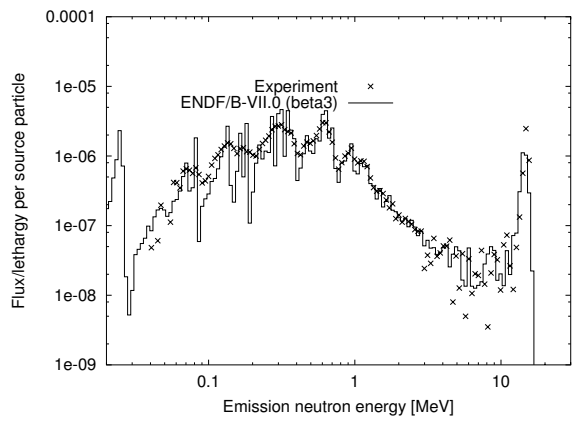

FIG. 81: Neutron spectrum for the FNS, Fe, d=40cm benchmark at 12.2° angle.

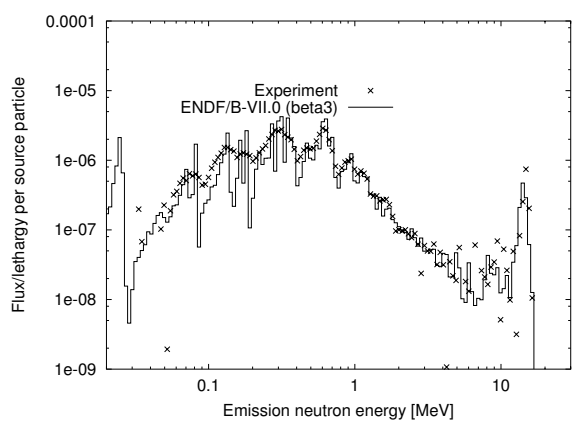

FIG. 82: Neutron spectrum for the FNS, Fe, d=40cm benchmark at 24.9° angle.

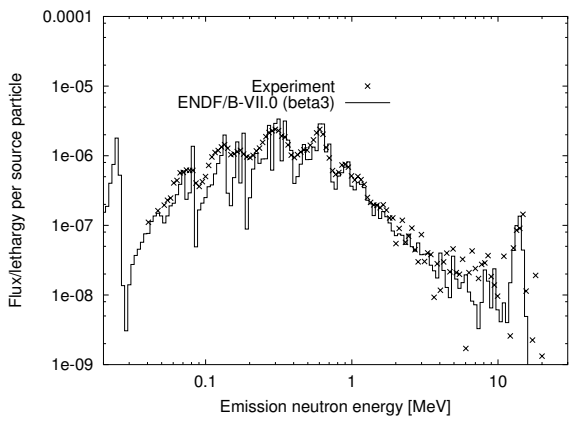

FIG. 83: Neutron spectrum for the FNS, Fe, d=40cm benchmark at 42.8° angle.

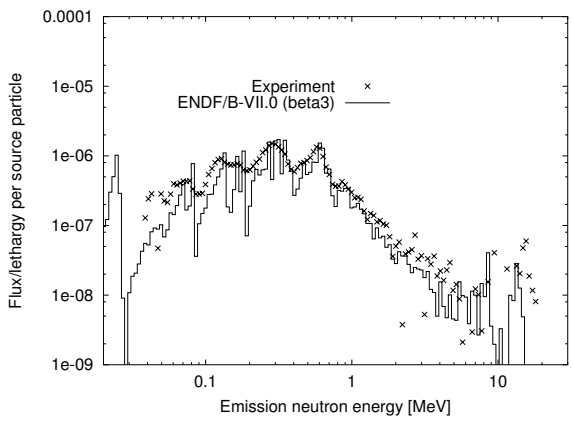

FIG. 84: Neutron spectrum for the FNS, Fe, d=40cm benchmark at 66.8° angle.

TABLE XLVII: C/E values for the spectrum of the FNS Fe 40cm benchmark.

energy [MeV]	0°	12.2°	24.9°	42.8°	66.8°
0.1−1.0	0.91±0.01	0.97±0.01	0.91±0.01	0.85±0.01	0.77±0.01
1.0−5.0	0.98±0.01	1.01±0.01	1.01±0.02	0.91±0.02	0.77±0.03
5.0−10.0	0.95±0.12	1.32±0.11	1.07±0.13	0.66±0.15	n.a.
10.0−20.0	0.76±0.02	0.71±0.05	0.86±0.08	0.84±0.14	n.a.

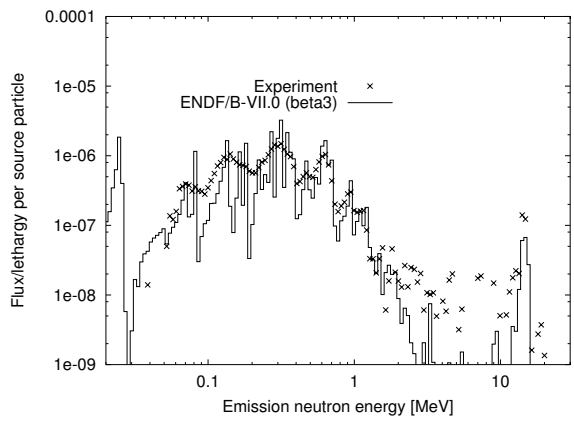

FIG. 85: Neutron spectrum for the FNS, Fe, d=60cm benchmark at 0° angle.

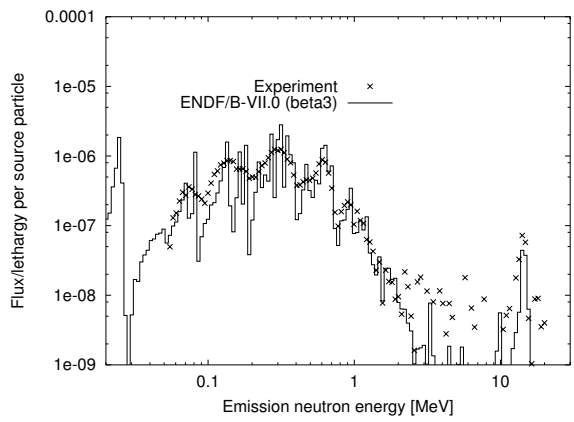

FIG. 86: Neutron spectrum for the FNS, Fe, d=60cm benchmark at 12.2° angle.

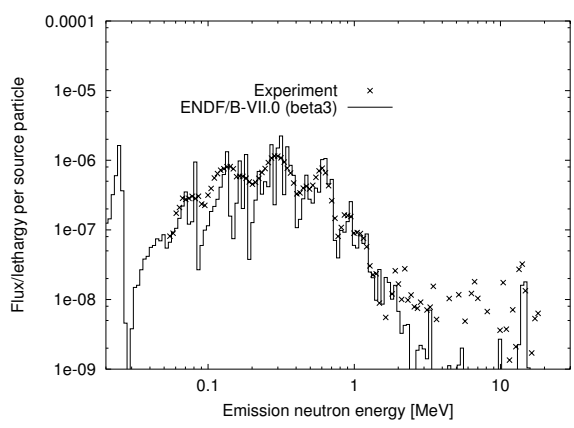

FIG. 87: Neutron spectrum for the FNS, Fe, d=60cm benchmark at 24.9° angle.

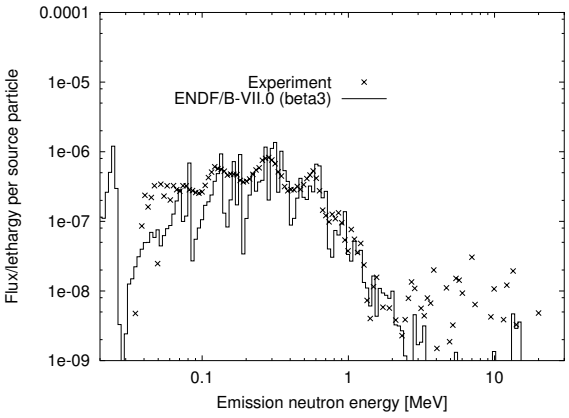

FIG. 88: Neutron spectrum for the FNS, Fe, d=60cm benchmark at 42.8° angle.

TABLE XLVIII: C/E values for the spectrum of the FNS Fe 60cm benchmark.

energy [MeV]	0°	12.2°	24.9°	42.8°	66.8°
0.1−1.0	0.91±0.01	0.98±0.01	0.90±0.01	0.91±0.01	n.a.
1.0−5.0	0.85±0.03	0.94±0.03	1.04±0.04	0.90±0.07	n.a.
5.0−10.0	n.a.	n.a.	n.a.	n.a.	n.a.
10.0−20.0	0.52±0.10	0.49±0.19	n.a.	n.a.	n.a.

7. *FNS, Pb, 5 cm, 20 cm and 40 cm*

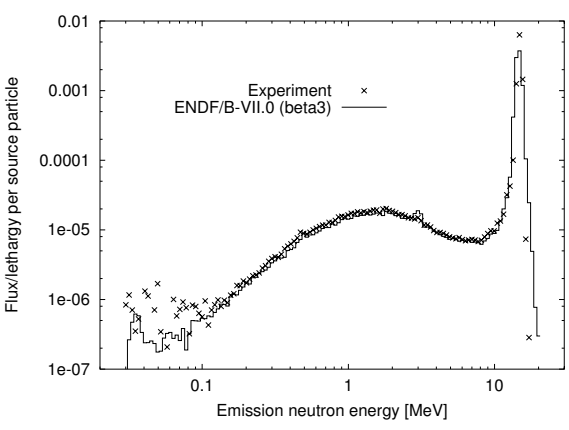

FIG. 89: Neutron spectrum for the FNS, Pb, d=5cm benchmark at 0° angle.

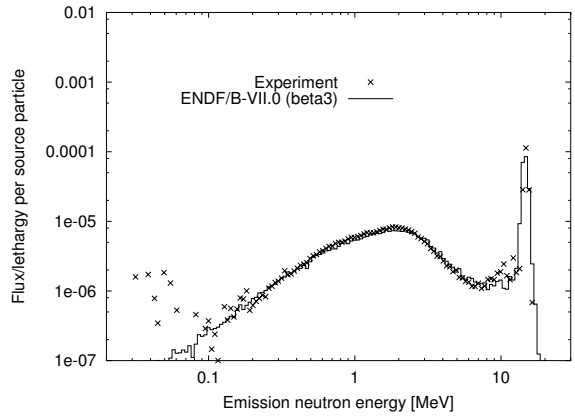

FIG. 90: Neutron spectrum for the FNS, Pb, d=5cm benchmark at 24.9° angle.

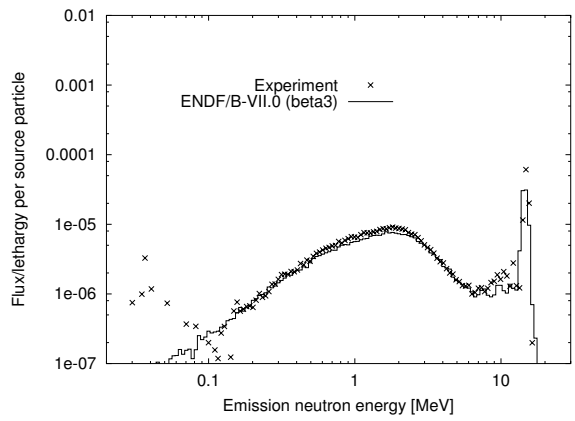

FIG. 91: Neutron spectrum for the FNS, Pb, d=5cm benchmark at 42.8° angle.

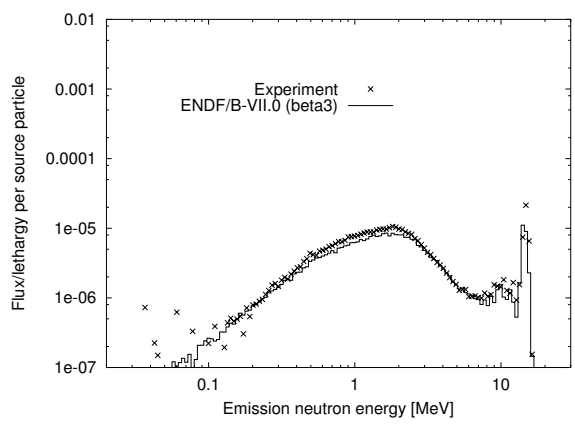

FIG. 92: Neutron spectrum for the FNS, Pb, d=5cm benchmark at 66.8° angle.

TABLE XLIX: C/E values for the spectrum of the FNS Pb 5cm benchmark.

energy [MeV]	0°	12.2°	24.9°	42.8°	66.8°
0.1−1.0	0.83±0.01	n.a.	0.88±0.01	0.85±0.01	0.80±0.01
1.0−5.0	0.96±0.01	n.a.	0.98±0.01	0.90±0.01	0.88±0.01
5.0−10.0	0.91±0.01	n.a.	1.02±0.02	0.87±0.02	0.90±0.02
10.0−20.0	0.93±0.01	n.a.	1.12±0.01	0.81±0.01	0.69±0.02

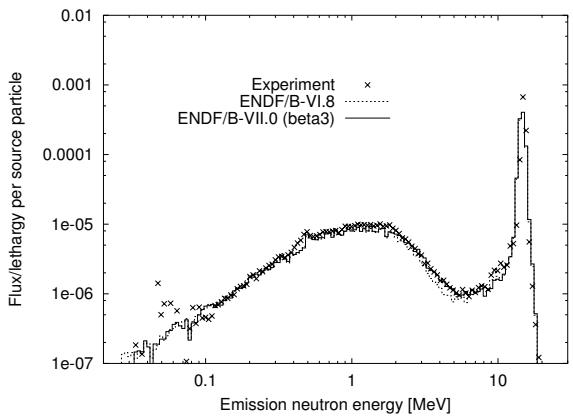

FIG. 93: Neutron spectrum for the FNS, Pb, d=20cm benchmark at 0° angle.

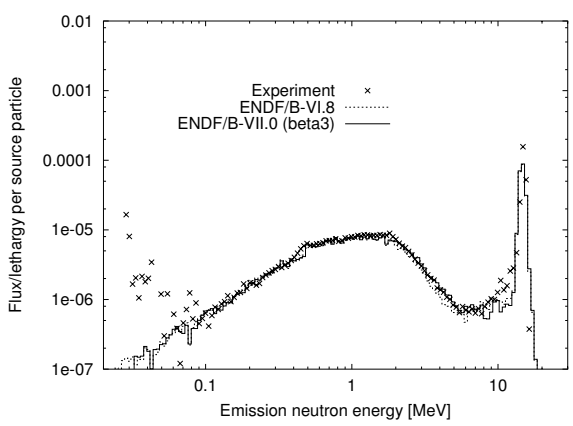

FIG. 94: Neutron spectrum for the FNS, Pb, d=20cm benchmark at 12.2° angle.

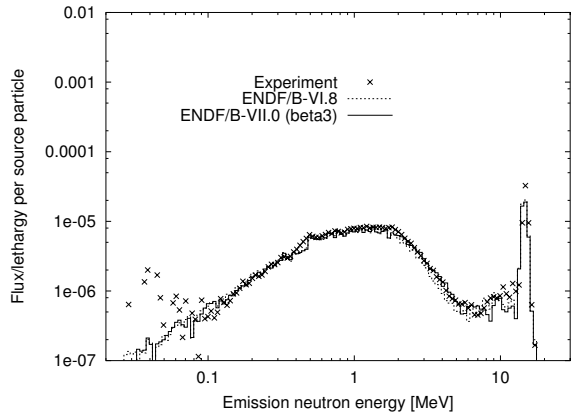

FIG. 95: Neutron spectrum for the FNS, Pb, d=20cm benchmark at 24.9° angle.

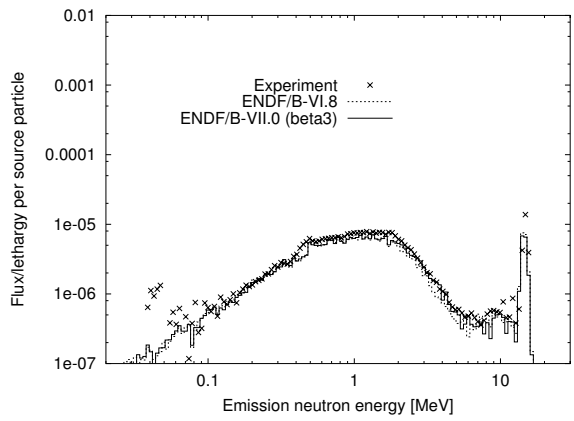

FIG. 96: Neutron spectrum for the FNS, Pb, d=20cm benchmark at 42.8° angle.

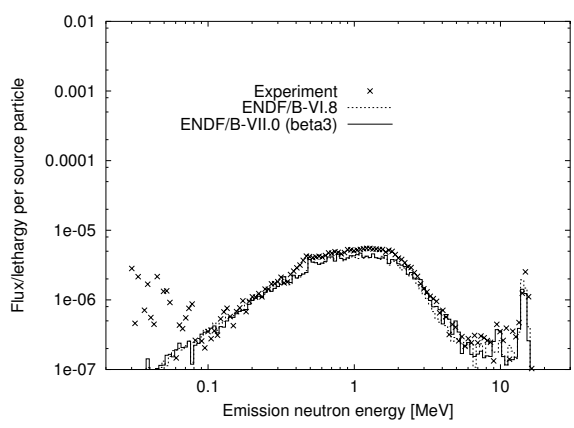

FIG. 97: Neutron spectrum for the FNS, Pb, d=20cm benchmark at 66.8° angle.

TABLE L: C/E values for the spectrum of the FNS Pb 20cm benchmark.

energy [MeV]	0°	12.2°	24.9°	42.8°	66.8°
0.1−1.0	0.85±0.01	0.91±0.01	0.89±0.01	0.83±0.01	0.80±0.01
1.0−5.0	0.93±0.01	0.99±0.01	0.95±0.01	0.90±0.01	0.86±0.01
5.0−10.0	0.83±0.03	0.92±0.03	0.88±0.04	0.78±0.04	0.84±0.07
10.0−20.0	0.93±0.01	0.84±0.01	0.81±0.02	0.73±0.03	0.63±0.05

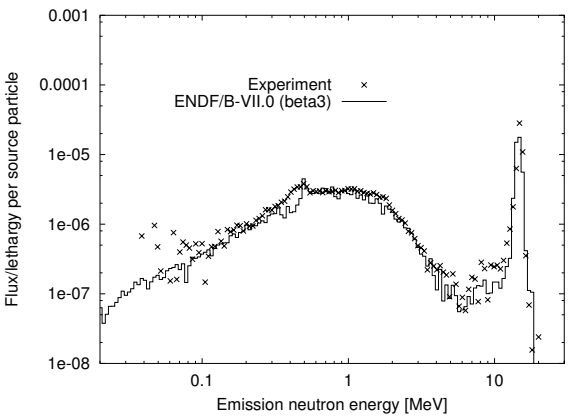

FIG. 98: Neutron spectrum for the FNS, Pb, d=40cm benchmark at 0° angle.

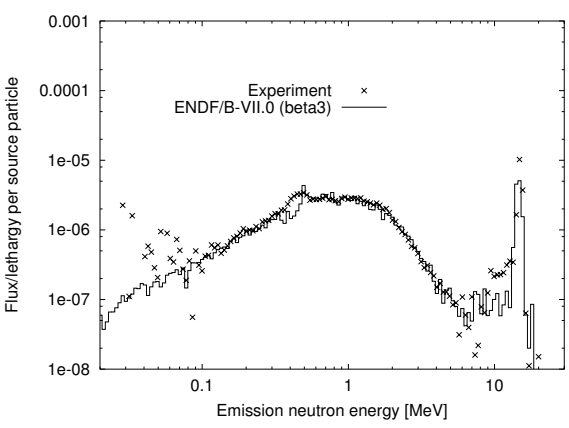

FIG. 99: Neutron spectrum for the FNS, Pb, d=40cm benchmark at 12.2° angle.

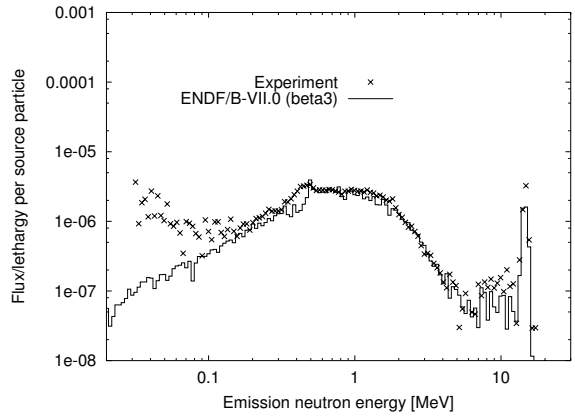

FIG. 100: Neutron spectrum for the FNS, Pb, d=40cm benchmark at 24.9° angle.

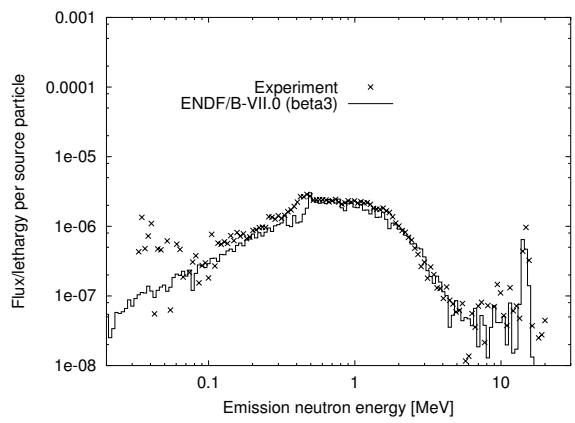

FIG. 101: Neutron spectrum for the FNS, Pb, d=40cm benchmark at 42.8° angle.

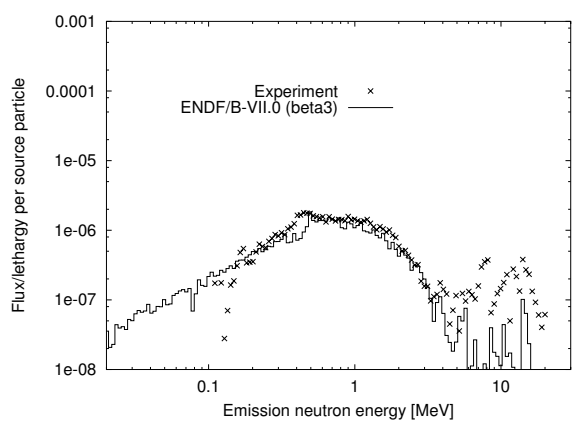

FIG. 102: Neutron spectrum for the FNS, Pb, d=40cm benchmark at 66.8° angle.

TABLE LI: C/E values for the spectrum of the FNS Pb 40cm benchmark.

energy [MeV]	0°	12.2°	24.9°	42.8°	66.8°
0.1−1.0	0.84±0.01	0.90±0.01	0.80±0.01	0.79±0.01	0.84±0.01
1.0−5.0	0.89±0.01	0.99±0.01	0.92±0.01	0.92±0.01	0.84±0.01
5.0−10.0	0.64±0.08	0.91±0.10	0.75±0.12	0.83±0.13	0.16±0.20
10.0−20.0	0.85±0.02	0.72±0.04	0.67±0.06	0.71±0.11	0.13±0.14

C. LLNL Pulsed Spheres

1. *LLNL Pulsed Spheres, ^6Li and ^7Li*

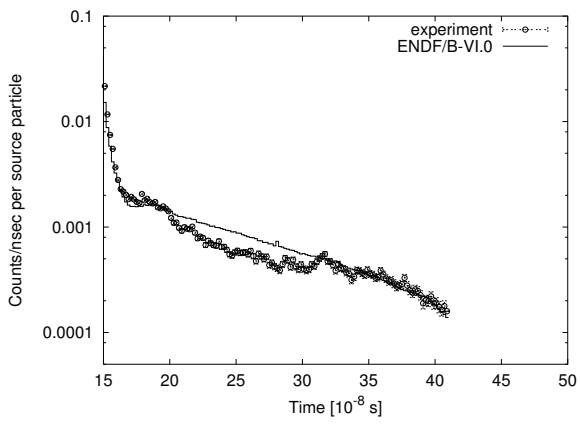

FIG. 103: Neutron spectrum for the LLNL Pulsed Sphere, ^{6}Li (0.5 mfp) benchmark, angle=39°.

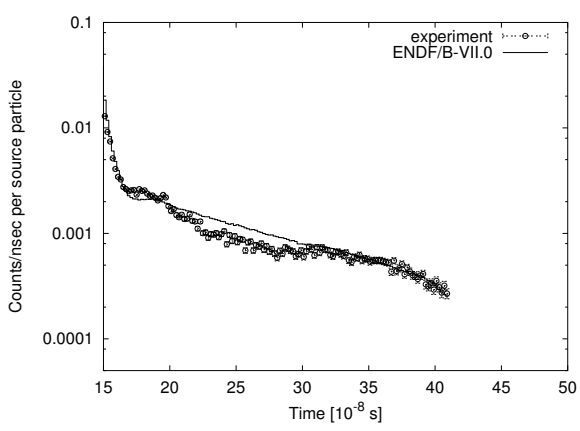

FIG. 104: Neutron spectrum for the LLNL Pulsed Sphere, ^{6}Li (1.1 mfp) benchmark, angle=39°.

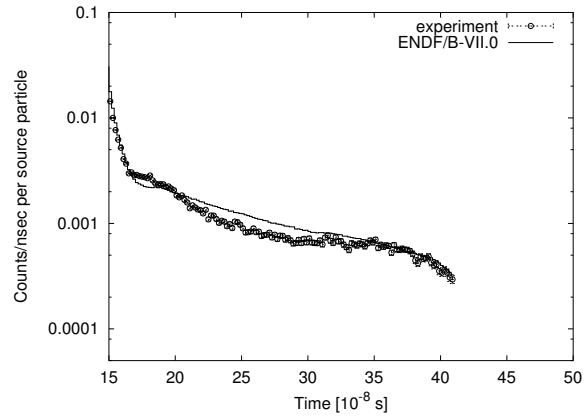

FIG. 105: Neutron spectrum for the LLNL Pulsed Sphere, ^{6}Li (1.6 mfp) benchmark, angle=39°.

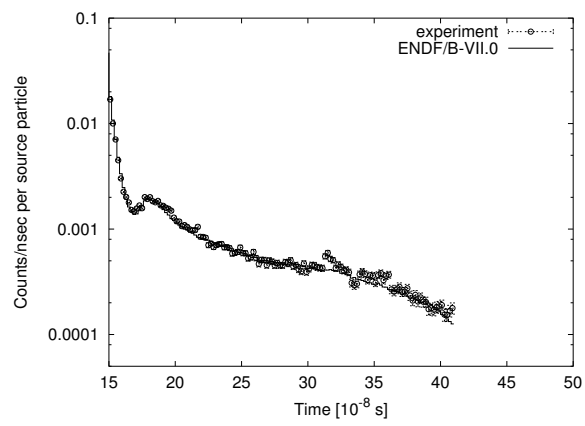

FIG. 106: Neutron spectrum for the LLNL Pulsed Sphere, ^{7}Li (0.5 mfp) benchmark, angle=39°.

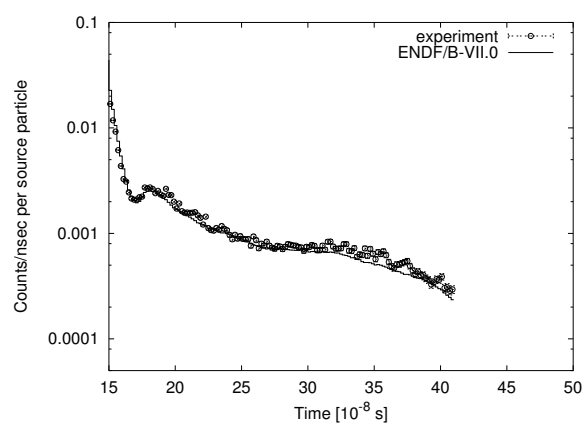

FIG. 107: Neutron spectrum for the LLNL Pulsed Sphere, ^{7}Li (1.1 mfp) benchmark, angle=39°.

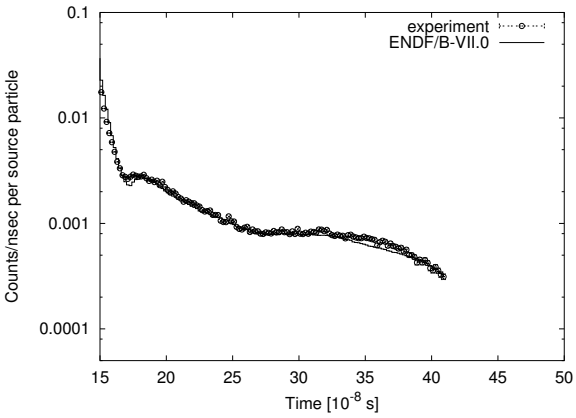

FIG. 108: Neutron spectrum for the LLNL Pulsed Sphere, ^{7}Li (1.6 mfp) benchmark, angle=39°.

2. LLNL Pulsed Spheres, Be

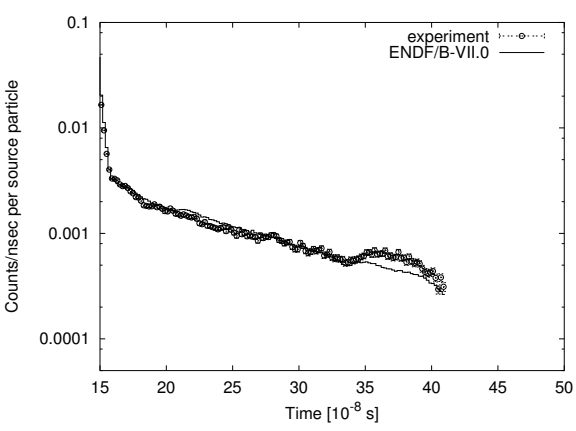

FIG. 109: Neutron spectrum for the LLNL Pulsed Sphere, Be (0.8 mfp) benchmark, angle=39°.

3. LLNL Pulsed Spheres, C

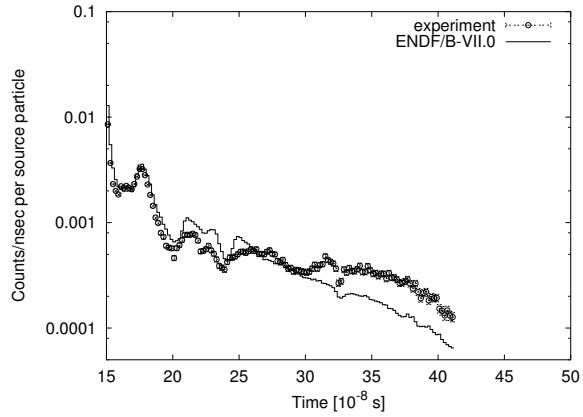

FIG. 110: Neutron spectrum for the LLNL Pulsed Sphere, C (0.5 mfp) benchmark, angle=39°.

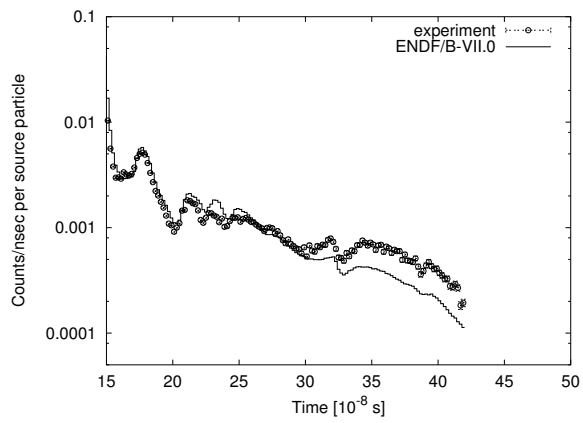

FIG. 111: Neutron spectrum for the LLNL Pulsed Sphere, C (1.3 mfp) benchmark, angle=39°.

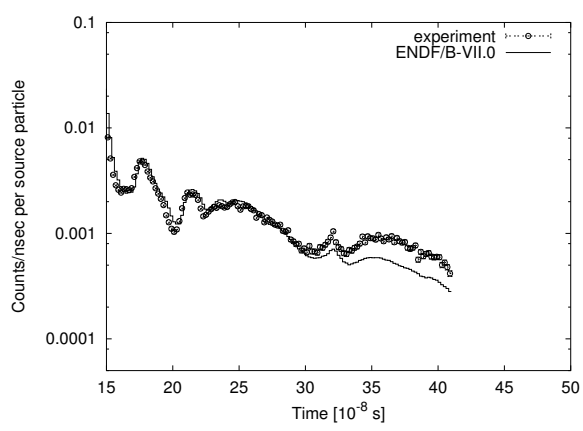

FIG. 112: Neutron spectrum for the LLNL Pulsed Sphere, C (2.9 mfp) benchmark, angle=39°.

4. LLNL Pulsed Spheres, N

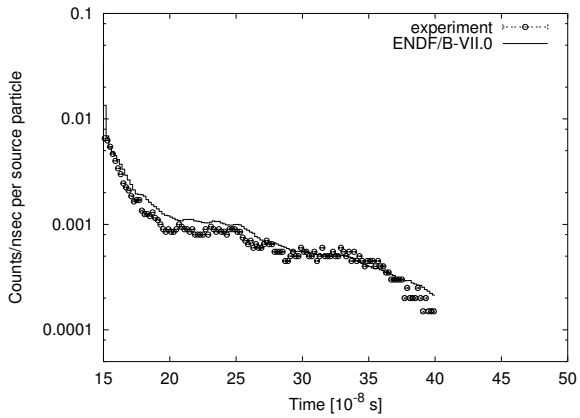

FIG. 113: Neutron spectrum for the LLNL Pulsed Sphere, N (1.1 mfp) benchmark, angle=39°.

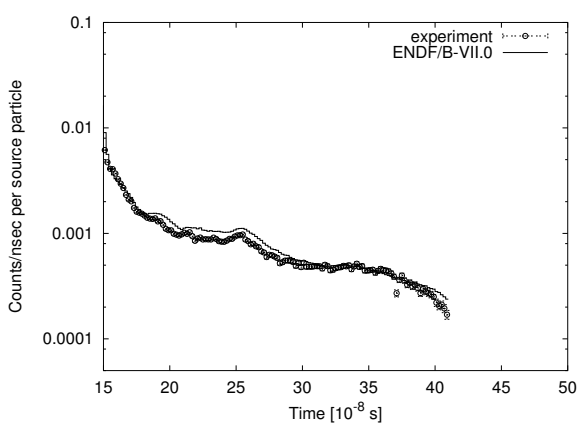

FIG. 114: Neutron spectrum for the LLNL Pulsed Sphere, N (3.1 mfp) benchmark, angle=39°.

5. LLNL Pulsed Spheres, O

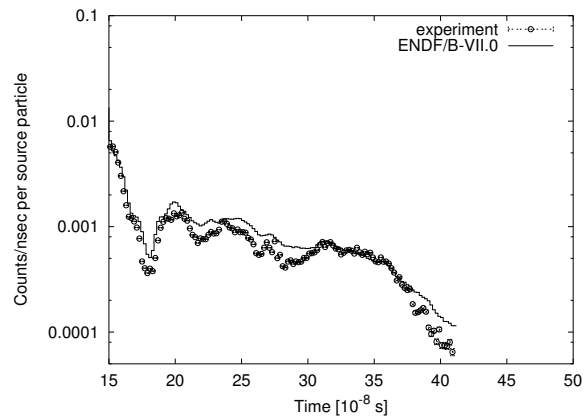

FIG. 115: Neutron spectrum for the LLNL Pulsed Sphere, O (0.7 mfp) benchmark, angle=39°.

6. LLNL Pulsed Spheres, Mg

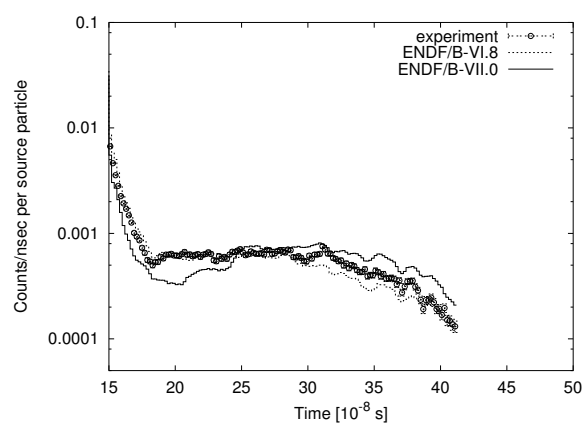

FIG. 116: Neutron spectrum for the LLNL Pulsed Sphere, Mg (0.7 mfp) benchmark, angle=39°.

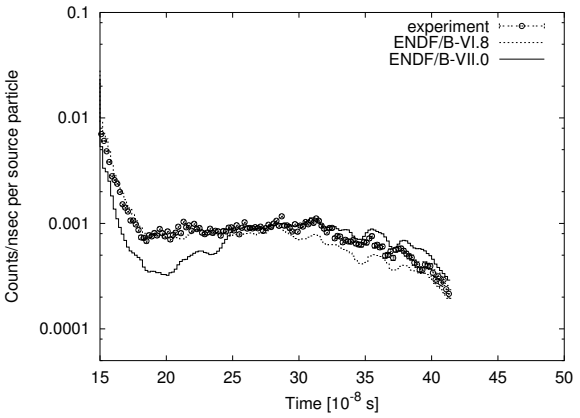

FIG. 117: Neutron spectrum for the LLNL Pulsed Sphere, Mg (1.2 mfp) benchmark, angle=39°.

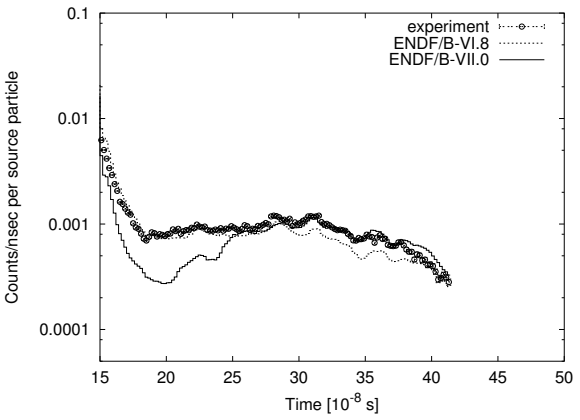

FIG. 118: Neutron spectrum for the LLNL Pulsed Sphere, Mg (1.9 mfp) benchmark, angle=39°.

7. *LLNL Pulsed Spheres, Al*

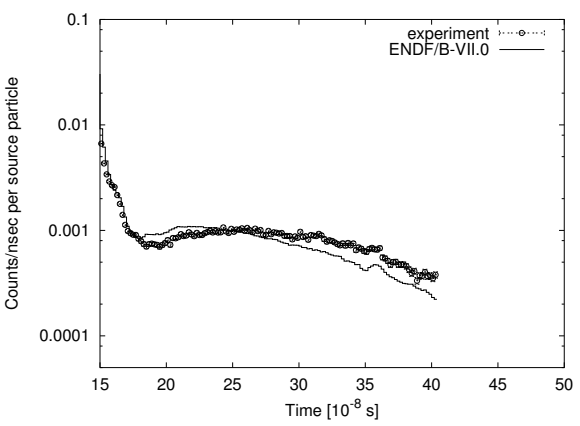

FIG. 119: Neutron spectrum for the LLNL Pulsed Sphere, Al (0.9 mfp) benchmark, angle=39°.

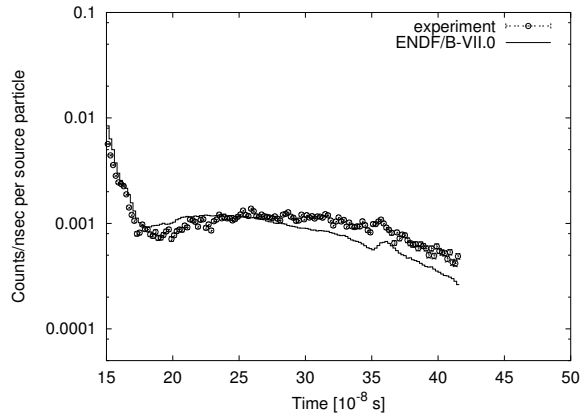

FIG. 120: Neutron spectrum for the LLNL Pulsed Sphere, Al (1.6 mfp) benchmark, angle=39°.

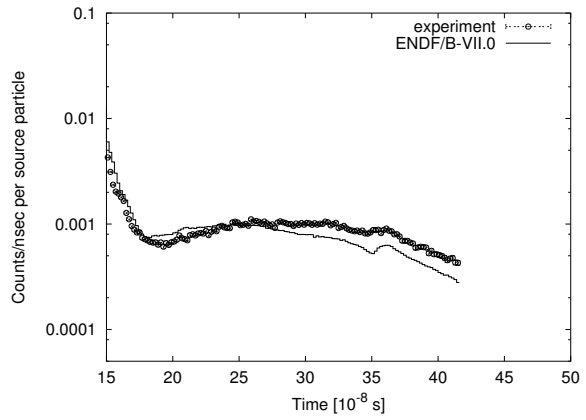

FIG. 121: Neutron spectrum for the LLNL Pulsed Sphere, Al (2.6 mfp) benchmark, angle=39°.

8. *LLNL Pulsed Spheres, Ti*

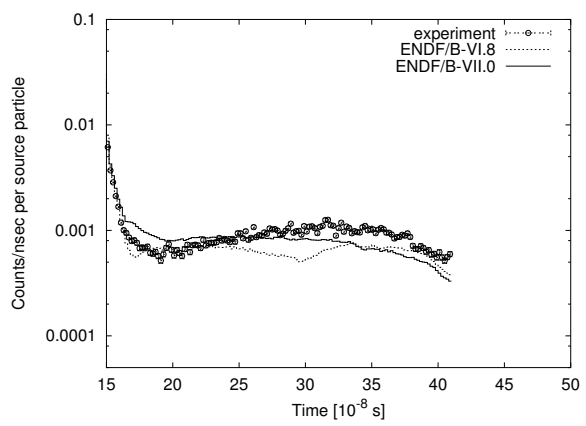

FIG. 122: Neutron spectrum for the LLNL Pulsed Sphere, Ti (1.2 mfp) benchmark, angle=39°.

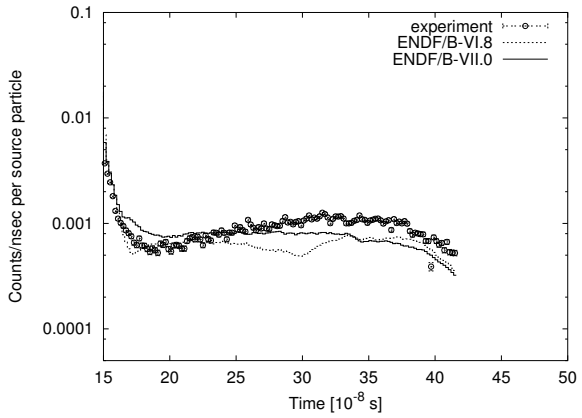

FIG. 123: Neutron spectrum for the LLNL Pulsed Sphere, Ti (2.2 mfp) benchmark, angle=39°.

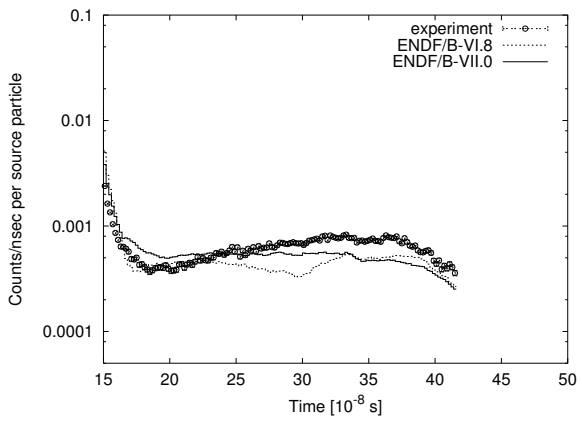

FIG. 124: Neutron spectrum for the LLNL Pulsed Sphere, Ti (3.5 mfp) benchmark, angle=39°.

9. *LLNL Pulsed Spheres, Fe*

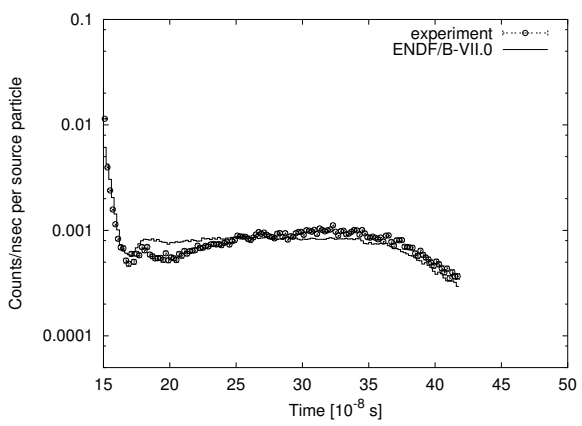

FIG. 125: Neutron spectrum for the LLNL Pulsed Sphere, Fe (0.9 mfp) benchmark, angle=39°.

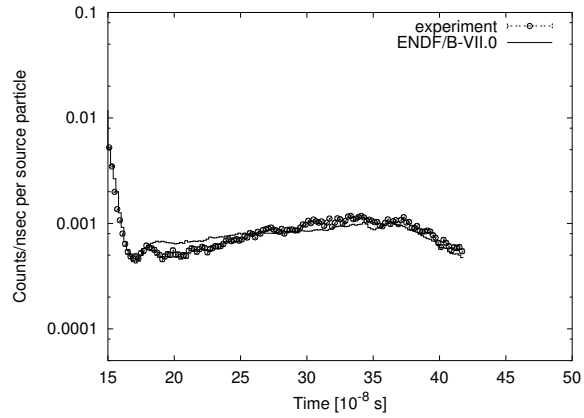

FIG. 126: Neutron spectrum for the LLNL Pulsed Sphere, Fe (2.9 mfp) benchmark, angle=39°.

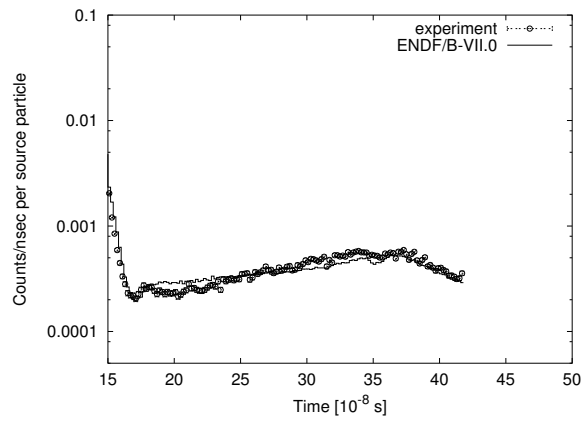

FIG. 127: Neutron spectrum for the LLNL Pulsed Sphere, Fe (4.8 mfp) benchmark, angle=39°.

10. *LLNL Pulsed Spheres, Pb*

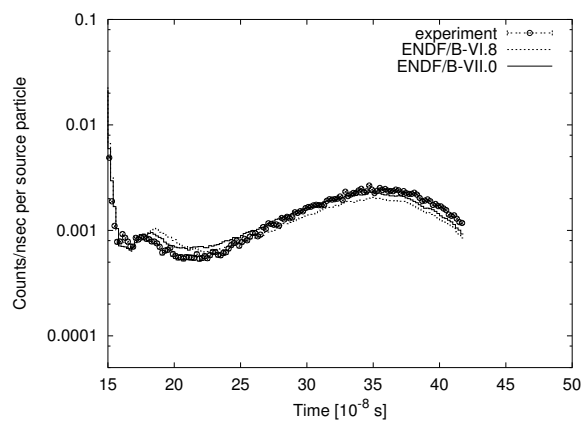

FIG. 128: Neutron spectrum for the LLNL Pulsed Sphere, Pb (1.4 mfp) benchmark, angle=39°.

11. *LLNL Pulsed Spheres, D_2O and H_2O*

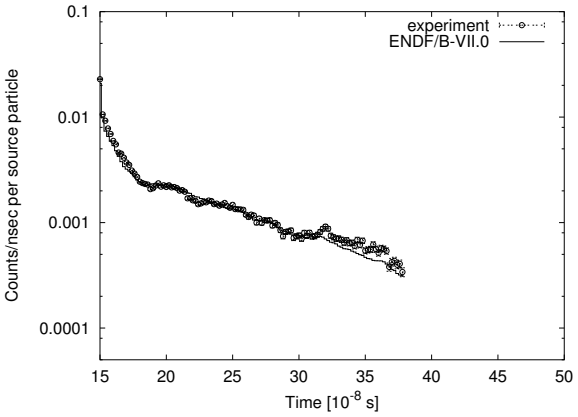

FIG. 129: Neutron spectrum for the LLNL Pulsed Sphere, D_2O (1.2 mfp) benchmark, angle=39°.

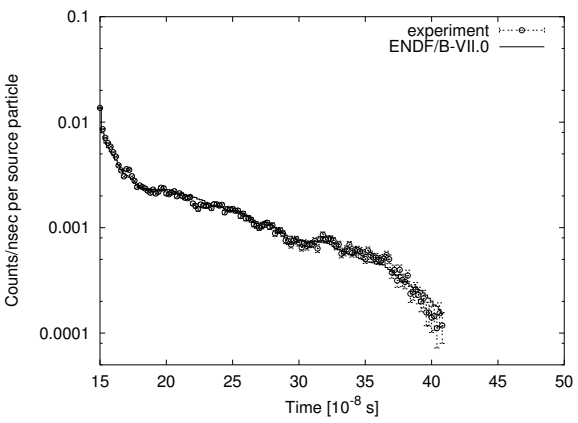

FIG. 130: Neutron spectrum for the LLNL Pulsed Sphere, D_2O (2.1 mfp) benchmark, angle=39°.

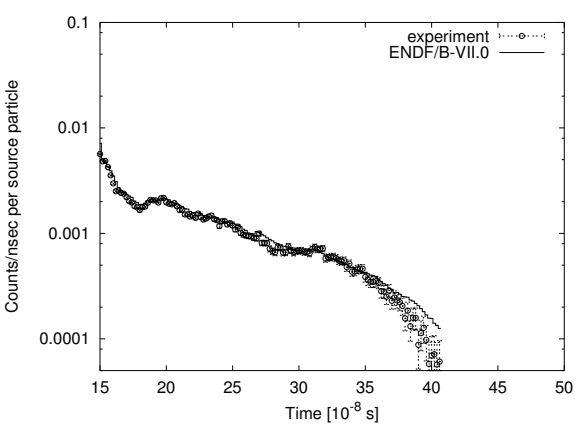

FIG. 131: Neutron spectrum for the LLNL Pulsed Sphere, H_2O (1.1 mfp) benchmark, angle=39°.

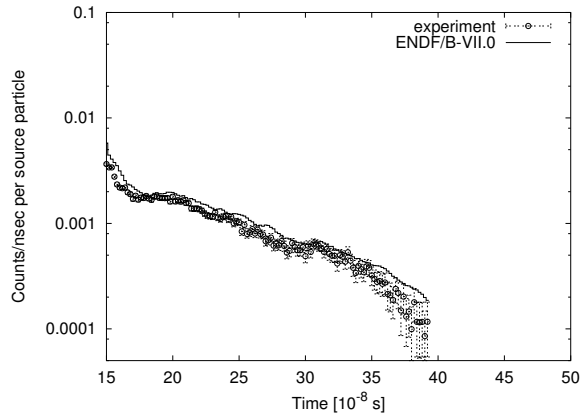

FIG. 132: Neutron spectrum for the LLNL Pulsed Sphere, H_2O (1.9 mfp) benchmark, angle=39°.

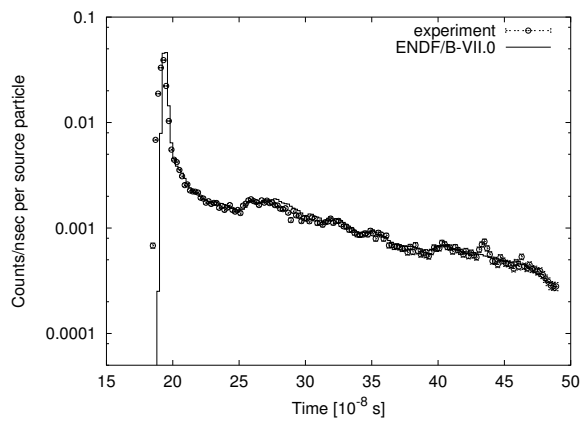

FIG. 133: Neutron spectrum for the LLNL Pulsed Sphere, H_2O (1.9 mfp) benchmark, angle=117°.

12. *LLNL Pulsed Spheres, Concrete*

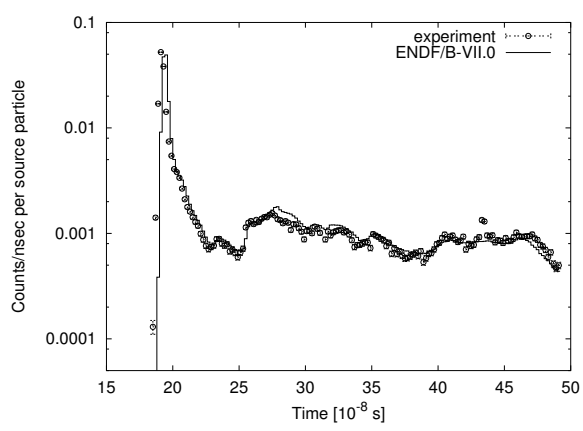

FIG. 134: Neutron spectrum for the LLNL Pulsed Sphere, Concrete (2.0 mfp) benchmark, angle=117°.

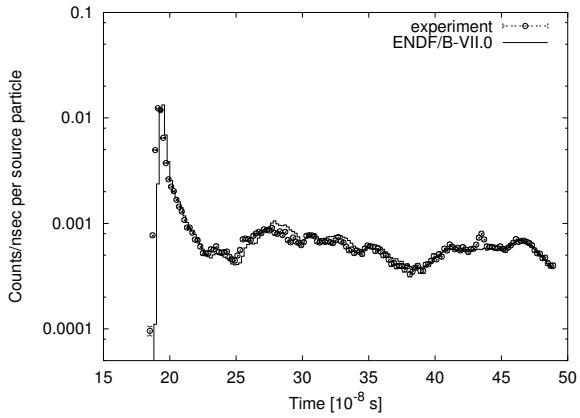

FIG. 135: Neutron spectrum for the LLNL Pulsed Sphere, Concrete (3.8 mfp) benchmark, angle=117°.

13. LLNL Pulsed Spheres, Polyethylene

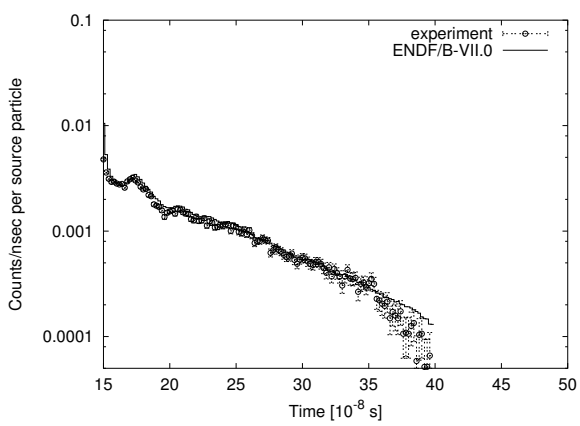

FIG. 136: Neutron spectrum for the LLNL Pulsed Sphere, Polyethylene (0.8 mfp) benchmark, angle=39°.

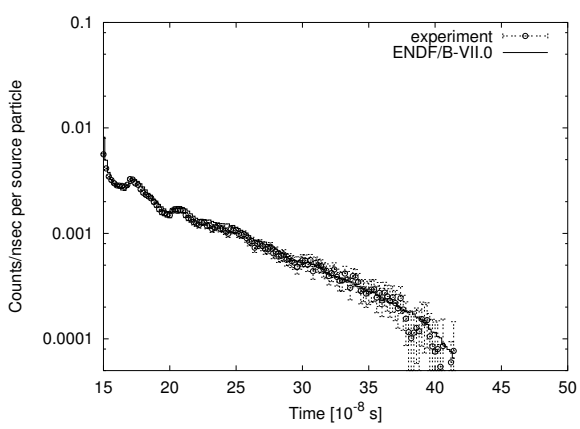

FIG. 137: Neutron spectrum for the LLNL Pulsed Sphere, Polyethylene (1.8 mfp) benchmark, angle=39°.

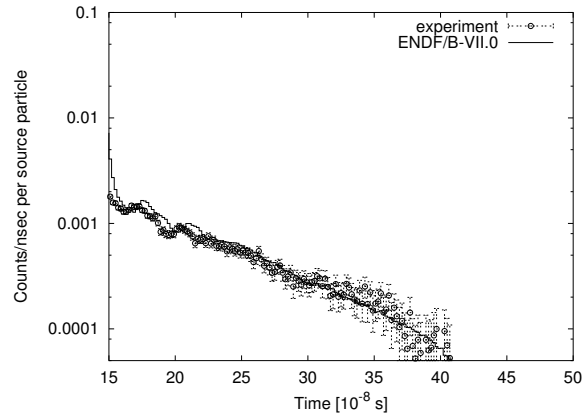

FIG. 138: Neutron spectrum for the LLNL Pulsed Sphere, Polyethylene (3.5 mfp) benchmark, angle=39°.

14. LLNL Pulsed Spheres, Teflon

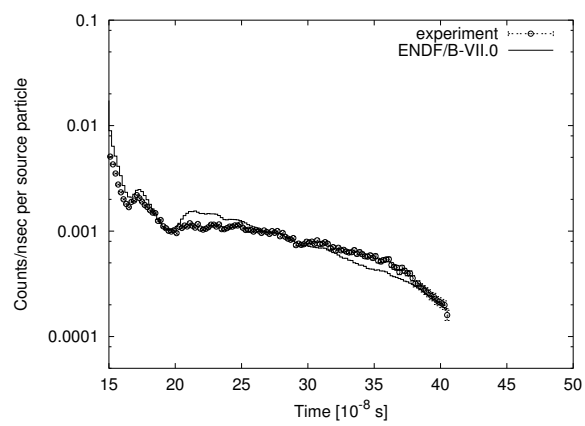

FIG. 139: Neutron spectrum for the LLNL Pulsed Sphere, Teflon (0.9 mfp) benchmark, angle=39°.

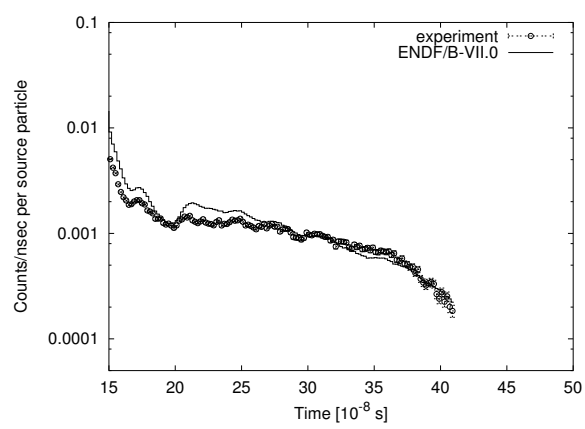

FIG. 140: Neutron spectrum for the LLNL Pulsed Sphere, Teflon (1.8 mfp) benchmark, angle=39°.

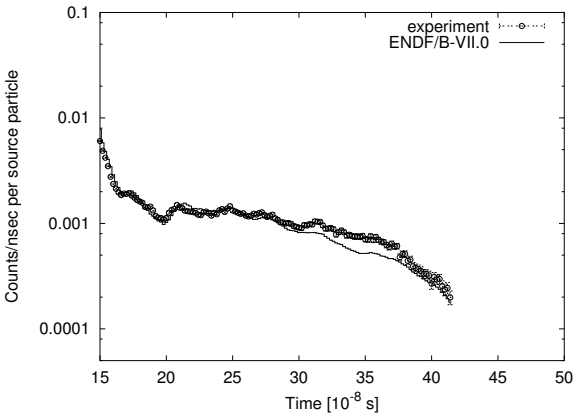

FIG. 141: Neutron spectrum for the LLNL Pulsed Sphere, Teflon (2.9 mfp) benchmark, angle=39°.

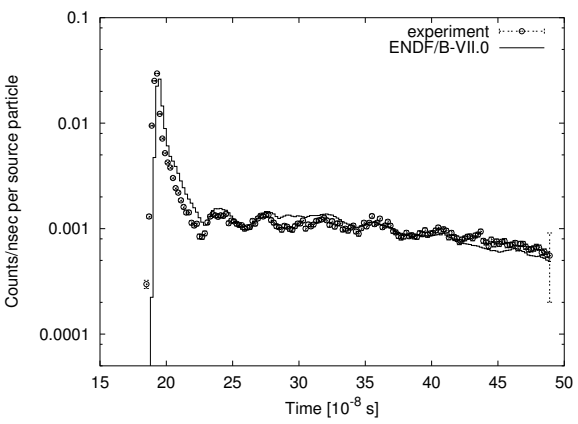

FIG. 142: Neutron spectrum for the LLNL Pulsed Sphere, Teflon (2.9 mfp) benchmark, angle=117°.

D. NIST Water Spheres

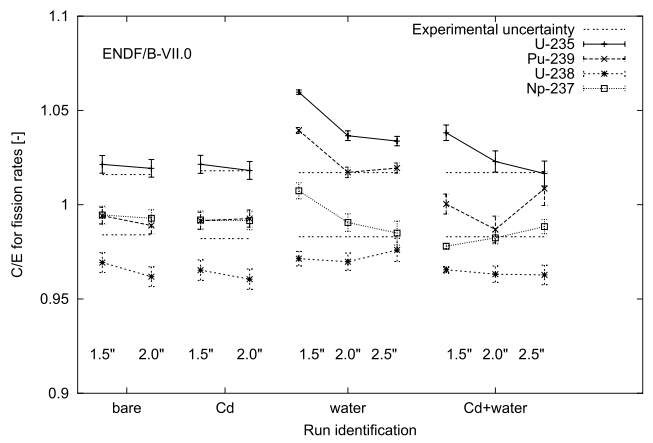

FIG. 143: C/E values for the fission rate in fission foils in the NIST experiments.

TABLE LII: C/E values for the fission rates in the NIST benchmark.

material	radius	U-235	Pu-239	U-238	Np-237
bare	1.5"	1.021±0.005	0.994±0.005	0.969±0.005	0.995±0.005
bare	2.0"	1.019±0.005	0.989±0.005	0.962±0.005	0.993±0.005
Cd	1.5"	1.021±0.005	0.991±0.005	0.965±0.005	0.992±0.005
Cd	2.0"	1.018±0.005	0.993±0.005	0.961±0.005	0.992±0.005
H_2O	1.5"	1.060±0.001	1.039±0.002	0.971±0.004	1.007±0.004
H_2O	2.0"	1.037±0.003	1.017±0.003	0.970±0.005	0.991±0.005
H_2O	2.5"	1.034±0.002	1.019±0.003	0.976±0.006	0.985±0.006
Cd+H_2O	1.5"	1.038±0.004	1.000±0.005	0.965±0.002	0.978±0.001
Cd+H_2O	2.0"	1.023±0.006	0.987±0.007	0.963±0.004	0.982±0.003
Cd+H_2O	2.5"	1.017±0.007	1.009±0.009	0.963±0.005	0.988±0.004

E. Summary

In the preceding pages, results for many benchmarks are presented. Most of these benchmarks have been defined with a view to fusion neutronics, focussing on the fast part of the spectrum, from 0.1 MeV to 15 MeV. For most of these benchmarks, the results based on ENDF/B-VII.0 have not changed considerably from results based on ENDF/B-VI.8.

For a few cases where there is a significant difference, we plotted the ENDF/B-VI.8 curve as well. This is for in-

stance the case for Mg, for which the results have gotten worse, and Zr, for which the results have improved considerably. Also for Mo the results have improved quite a bit, whilst for Ti the results above 1 MeV are somewhat better, whereas below 1 MeV they look slightly worse. Finally for Pb some small improvements can be observed between 1 and 10 MeV, which is illustrated in the results for the FNS 20cm case (Figs. 93−97) and for the LLNL Pulsed Sphere Pb case (Fig. 128).

In all, however, the results for these types of benchmarks have mostly stayed the same.

VI. DELAYED NEUTRON DATA TESTING

To validate the results that can be obtained with the delayed neutron data, we have calculated $\beta_{\rm eff}$ for many systems for which measurements have been reported in the open literature. The results of these calculations are reported here.

The results in this report have been obtained using MCNP-4C3 [10], extended with a method to calculate $\beta_{\rm eff}$ [20]. The standard versions of MCNP-4C3, MCNP-5, and MCNPX can all work with delayed neutron data. However, because these codes do not calculate a value for $\beta_{\rm eff}$, we included our own $\beta_{\rm eff}$ method into MCNP-4C3. This method has been used earlier to calculate $\beta_{\rm eff}$ for other nuclear data libraries, *viz.* JEFF-3.1, ENDF/B-VI.8, and JENDL-3.3 [21].

A. Brief description of the experiments

We have searched in the literature for measurements of the effective delayed neutron fraction, the result of which is listed below. We will use these experiments as benchmarks for the calculation of $\beta_{\rm eff}$ on the basis of ENDF/B-VII.0 nuclear data. For some systems we have found experimental values for the parameter α, which is linked to $\beta_{\rm eff}$ through $\alpha = [k(1-\beta_{\rm eff})-1]/l$, where l is the prompt neutron life time. All systems described below are at delayed criticality, so that the parameter we can compare with is the value $\alpha_{\rm dc} = \alpha(k=1) = -\beta_{\rm eff}/l$.

When not stated explicitly, the MCNP [10] model for the experiment was taken, without modifications, from the ICSBEP data [2]. Where possible, the ICSBEP identification is given in brackets after the benchmark name.

- **Godiva** (heu-met-fast-001)
  A bare sphere of highly enriched (94 wt%) uranium.
- **Jezebel** (pu-met-fast-001)
  A bare sphere of plutonium (95 at% Pu-239).
- **Skidoo** (u233-met-fast-001)
  A bare sphere of uranium, of which 98 at% U-233.
- **Topsy** (Flattop 25, heu-met-fast-028)
  A highly enriched (93 wt%) uranium sphere surrounded by a thick reflector of normal uranium. Experimental results are given in Ref. [22].
- **Popsy** (Flattop-Pu, pu-met-fast-006)
  A plutonium (94 wt% Pu-239) sphere surrounded by a thick reflector of normal uranium. Experimental results are given in Ref. [22].
- **Flattop 23** (u233-met-fast-006)
  A uranium (98 at% U-233) sphere surrounded by a thick reflector of normal uranium. Experimental results are given in Ref. [22].
- **Big Ten** (ieu-met-fast-007)
  A large, mixed-uranium-metal cylindrical core with 10% average U-235 enrichment, surrounded by a thick reflector of depleted uranium [23].
- **ZPR** (heu-met-inter-001, ieu-met-fast-010, mix-met-fast-011 case 1, pu-met-inter-002)
  Four cores in the Zero Power Reactor at ANL. The first one is a highly enriched uranium/iron benchmark, reflected by steel. The second is a heterogeneous cylindrical core of uranium (average enrichment 9%). The third has plutonium/uranium/zirconium fuel, reflected by graphite. The last core had heterogeneous plutonium metal fuel with carbon/stainless steel dilutions, and a steel reflector. Measured values for $\beta_{\rm eff}$ are given in e.g. Ref. [24].
- **SNEAK** (cores 7A, 7B, 9C1, and 9C2)
  Measurements of $\beta_{\rm eff}$ in four unmoderated PuO_2-UO_2 cores, surrounded by a depleted uranium reflector [25]. One core, 9C1, had only uranium as fuel. The 9C2 core was diluted with sodium. MCNP models were built based on the R-Z model descriptions in Ref. [25].
- **Masurca** (cores R2 and ZONA2)
  Measurements of $\beta_{\rm eff}$ by several international groups in two unmoderated cores, *viz.* R2 and ZONA2 [7]. Core R2 had of $\sim$ 30% enriched uranium as fuel, whereas ZONA2 had both plutonium and depleted uranium. Both cores were surrounded by a 50-50 UO_2-Na mixture blanket, and by steel shielding. MCNP models were built based on the R-Z model descriptions in Ref. [7].
- **FCA** (cores XIX-1, XIX-2, and XIX-3)
  Measurements of $\beta_{\rm eff}$ by several international groups in three unmoderated cores in the Fast Critical Assembly [7]. One core had highly enriched uranium, one had plutonium and natural uranium, and the third one had plutonium as fuel. The cores were surrounded by two blanket regions, one with depleted uranium oxide and sodium, and another one with only depleted uranium metal. MCNP models were built based on the R-Z model descriptions in Ref. [7].

- **TCA** (related to leu-comp-therm-006)
  A light water moderated low-enriched UO_2 core in the Tank-type Critical Assembly. From the description of this experiment in Ref. [8] it is clear that this experiment is closely related to benchmark leu-comp-therm-006 [2]. We have taken the MCNP input decks given in Ref. [2], and changed the loading pattern, the water height and lattice pitch.

- **IPEN/MB-01** (related to leu-comp-therm-077)
  Measurement of β_{eff} in the research reactor IPEN/MB-01, with a core consisting of 28×26 UO_2 (4.3% enriched) fuel rods inside a light water filled tank [9]. An MCNP input deck was made available by the authors of Ref. [9].

- **Winco slab tanks** (related to heu-sol-therm-038 case 5)
  Measurement of α in the Westinghouse Idaho Nuclear Company Slab Tank Assembly. The experiment consisted of two thin coaxial slab tanks with 93% enriched uranyl nitrate solution. From the description of this experiment in Ref.[26] it is clear that this experiment is closely related to heu-sol-therm-038, case 5 [2]. We have taken the MCNP input deck given in Ref. [2], and removed the stainless steel absorber between the two slab tanks.

- **Stacy** (leu-sol-therm-004, -007, -016, -021)
  Measurements of β_{eff}/l in uranyl nitrate solution (10 % enrichment) in several cores in the STACY facility. From the description of these experiments in Ref. [27], one can identify several experiments that have been included in the criticality benchmark collection [2].

- **Sheba** (core II)
  Measurement of β_{eff}/l in a critical assembly vessel, filled with 5% enriched uranyl fluoride, UO_2F_2, the Solution High-Energy Burst Assembly [28]. The vessel had a cylindrical shape, and there was no reflector. An MCNP model was built from scratch.

- **SHE-8**
  Measurement of β_{eff}/l in a split table type critical assembly called Semi-Homogeneous Assembly [29]. The core was shaped in a hexagonal prism, with graphite matrix tubes and graphite rods. There was no axial reflector. The central region in core 8 consisted of 73 fuel rods with 2.9% enriched UO_2 dispersed in graphite. An MCNP model was built from scratch.

- **Proteus** (core 5)
  Measurement of β_{eff}/l in a graphite reflected pebble bed reactor, containing uranium-carbon fuel pebbles (16.7% enrichment) and graphite moderator pebbles. As the reactor was operated below 1 kW, no coolant was needed. An MCNP model was made available by the authors of Ref. [11].

For Godiva, Jezebel, and Skidoo, both Keepin [30] and Paxton [22] give experimental values for β_{eff}. Although these values are not identical, the differences are small and have no significant impact on the conclusions drawn in this paper. Therefore we will use the numbers given by Keepin, because this is the commonly used reference.

For the Stacy, Winco, SHE-8, Sheba-II, and Proteus experiments, we will compare with the α values given in the respective references, because that is the measured quantity. Also, for the Winco experiment, there is some uncertainty in deriving a value for β_{eff} from the measured α. The comparison in the next section is done by dividing the calculated β_{eff} by the prompt neutron fission life time. This life time is calculated by MCNP by default, and is given in the output as the 'fission lifespan' (see the discussion of life time estimation in section 2.VIII.B of the manual [10]).

B. Results

The results for the Sheba-II, SHE-8, TCA and Winco experiments should be viewed with some caution, since the preparation of the MCNP models for these experiments involved interpretation on our part, based on the references given earlier. However, since the computational results for these cases are close to the experimental values, we judge the models to be appropriate for calculating β_{eff} and α.

Concerning the Winco slab tank experiment, another remark is in order. Our calculation of β_{eff} yields a value of 827 ± 4 pcm, contradicting the value 1500 ± 120 calculated in Ref. [26], based on the experimental α-value and other experimental information, not involving the prompt neutron fission life time. However, in Ref. [26] it is noted that its calculated value is higher than the expected value of roughly 900 pcm, the reason for which was not well understood. Our value for α is close to the experimental value.

The results for the fast cases are all close to the experimental values. The most reliable measurements in the fast range are the FCA and Masurca cores, since these have been measured independently by several international groups. For these systems, the results are well within 3% of the experimental values, which is the targeted accuracy proposed by Subgroup 6 of the Working Party on International Evaluation Co-operation (WPEC) of the Nuclear Energy Agency Science Committee [31].

For thermal systems we have only two cases in which β_{eff} was measured, *viz.* TCA and IPEN/MB-01. For all the others, where $\alpha = \beta_{\text{eff}}/l$ was measured, we also have to calculate the life time l, which can introduce an inaccuracy as well. Therefore we prefer to look mostly at the results for TCA and IPEN/MB-01, which are well within the targeted 3% accuracy.

TABLE LIII: The experimental and calculated β_{eff} (in pcm). The uncertainty for C/E includes only the statistical uncertainty of the calculation. This corresponds to the error bar in Fig. 144. The experimental uncertainty range is shown with dashed lines in Fig. 144.

	Experiment	Calculation		C/E
		ENDF/B-VI.8	ENDF/B-VII.0	ENDF/B-VII.0
TCA	771±17	812±9	769.2±1.3	0.998±0.002
IPEN	742±7	782±4	747.6±4.0	1.008±0.005
Masurca_R2	721±11	746±7	729.3±6.9	1.012±0.009
Masurca_Z2	349±6	343±5	339.5±4.5	0.973±0.013
FCA-XIX-1	742±24	746±8	732.4±7.5	0.987±0.010
FCA-XIX-2	364±9	365±5	367.6±4.8	1.010±0.013
FCA-XIX-3	251±4	255±4	246.2±4.1	0.981±0.017
Sneak-9C1	758±24	741±7	739.2±7.0	0.975±0.009
Sneak-7A	395±12	368±5	361.6±4.7	0.915±0.013
Sneak-7B	429±13	421±5	416.0±4.9	0.970±0.012
Sneak-9C2	426±19	388±5	376.4±4.8	0.884±0.013
Zpr-Heu	667±15	692±9	689.3±8.9	1.033±0.013
Zpr-U9	725±17	732±8	714.9±8.0	0.986±0.011
Zpr-Mox	381±9	363±6	367.0±5.1	0.963±0.014
Zpr-Pu	222±5	223±5	236.9±5.2	1.067±0.022
Godiva	659±10	670±8	668.7±4.0	1.015±0.006
Topsy	665±13	640±8	643.2±3.8	0.967±0.006
Jezebel	194±10	187±5	197.3±2.1	1.017±0.011
Popsy	276±7	278±5	266.4±2.4	0.965±0.009
Skidoo	290±10	313±6	312.1±2.7	1.076±0.009
Flattop-23	360±9	359±6	356.9±2.8	0.991±0.008

TABLE LIV: The experimental and calculated α (in $s^{-}1$). The uncertainty for C/E includes only the statistical uncertainty of the calculation. This corresponds to the error bar in Fig. 144. The experimental uncertainty range is shown with dashed lines in Fig. 144.

	Experiment	Calculation		C/E
		ENDF/B-VI.8	ENDF/B-VII.0	ENDF/B-VII.0
Proteus	3.60±0.02	3.78±0.07	3.61±0.03	1.003±0.008
SHE-8	6.53±0.34	6.22±0.07	5.99±0.15	0.917±0.025
Sheba-II	200.3±3.6	204.3±4.3	199.73±1.39	0.997±0.007
Stacy-029	122.7±4.1	124.4±2.6	116.88±0.75	0.953±0.006
Stacy-033	116.7±3.9	118.5±2.5	111.99±0.71	0.960±0.006
Stacy-046	106.2±3.7	107.5±2.2	102.87±0.64	0.969±0.006
Stacy-030	126.8±2.9	133.8±2.7	125.47±0.81	0.990±0.006
Stacy-125	152.8±2.6	159.5±3.3	152.06±0.99	0.995±0.007
Stacy-215	109.2±1.8	115.6±2.3	108.11±0.68	0.990±0.006
Winco	1109.3±0.3	1166.±13.	1111.24±5.54	1.002±0.005
BigTen	$(1.17\pm0.01)\times10^5$	$(1.19\pm0.01)\times10^5$	$(1.11\pm0.01)\times10^5$	0.952±0.008

VII. CONCLUSIONS

The introduction of the new data library ENDF/B-VII.0 has been made possible by much work, diligent and thorough, by many people. In this paper we have shown that the resulting library withstands the tests of many benchmarks. The library will doubtless be tested even more severely in the near future, but from the present work some conclusions can already be drawn. The underprediction of k_{eff} for LEU-COMP-THERM type systems, which was present in most recent data libraries, has been removed. The average calculated k_{eff} is now within 20 pcm of unity, compared to −452 for ENDF/B-VI.8. Moreover, for some benchmark series, such as LEU-COMP-THERM-007, the pitch dependence that was observed in the ENDF/B-VI.8 results, has also been removed. In the LEU-COMP-THERM category, there are no clear tendencies with any parameter, except for a few cases with special reflector materials (such as lead in LEU-COMP-THERM-010). While the prediction of k_{eff} for LEU-COMP-THERM has been improved considerably by making it higher, the predictions for LEU-

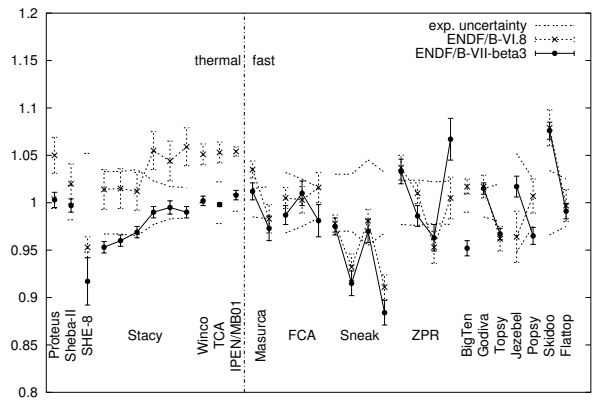

FIG. 144: C/E for β_{eff} (or β_{eff}/l, see text) for many benchmark systems. The systems are roughly ordered with respect to the average energy at which fission takes place, from low energy (left) to high (right).

SOL-THERM have stayed almost the same, compared to ENDF/B-VI.8, which is a good result.

Another area of improvement is IEU-MET-FAST, specifically -007 (Big Ten) and -010 (ZPR-U9), where the calculated values are now well inside the experimental uncertainty margins. For thermal HEU systems, the differences with ENDF/B-VI.8 are not big, but for some of the HEU-MET-FAST systems, fairly large improvements are seen. This is true of bare systems, as well as for ^{238}U reflected systems. However, for lead reflected systems, not all calculated values are satisfactory yet. Also, there are several IEU and HEU benchmarks based on cores in the Zero Power Reactor at Argonne, for which the calculational results are too high. It appears that the nuclear data for tungsten may be (partly) to blame. The predictions for the PU-SOL-THERM systems are, on average, somewhat on the high side. The calculational results are close the those based on ENDF/B-VI.8, reflecting the fact that the thermal part of the plutonium evaluations has not yet received the kind of attention that the uranium evaluations have. Results for the PU-MET-FAST systems have improved, with the exception of PU-MET-FAST-005, which is a tungsten reflected system. The PU-MET-INTER-002 benchmark (ZPR-6/10) remains a glaring outlier, which is confirmed by independent calculations, but not understood at present.

The results for the fusion shielding benchmarks have not changed much compared to ENDF/B-VI.8, except for certain elements. Especially noticeable is that results for Mg have deteriorated, whereas those for Mo and Zr have improved considerably. The NIST shielding benchmark still reveals a tendency of the thermal fission foil results with the thickness of the water layer, again comparable to ENDF/B-VI.8. The delayed neutron testing (β_{eff}) shows that the results for the fast spectrum cases are fine, and that the thermal spectrum cases are now also well reproduced, whereas the latter were calculated 5% high with ENDF/B-VI.8.

On the whole, the benchmark results show much improvement, worthy of a new major release of a nuclear data library.

Acknowledgments

The author wishes to acknowledge A. Hogenbirk for initiating the work on various benchmark series, and for processing the nuclear data files, in collaboration with M.C. Duijvestijn. Also, thanks are due to A.C. Kahler and J.C. Sublet for extensive comparisons with results from MCNP5 and TRIPOLI respectively, thus eliminating many errors along the way. The contribution of W. Haeck, who supplied the MCNP input decks for the LLNL Pulsed Sphere benchmarks, is gratefully acknowledged.

[1] M.B. Chadwick, P. Obložinský, M. Herman, N.M. Greene, R.D. McKnight, D.L. Smith, P.G. Young, R.E. MacFarlane, G.M. Hale, S.C. Frankle, A.C. Kahler, T. Kawano, R.C. Little, D.G. Madland, P. Moller, R.D. Mosteller, P.R. Page, P. Talou, H. Trellue, M.C. White, W.B. Wilson, R. Arcilla, C.L. Dunford, S.F. Mughabghab, B. Pritychenko, D. Rochman, A.A. Sonzogni, C.R. Lubitz, T.H. Trumbull, J.P. Weinman, D.A. Brown, D.E. Cullen, D.P. Heinrichs, D.P. McNabb, H. Derrien, M.E. Dunn, N.M. Larson, L.C. Leal, A.D. Carlson, R.C. Block, J.B. Briggs, E.T. Cheng, H.C. Huria, M.L. Zerkle, K.S. Kozier, A. Courcelle, V. Pronyaev, S.C. van der Marck, *ENDF/B-VII.0: Next Generation Evaluated Nuclear Data Library for Nuclear Science and Technology Applications*, Nuclear Data Sheets, this volume.

[2] J. Blair Briggs (ed.), *International Handbook of Evaluated Criticality Safety Benchmark Experiments,* NEA/NSC/DOC(95)03/I, Nuclear Energy Agency, Paris (September 2004 Edition).

[3] http://www-nds.iaea.or.at/fendl2/validation/benchmarks/jaerim94014/oktavian/n-leak

[4] http://www-nds.iaea.or.at/fendl2/validation/benchmarks/jaerim94014/fns-tof

[5] C. Wong, J.D. Anderson, P. Brown, L.F. Hansen, J.L. Kammerdiener, C. Logan, and B. Pohl, *Livermore Pulsed Sphere Program: Program Summary through July 1971,* UCRL-51144, Rev. 1, 1972.

[6] Sinbad data base, NEA (2004), http://www.nea.fr/html/science/shielding/sinbad/nist_h2o/nist-abs.htm

[7] S. Okajima, T. Sakurai, J.F. Lebrat, V.Z. Averlant, and M. Martini, *Summary on International Benchmark Experiments for Effective Delayed Neutron Fraction*, Progress in Nuclear Energy, **41** pp. 285-301, 2002.

[8] K. Nakajima, *Re-evaluation of the Effective Delayed Neu-*

tron Fraction Measured by the Substitution Technique for a Light Water Moderated Low-Enriched Uranium Core, J. Nucl. Sci. Technol. **38** pp. 1120-1125, 2001.

[9] A. dos Santos, R. Diniz, L.C.C.B. Fanaro, R. Jerez, G.S. de Andrade e Silva, and M. Yamaguchi, *The experimental determination of the effective delayed neutron parameters of the IPEN/MB-01 reactor*, Proc. Physor-2004, Chicago.

[10] J.F. Briesmeister (Ed.), *MCNP - A General Monte Carlo N-Particle Transport Code, Version 4C,* Technical Report LA-13709-M, Los Alamos National Laboratory, USA, 2000. J.S. Hendricks, *MCNP4C3*, Report X-5:RN(U)-JSH-01-17, Los Alamos National Laboratory, USA, 2001.

[11] T. Williams, M. Rosselet, and W. Scherer (Eds.), *Critical Experiments and Reactor Physics Calculations for Low-Enriched High Temperature Gas Cooled Reactors*, IAEA Tecdoc 1249 (advance electronic version, 2001).

[12] A. D. Knipe, *Specifications of the Dimple S01 Benchmark Assemblies*, Report AEA TSD 0375 (JEF/DOC-504), AEA Technology, 1994.

[13] J. Hardy, D. Klein and J. J. Volpe, *A study of physics parameters in several H_2O-moderated lattices of slightly enriched and natural uranium*, Nuc. Sci. Eng. **40** p. 101, 1970.
Cross Section Evaluation Working Group (CSEWG), *Benchmark Specifications*, ENDF-202, 1986.

[14] I. Remec, J. C. Gehin, and R. J. Ellis, *KRITZ-2:19 experiment on regular H2O/fuel pin lattices with mixed oxide fuel at temperatures up to 245° C, A Study (Draft) by the OECD/NEA Working Party on Scientific Issues of Reactor Systems (WPRS)*, to be published as part of the International Reactor Physics Benchmark Project.

[15] S.C. van der Marck, A. Hogenbirk, and R. Klein Meulekamp, *New temperature interpolation in MCNP*, Proc. M&C-2005, Avignon (France), 2005.

[16] C. Ichihara, I. Kimura, S.A. Hayashi, J. Yamamoto, and A. Takahashi, *Measurement of leakage neutron spectra from a spherical pile of zirconium irradiated with 14 MeV neutrons and validation of its nuclear data,* J. Nucl. Sci. Techn. **40** pp. 417-422, 2003.

[17] Y. Oyama, S. Yamaguchi, and H. Maekawa *Measruements and analyses of angular neutron flux spectra on graphite and lithium-oxide slabs irradiated with 14.8 MeV neutrons,* J. Nucl. Sci. Techn. **25** pp. 419–428, 1988.

[18] W. Haeck, *JEFF 3.1 validation results on LLNL pulsed spheres,* JEF/DOC-1141, 2006.

[19] M.Z. Youssef, A. Kumar, M.A. Abdou, Ch. Konno, F. Maekawa, M. Wada, Y. Oyama, H. Maekawa, and Y. Ikeda, *Verification of ITER shielding capability and FENDL data benchmarking through analysis of bulk shielding experiment on large SS316/water assembly bombarded with 14 MeV neutrons*, Fusion Engineering and Design **42** pp. 235-245, 1998.

[20] S.C. van der Marck and R. Klein Meulekamp, *Calculation of the effective delayed neutron fraction by Monte Carlo*, Proc. Physor-2004, Chicago, USA, 2004. R. Klein Meulekamp and S.C. van der Marck, *Calculation of the effective delayed neutron fraction by Monte Carlo*, Nucl. Sci. Eng. **152** pp. 142-148, 2006.

[21] S.C. van der Marck, R. Klein Meulekamp, A. Hogenbirk, and A.J. Koning, *Benchmark results for delayed neutron data*, Proc. ND-2004, Santa Fe, USA, pp. 531-534, 2004.

[22] H.C. Paxton, *Fast Critical Experiments*, Progress in Nuclear Energy **7** pp. 151-174, 1981.

[23] L.J. Sapir, H.H. Helmick, and J.D. Orndoff, *Big Ten, a 10% Enriched Uranium Critical Assembly: Kinetic Studies*, Trans. Am. Nucl. Soc. **15**, p. 312, 1975.

[24] E. Fort, V. Zammit-Averlant, M. Salvatores, and A. Filip, *Recommended values of the delayed neutron yield for U-235, U-238, and Pu-239*, JEFDOC-820.

[25] E.A. Fischer, *Integral measurements of the effective delayed neutron fractions in the fast critical assembly SNEAK*, Nucl. Sci. Eng. **62** pp. 105-116, 1977.

[26] G.D. Spriggs, *A Measurement of the Effective Delayed Neutron Fraction of the Westinghouse Idaho Nuclear Company Slab Tank Assembly using Rossi-α Techniques*, Nucl. Sci. Eng. **115** pp. 76-80, 1993.

[27] K. Tonoike, Y. Miyoshi, T. Kikuchi, and T. Yamamoto, *Kinetic Parameter β_{eff}/l Measurement on Low Enriched Uranyl Nitrate Solution with Single Unit Cores (600ϕ, 280T, 800ϕ) of STACY*, J. Nucl. Sci. Technol. **39** pp. 1227-1236, 2002.

[28] K.B. Butterfield, *The SHEBA experiment*, Trans. Am. Nucl. Soc. **74** pp. 199-200, 1994. R. Sanchez and P. Jaegers, *Prompt neutron decay constants in SHEBA*, Trans. Am. Nucl. Soc. **76** pp. 363–364, 1997.

[29] M. Takano, M. Hirano, R. Shindo, and T. Doi, *Analysis of SHE critical experiments by neutronic design codes for experimental Very High Temperature Reactor*, J. Nucl. Sci. Techn. **22** pp. 358-370, 1985. Y. Kaneko, F. Akino, and T. Yamane, *Evaluation of delayed neutron data for thermal fission of U-235 based on integral experiments at Semi-Homogeneous Experiment*, J. Nucl. Sci. Techn. **25** pp. 673–681, 1988.

[30] G.R. Keepin, *Physics of Nuclear Kinetics*, Addison-Wesley, Reading, USA, 1965.

[31] A. d'Angelo and J. Rowlands, *Delayed neutron data for the major actinides*, Tech. Rep. WPEC/SG6, NEA, Paris, 2002.